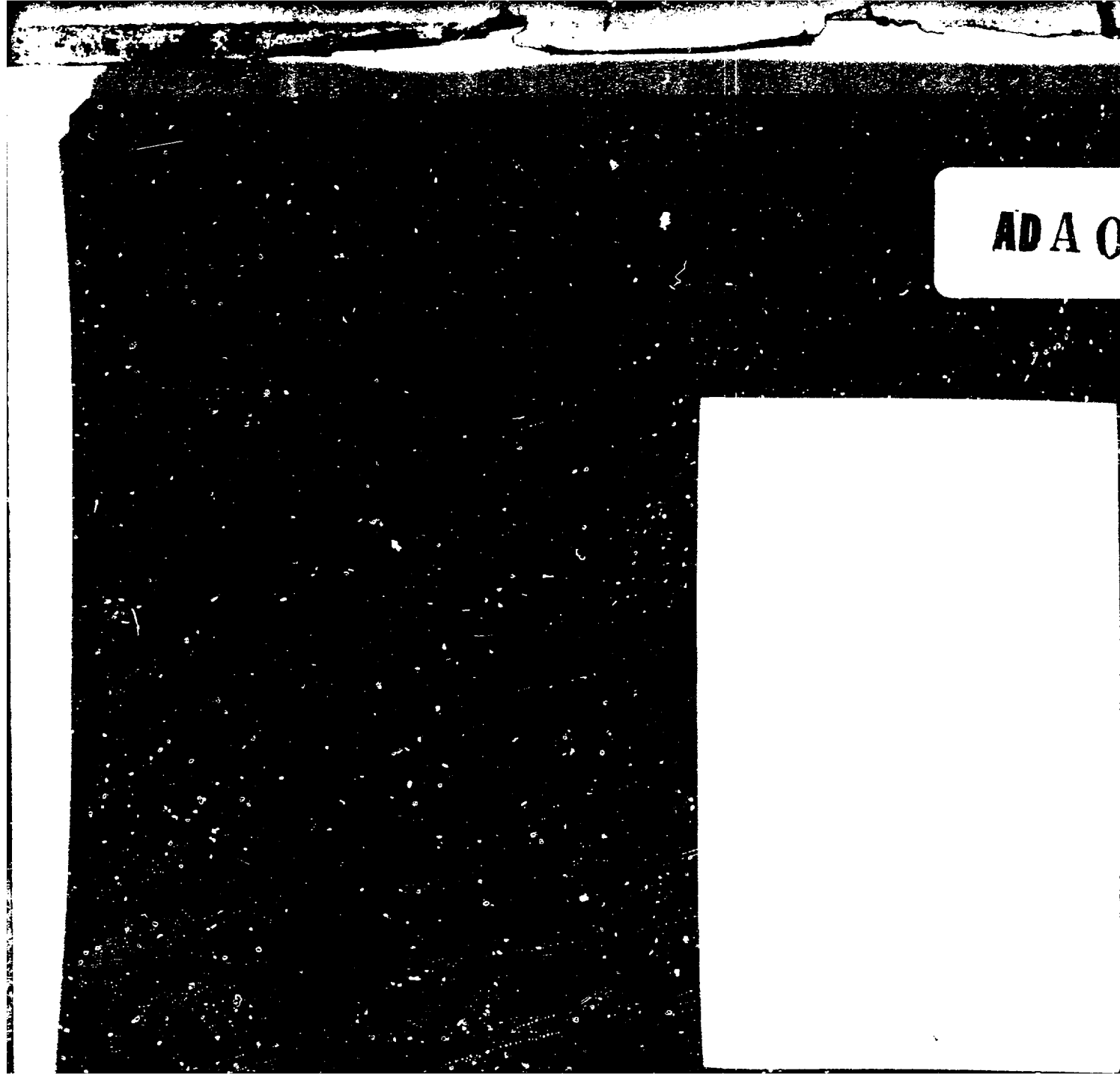
AD A C

SECURITY CLASSIFICATION OF THIS PAGE (When Data Entered)

(19) REPORT DOCUMENTATION PAGE

READ INSTRUCTIONS BEFORE COMPLETING FORM

(18) 1. REPORT NUMBER: AFOSR - TR-76-1168

2. GOVT ACCESSION NO.

3. RECIPIENT'S CATALOG NUMBER

(6) 4. TITLE (and Subtitle): STUDIES OF TRANSVERSE LIQUID FUEL JETS IN HIGH-SPEED AIR STREAMS

(9) 5. TYPE OF REPORT & PERIOD COVERED: INTERIM rept.

(14) 6. PERFORMING ORG. REPORT NUMBER: VPI-Aero-049

(10) 7. AUTHOR(s): J. SCHETZ, W. MOVEY, A. PADHYE, F. MUNTEANU

(15) AF - AFOSR [redacted]-2584-74

8. CONTRACT OR GRANT NUMBER(s)

9. PERFORMING ORGANIZATION NAME AND ADDRESS
VIRGINIA POLYTECHNIC INSTITUTE & STATE UNIVERSITY
~~AEROSPACE AND OCEAN ENGINEERING DEPARTMENT~~
BLACKSBURG, VIRGINIA 24061

10. PROGRAM ELEMENT, PROJECT, TASK AREA & WORK UNIT NUMBERS
~~61308~~
(16) 9711-02 (17) 02
61102F

11. CONTROLLING OFFICE NAME AND ADDRESS
AIR FORCE OFFICE OF SCIENTIFIC RESEARCH/NA
BLDG 410
BOLLING AIR FORCE BASE, D C 20332

(11) 12. REPORT DATE: Jul [redacted] 76

13. NUMBER OF PAGES: 135

14. MONITORING AGENCY NAME & ADDRESS (if different from Controlling Office)

(12) 136 p.

15. SECURITY CLASS. (of this report): UNCLASSIFIED

15a. DECLASSIFICATION/DOWNGRADING SCHEDULE

16. DISTRIBUTION STATEMENT (of this Report)

Approved for public release; distribution unlimited.

17. DISTRIBUTION STATEMENT (of the abstract entered in Block 20, if different from Report)

18. SUPPLEMENTARY NOTES

19. KEY WORDS (Continue on reverse side if necessary and identify by block number)

LIQUID FUEL INJECTION
FUEL ATOMIZATION
FUEL IGNITION

20. ABSTRACT (Continue on reverse side if necessary and identify by block number)

This report is in two parts describing two related studies of liquid fuel jet injection. The first study was concerned with the flowfield in the immediate vicinity of the injection port for the case of a hot, supersonic main air stream. Water, kerosene and carbon disulphide were studied as the injectants. The second study dealt with the details of penetration and break-up of liquid jets in high subsonic speed air streams.

DD FORM 1 JAN 73 1473 EDITION OF 1 NOV 65 IS OBSOLETE

UNCLASSIFIED 406 922

SECURITY CLASSIFICATION OF THIS PAGE (When Data Entered)

AFOSR INTERIM SCIENTIFIC REPORT VPI-Aero-049

AFOSR-TR- July 1976
AFOSR - TR - 76 - 1168

STUDIES OF TRANSVERSE LIQUID FUEL JETS IN HIGH-SPEED AIR STREAMS

J. Schetz, W. McVey, A. Padhye
and F. Munteanu

Approved for public release; distribution unlimited

This work was supported by the Air Force Office of Scientific Research under Grant AFOSR-74-2584. Dr. B. T. Wolfson was the Technical Monitor.

Mr. Munteanu's participation was supported through an East Europe Cooperative Science Program with the NSF. Mr. Robert Hull is the Program Monitor.

TABLE OF CONTENTS

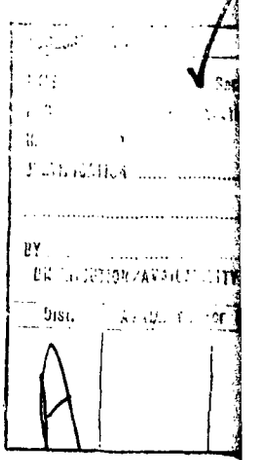

PART A: INJECTION INTO A HOT, SUPERSONIC AIRSTREAM

I. BACKGROUND

The flow field produced as a result of injecting liquid jets transverse to a supersonic stream is of great interest to present-day engineers. Fuel injection in scramjets, transpiration cooling of re-entry bodies, thrust vector control in rocket nozzles and external burning on projectiles are a few areas where these flow fields are important. Previous work has been conducted in the area of jet penetration, break-up and atomization of non-combustible jets (Refs. 1-11), but little work has been done where the combustion of these liquid jets are involved. Due to combustion being present in many of the practical applications, the combustion of liquid fuel jets injected into a supersonic stream merits study.

One aspect observed from the non-combustible testing which may prove important in the combustible case was the formation of a liquid layer on the solid surface in the region of the injector (Refs. 5-6). Since the flow velocity in the boundary layer above this liquid surface layer is less than that in the vicinity of the penetrating jet, one would expect combustion to occur near the liquid layer first due to the increased residence time.

This report describes a study of these liquid surface layers formed when liquid fuel jets are injected transverse to a hot, supersonic air stream. The tests were conducted in a specially constructed hot air facility that employed electrical resistance heating. The freestream conditions at the injection port were $M = 1.8$, $P_0 = 100$ psia and $500 \leq T_0 \leq 2100^{\circ}F$. Kerosene and carbon disulfide, CS_2, were used as the

liquid fuels and were injected through a 0.030 in. port perpendicular to the nozzle surface. Carbon disulfide was chosen as one of the fuels because of its lower minimum ignition temperature, 248°F as compared to 489°F for kerosene (Ref. 12). Water injections were conducted as control tests. In order to reach the highest air temperatures, an ethylene-oxygen-fueled dump combustor, or afterburner, was used upstream of the nozzle in addition to the electrical resistance heating.

Observations of the liquid surface layers were in the form of top-view direct photographs and infrared photographs using a thermographic camera to produce colored isotherms. Temperature probing with a fine thermocouple of the area above the liquid surface layer was also performed. In addition, wall temperatures beneath the liquid layer and away from the liquid layer were recorded for each test. A further, more complete description of the test facilities, data recording devices and results follows.

II. EXPERIMENTAL APPARATUS

A. Hot Air Facility

The hot supersonic air stream for the experiments was produced by a specially-designed facility. The facility consisted of a long, thick-walled Inconel 601 tube heated by means of electrical resistance (Fig. 1). The electric power was supplied by a bank of six Plasmatron PS-20 transformers producing approximately 40 kW. The entire facility was suspended from the ceiling in pendulum fashion with the nozzle rigidly supported. This allowed the pipe to expand when heated but at the same time held the nozzle in the same position for photography purposes.

The average wall temperature of the pipe was determined by means of a simple thermal expansion gauge. The gauge was constructed by considering the coefficient of thermal expansion for the Inconel 601 alloy as the wall temperature varied from room temperature up to 2000°F. Using this gauge provided a rough but adequate means of setting test conditions. Due to the long length of the pipe, the exit temperature, as measured in the settling chamber upstream of the nozzle throat, was nearly equal to the average pipe wall temperature as indicated by the expansion gauge. From rupture stress considerations for a pressure of 150 psia, a conservative maximum wall temperature of 1800°F was selected for the Inconel pipe.

The air supply came from a Bury VB-3-8, 600 psi compressor and was stored in a 70 cubic feet surge tank. The air flow from the tank to the pipewas regulated by a Grove dome pressure regulator operated parallel to a preset throttling valve and an on-off ball valve. Prior to entering

the surge tank, the air passes through a series of filters and dryers. All considered, this facility produces uncontaminated, dust-free air which is considered crucial in sensitive combustion studies.

B. Test Nozzle

The nozzle used for these tests was an axisymmetric nozzle constructed of stainless steel and designed to produce a Mach number of 1.8 at the injection station, approximately 0.25 in. from the end of the nozzle (Fig. 2). Located on the nozzle are stagnation and static pressure taps, two total temperature measuring devices and two wall temperature measuring devices (Fig. 3). One wall thermocouple is located at the same axial station as the injector but well around the nozzle 90 degrees to the injector. The other thermocouple is located near the injector in a region expected to be covered by the liquid layer based on previous work (Ref. 6). The total temperature thermocouples are located upstream of the nozzle throat in the settling chamber. These probes are located a distance 0.44 in. and 0.34 in. from the wall and 120 degrees apart.

C. Gas-Fired Afterburner

The gas-fired afterburner, or dump combustor, was used to facilitate reaching higher (>1650°F) air temperatures (Fig. 4). The combustor was constructed of a stainless steel tube 18.0 in. in length with a 3.0 in. outside diameter and a 0.5 in. wall thickness. The injection plate was constructed of stainless steel and was designed to inject the ethylene, C_2H_4, and oxygen into the recirculation region of the combustor (Fig. 5). Although the air temperature in the combustor was very high (1300°F to 1500°F), a spark plug was located near the flow recirculation region to

ensure ignition and for safety reasons. Four equally spaced thermocouples were located near the exit of the combustor in order to measure the temperature profile of the air leaving the combustor. These thermocouples were spaced at equal intervals from 0.25 in. above the wall out to the centerline, 1.0 in. above the wall.

The oxygen and ethylene were injected into the combustion zone in gaseous form. The flow of each was controlled by means of an orifice designed to operate in a choked condition. Therefore, increasing/decreasing the pressure would increase/decrease the flow rate as long as the pressure upstream of the orifice was approximately twice the downstream pressure. These orifices were calibrated to determine the discharge coefficient. The injection system was automatically controlled by a Cramer Type 540 cam-type timer. The system involved an interlocking purge (nitrogen) with a fail-safe valving system incorporated into the design. This design ensured safe, accurate and repeatable tests.

The spark plug, located near the injector, was fired by a Franceformer Ignition Transformer which delivers a terminal voltage of 6000 volts and provides a continuous spark. The spark plug was in operation from initial purge through fuel injection and final purge. This ensures that any lingering fuel will be ignited and eliminates the possibility of explosions du to a build-up of excess fuel.

Each of the four thermocouples located at the exit of the combustor was monitored once every four seconds by means of a Cramer Type 540 cam-type timer. As stated earlier, these thermocouples provided a means of measuring the temperature profile across the combustor exit. In addition to this, their readings were helpful in confirming that nothing unusual

was occurring in the combustor. Table 1 gives some typical output from these thermocouples and fig. 6 contains this data.

The theoretical temperature for a given inlet temperature to the combustor and a particular mass flow of ethylene was calculated and compared to that measured at the centerline of the combustor. The measured temperature was found to be twelve percent lower than the theoretical temperature. One can assume that this twelve percent loss in temperature is probably due to heat transfer along the 18 in. combustor. Indirect evidence for our belief that all of the ethylene is consumed in the afterburner can be found in the observed fact that there was no further temperature increase between the thermocouples at the end of the afterburner and those in the nozzle plenum (about 2 1/2 D). Then, by injecting the amount of oxygen consumed in the combustion process, we again have relatively "clean" air. The only extra elements are the product of combustion and since the mass flow of ethylene was very small, the amount of contamination is small.

D. Liquid Fuel Injection System

The liquid fuel was forced from a storage cylinder pressurized with nitrogen through a 0.030 in. port in the nozzle. Again, as in the combustor, the system involved an interlocking purge (nitrogen) with a fail-safe valving system incorporated into the design.

The injectant flow rate was measured by a Ramapo Model V-1/2-SS drag body flow meter. The flow meter was calibrated for each of the

injectants used. All tests reported here were conducted at a mass flow of 0.026 lbs/sec. but necessarily different volumetric flows as the densities of the three injectants differed.

E. Automatic Operation

The entire test facility was constructed such that its operation could be automatic. Cam-type timers, as described earlier, were used to control the injection of ethylene and oxygen into the combustor, the injection of liquid fuels into the supersonic air stream and the temperature monitoring at the exit of the combustor. The timer sequences are shown in Fig. 7. The use of these timers enabled the safe operation of the facility and also ensured the repeatability of the tests.

F. Instrumentation

The thermocouples used in these tests were of the Cromel-Alumel type. The output from these thermocouples was recorded on Hewlett-Packard Model 7100B strip chart recorders.

Strain gauge type pressure transducers were used to obtain pressure measurements. Again, the output was recorded on Hewlett-Packard Model 7100B strip chart recorders.

Visual observations of the liquid surface layer were performed by two methods; direct, top-view photographs and thermographic photographs. The direct, top-view photographs were made with an f 2.9, 2.75 in. diameter lens and a 4x5 Graflex camera using Polaroid type 57 sheet film. A Strobotac Type 1531-AB provided the light source by single pulses of 0.4 μsec duration. The physical arrangement of the lens and camera was such as to provide a magnification of approximately 2x1 (Fig. 8).

The most informative and probably the most impressive observations were those utilizing a Thermovision Model 680 Thermographic camera. This camera senses the infrared radiation emitted by a heated surface, processes these infrared images internally and produces ten color, isotherm band images of the field of view on a color television screen. The temperature difference for each isotherm band as well as the range of temperatures observed are adjustable over a wide range. Most of these tests were conducted with a camera setting of f 14, sensitivity of 200 and a 6.0 percent transmission gray filter for high temperature tests. Photographs of the color television image were taken with a 4x5 Graflex camera using Polaroid type 58 sheet film. The viewing path for the Thermographic camera was the same as that for the direct, top-view photographs (Fig. 9).

III. TEST PROCEDURE

For each test, the following were recorded from the beginning to the end of the test: total pressure at exit from the surge tank, total pressure in nozzle settling chamber, static pressure at injection port, two total temperature measurements in nozzle settling chamber, nozzle wall temperature away from liquid layer, nozzle wall temperature beneath the liquid layer and liquid injection flow rate. In addition to these, during the tests utilizing the gas-fired combustor, temperatures at four different radial positions at the exit of the combustor were recorded.

Prior to the beginning of each test, the Inconel pipe was heated to the desired temperature, and all fuel tanks and purge tanks were pressurized to the desired pressure. This included the oxygen and ethylene supplies when the gas-fired combustor was used. Upon reaching the desired pipe temperature, the air flow was initiated manually. As the nozzle wall temperature approached the desired value, the automatic timers were started. As indicated earlier, these cam-type timers controlled every aspect of the test except the air flow. There were three timers utilized; one main timer and two auxiliary timers. The main timer was used to start the remaining two timers and to control the injection of oxygen and ethylene into the combustor. One of the auxiliary timers was used to control the liquid fuel injection, flash for photography and the actuation of the Graflex camera. The remaining timer was used in the monitoring of the four temperatures at the exit of the combustor. A schematic of the timer sequences is shown in Fig. 7.

All photographs were taken two seconds after tne four second liquid fuel injection had begun. This ensured the stabilization of the liquid layer and the liquid jet.

IV. RESULTS

Numerous tests were conducted at various air temperatures for three different liquid injectants; water, kerosene and carbon disulfide (Table 2). For all tests, the temperature and mass flow of the injectant were constant. The air temperature ranged from 500°F to 2100°F as the nozzle wall temperature away from the liquid injection varied between 250°F to 900°F. Tables 3, 4 and 5 give a sample of the temperature data collected for tests with water, carbon disulfide and kerosene, respectively.

A. Direct, Top-View Photographs

Figures 10, 11, 12, and 13 are a few typical direct, top-view photographs for water, carbon disulfide and kerosene, respectively. In all of these photographs, the air flow is from left to right. The oblong hole in the center is the nozzle exit, and the white streak going off towards the right is the main liquid jet. To the left, above and below the front of the main jet, one can observe the liquid surface layer mentioned earlier. Notice that the thermocouple just above the front of the main jet is covered by this liquid layer. As the air temperature increases, the liquid layer becomes less distinct and apparently thinner but is still evident with an air temperature of 1800°F for the water injection case. The fact that the wall temperature is reduced a large amount is again evidence that a liquid layer exists.

The carbon disulfide injection cases are shown in Figs. 11a and 11b. These are for the same mass flow, but since carbon disulfide has a specific gravity of 1.26, the volume flow is reduced. The jets still appear larger when viewed from above. This, apparently, is a result of

the lower vapor pressure of carbon disulfide which produced more rapid spreading. Again, the surface layers are visible at all air temperatures.

The kerosene injection photographs also show the presence of the liquid surface layer. In addition, due to slight differences in lighting, one can see indications of the waves on the liquid surface that were observed before (Ref. 6). This is particularly evident below the front of the main jet in Fig. 12a.

While the photographs are interesting and show many features of the flow, they do not reliably provide evidence of combustion. For example, Figs. 13a and 13b show kerosene injection at an air temperature of 1500°F and 1600°F. These were taken at a slightly different optical path and had a higher magnification. Note the difference in the "brightness" of the liquid layer in each case. The brighter, Fig. 13b, appears to indicate combustion, but it is not possible to be certain on this basis alone.

B. Infrared, Top-View Photographs

As mentioned before, the Thermographic camera produces isotherms graduated into ten color images on a television screen. The screen was photographed with Polaroid color sheet film to produce the photographs shown in Figs. 14, 15 and 16.* In these photographs, the flow is from left to right, with the oblong image in the center being the nozzle exit. The main jet produces the jagged protrusion to the right of the nozzle exit. The liquid layer is the multi-banded region bulging inward toward the left. These photographs can best be understood by referring back to Figs. 10, 11 and 12, as the optical path was similar. Also in the photographs, the color black is the coolest with the temperature increasing up the scale to white, the hottest.

* These figures are in color in the official library copy of McVey's Thesis at VPI&SU. They are reproduced here in B&W because of cost.

All three of these photographs indicate the cooling effect of the liquid injection. The wall is coolest in the vicinity where the liquid layer is located, then increases in temperature as one moves upstream (to the left in the photographs). The difference in area covered by the color white (hottest) from Figs. 14, 15 and 16 is due to the increasing wall temperature, T_w, as one goes from Fig. 14 to Figs. 15 and 16.

These results were obtained using the Thermographic camera outside of its normal calibration range for direct temperature measurements. Also, the emissivity for the nozzle wall and the liquid layer are difficult to model accurately. In addition, the "shape factor" for the surfaces involved is difficult to obtain. All of these effects combine to make it difficult to use these photographs to accurately determine temperature levels in the flow field. Nonetheless, this method can be used to quantitatively observe the flow. That is, if combustion should occur, the region around the liquid surface layer should appear white, thus showing a definite change in the pattern. This was not observed, only the same repeating cooling pattern with uniform changes, if any.

C. Wall Temperature Measurements

The wall temperature was measured by two thermocouples; one under the liquid layer and one well away from this layer. The direct, top-view photographs, discussed earlier, were used to ensure that one of the thermocouples was covered by the liquid on the surface. One would expect a difference between the two thermocouples due to the cooling effect of the liquid layer or the heat released due to the combustion of this liquid layer. Indeed, this was observed.

Figures 17, 18 and 19 show one way in which this data can be viewed, as T_w and T_w' are compared for water, carbon disulfide and kerosene injections, respectively. The first and most obvious observation is that there is a great deal of cooling that occurs in the area of the injectant. For example, in the case of water injection with a wall temperature of 600°F, the wall temperature beneath the liquid layer was 160°F. This type of reduction in temperature occurs for all three injectants.

The second observation would be that the wall temperature is not reduced as much for the two fuels as it is for water injection. At first, one would be tempted to state that the liquid layer was burning, but further observation shows that, in fact, a good majority of tne carbon disulfide data lie in the same range as the water data. Only the kerosene data is consistently higher. Possible explanations for this are the differences in specific heats and thermal conductivities, which would produce different rates of heat transfer.

A third observation can be noted from these plots. For the two fuels, there is a discontinuity in the data when T_w is near 700°F. This sudden rise in wall temperature under the liquid layer seems to be totally confined to data taken while the gas-fired combustor was in use (allowing for some scatter). One could speculate that unburned fuel from the gas-fired combustor was burning behind the shock-wave generated by the presence of the liquid jet, thus increasing the wall temperature and accounting for the jump when the combustor is used. The water data, however, appears to lie about one line with no sudden changes. This tends to nullify that explanation. Another explanation could be that there is actual burning taking place in the liquid layer. Since there was some overlap region

on the data, it was possible to compare two cases with nearly the same T_w but with a T_w' that differed by as much as 75°F. This comparison showed absolutely no change in the pattern of cooling as depicted by the thermographic photographs. Thus this explanation tends to fade. Therefore, this phenomenon goes unexplained at present and it needs further study.

Although these results are interesting, independently they do not indicate combustion occurring in the liquid layer. They do indicate the cooling effect mass injection has upon the heated surface.

It should be noted that in some cases T_w' was almost double the minimum ignition temperature for carbon disulfide and equal to that for kerosene. Therefore, it is evident that the methods used to determine these ignition temperatures (as in Ref. 12) are not applicable to this situation.

D. Temperature Probing

Tests were also conducted in which an exploratory study with a small (0.010 in. diameter) sheathed thermocouple held just above the liquid surface layer to the side of the main jet was made. These tests were conducted using carbon disulfide and water as injectants. In one of the tests, these probes indicated a large temperature difference between the carbon disulfide and water injections at the same nominal conditions; carbon disulfide produced the higher temperature. Again, this would might indicate ignition, however, severe problems with frequent thermocouple burn-up were encountered. In addition, single point probing is tedious and difficult. Further tests of this type are planned.

V. CONCLUSIONS

Liquid fuel jet injection into a hot, supersonic air stream was studied for three different liquids: kerosene, carbon disulfide and water as a non-burning control case. The flow field was analyzed by means of nozzle wall temperature measurements, direct, top-view photographs, infrared, top-view photographs (utilizing a Thermographic camera) and temperature probing of the area above the liquid surface layer. Of these methods of viewing the flow field, there were cases from all that seemed to give indications of combustion on the liquid surface area, except the infrared photographs. These cases were random and none of the conditions overlapped from one method of observation to the other. Therefore, on an individual basis, it was difficult to unequivocally state that combustion did occur.

Wall temperature measurements, infrared photographs and temperature probing seem to be the most effective methods in terms of observing combustion in the flow field. The direct photographs would probably be useful, once combustion was detected, by using no flash and exposing the film with the light generated as a result of the combustion.

These tests were made over a wide range of air temperatures and wall temperatures but did not completely utilize the capabilities of the facility. Thus, suggestions for further testing would be:

1. Investigate the discontinuous jumps in the T_w' vs T_w plots for kerosene and carbon disulfide.

2. Investigate the effects of decreasing or increasing $\dot{m}_j$.

3. Investigate the effects of heating the liquid injectant to various temperatures.

4. Conduct additional temperature probing tests using a temperature rake to eliminate the aggravating point by point probing.

VI. REFERENCES

1. Schetz, J. A., Gilreath, H. E., and Lubard, S. C., "Fuel Injection and Mixing in Supersonic Flow," 12th International Symposium on Combustion, Poitiers, France, July 1968.

2. Lubard, S. C. and Schetz, J. A., "Atomization and Vaporization of a Liquid Sheet Exposed to a Supersonic Airstream," AIAA Propulsion Specialist Meeting, Paper No. 68-643, Cleveland, Ohio, June 1968.

3. Schetz, J. A., Kush, E. A., Jr., and van Overeem, J., "High Speed Photographic Study of Liquid Jet Breakup," 9th International Congress on High Speed Photography, August 1970.

4. Sherman, A. and Schetz, J. A., "The Break-up of Liquid Sheets and Jets in a Supersonic Gas Stream," AIAA Journal, Vol. 9, No. 4, April 1971.

5. Kush, E. A., Jr. and Schetz, J. A., "Liquid Jet Injection into a Supersonic Flow," AIAA Journal, Vol. 11, No. 9, September 1973.

6. Joshi, P. B. and Schetz, J. A., "Effect of Injector Geometry on the Structure of a Liquid Jet Injected Normal to a Supersonic Airstream," AIAA/SAE, 10th Propulsion Conference, AIAA Paper No. 74-1156, October 1974.

7. Dowdy, M. W. and Newton, J. F., "Investigation of Liquid and Gaseous Secondary Injection Phenomena on a Flat Plate with M = 2.01 to M = 4.54," Jet Propulsion Lab., TR 32-542, 1963.

8. Kolpin, M., Horn, K., and Reichenbach, R., "Study of Penetration of a Liquid Injectant into a Supersonic Flow," AIAA Journal, Vol. 6, No. 5, May 1968.

9. Yates, C. L. and Rice, J. L., "Liquid Jet Penetration," Research and Development Programs Quarterly Report, U-RQR/69-2, Applied Physics Lab., Johns Hopkins University, 1969.

10. Reichenbach, R. E. and Horn, K. P., "Investigation of Injectant Properties on Jet Penetration in a Supersonic Stream," AIAA Journal, Vol. 9, No. 3, March 1971.

11. Weiss, M. A. and Worsham, C. H., "Atomization in High Velocity Air Streams," ARS Journal, Vol. 29, No. 4, April 1959.

12. Scott, G. S., Jones, G. W., and Scott, F. E., "Determination of Ignition Temperatures of Combustible Liquids and Gases," Analytical Chemistry, Vol. 20, No. 3, March 1948.

13. McVey, W. J. and Scheitz, C. A. "Flowfield Near Liquid Fuel Jets Injected Transverse to a Hot Supersonic Air Stream," AIAA/SAE 11th Propulsion Conference. AIAA Paper No. 75-1230, September 1975.

Table 1. Typical Temperature Measurements at Exit of Gas-Fired Combustor

Station No.	1	2	3	4
Distance From Wall (in.)	1	0.75	0.50	0.25

Test No.	Temperature in °F at Station			
	1	2	3	4
38	1673	1673	1673	1609
43	1727	1727	1712	1640
60	1834	1834	1811	1731
63	1845	1845	1834	1749
61	1852	1842	1834	1760
70	1868	1868	1861	1786
58	1877	1877	1863	1784
66	1891	1891	1881	1799
65	1912	1912	1903	1822
74	1938	1938	1931	1836
68	1949	1949	1933	1857
75	1966	1966	1958	1880
87	1978	1978	1952	1866
77	1984	1984	1973	1891
71	1996	1996	1991	1914
86	2013	2013	1996	1924
91	2027	2027	1978	1926
90	2039	2039	2010	1942
85	2050	2050	2043	1952
94	2091	2091	2068	1992
96	2122	2122	2122	2022
95	2134	2134	2134	2006

Table 2. Test Conditions Investigated

Test No.	Average T_o in Settling Chamber, °F	T_w, °F	T_w', °F	Injectant		
				Kerosene	CS_2	H_2O
1	580	290	130			X
2	590	255	110			X
3	720	300	125			X
4	775	315	125			X
5	780	320	145			X
6	800	310	140			X
7	855	390	130			X
8	1015	445	150			X
9	1075	480	250	X		
10	1110	490	135		X	
11	1160	480	155			X
12	1210	470	145			X
13	1220	530	155			X
14	1245	550	195			X
15	1250	525	290	X		
16	1270	405	145			X
17	1275	500	160		X	
18	1275	535	160		X	
19	1280	490	150		X	
20	1290	450	145			X
21	1310	520	155			X
22	1320	505	135		X	
23	1335	545	155			X
24	1370	520	150			X
25	1390	455	280	X		
26	1400	610	180		X	
27	1400	590	300	X		
28	1410	510	160		X	
29	1425	535	160		X	
30	1425	655	205			X
31	1455	590	320	X		
32	1465	525	205			X
33	1480	520	155			X
34	1485	570	315	X		
35	1490	535	160		X	
36	1500	525	160		X	
37	1500	710	215		X	
*38	1510	715	180			X
39	1535	710	345	X		
40	1545	555	170		X	
41	1545	700	225		X	
42	1550	530	160			X
*43	1560	625	175			X

Table 2. Continued

Test No.	Average T_o in Settling Chamber, °F	T_w, °F	T_w', °F	Injectant		
				Kerosene	CS_2	H_2O
44	1560	710	205		X	
45	1560	685	345	X		
46	1565	665	340	X		
47	1570	555	160		X	
48	1575	620	205		X	
49	1585	645	330	X		
50	1585	665	170		X	
51	1610	605	160			X
52	1610	605	170		X	
53	1620	585	175		X	
54	1620	700	200		X	
55	1630	590	180		X	
56	1630	610	165		X	
57	1640	630	195		X	
*58	1640	655	205		X	
59	1645	600	180		X	
*60	1655	645	250		X	
*61	1665	715	290		X	
*62	1695	730	320		X	
*63	1695	675	390	X		
*64	1700	710	220		X	
*65	1710	735	360		X	
*66	1725	655	220		X	
*67	1735	780	400	X		
*68	1740	730	310		X	
*69	1740	790	320		X	
*70	1745	790	430	X		
*71	1750	805	410		X	
*72	1765	830	225			X
*73	1770	695	185			X
*74	1770	680	400	X		
*75	1790	795	235			X
*76	1790	720	260		X	
*77	1790	720	310		X	
*78	1800	705	215			X
*79	1805	745	425	X		
*80	1810	700	250		X	
*81	1820	750	365		X	
*82	1820	820	450	X		
*83	1820	800	430	X		
*84	1825	740	270		X	
*85	1830	700	335		X	
*86	1840	710	340		X	
*87	1845	700	425	X		

Table 2. Continued

Test No.	Average T_o in Settling Chamber, °F	T_w, °F	T_w', °F	Injectant		
				Kerosene	CS_2	H_2O
*88	1850	775	440	X		
*89	1860	840	450	X		
*90	1865	795	455	X		
*91	1915	840	460	X		
*92	1925	900	480	X		
*93	1925	845	480		X	
*94	1935	785	470	X		
*95	1960	785	400		X	
*96	1965	840	480	X		

*Indicates gas-fired combustor used.

Table 3. Typical Temperature Measurements for Water Injection Tests, $\dot{m}_j$ = 0.026 lb/sec

Test No.	Centerline Temperature at Exit of Combustor, °F	Average T_o in Settling Chamber, °F	T_w, °F	T_w', °F
1	--	580	290	130
4	--	775	315	125
7	--	855	390	130
8	--	1015	445	150
11	--	1160	480	155
13	--	1220	530	155
20	--	1290	450	145
23	--	1335	545	155
30	--	1425	655	205
32	--	1465	525	205
38	1675	1510	715	180
42	--	1550	530	160
43	1730	1560	625	175
51	--	1610	605	160
72	1920	1765	830	225
73	1900	1770	695	185
75	1965	1790	795	235
78	1950	1800	705	215

Table 4. Typical Temperature Measurements for Carbon Disulfide Injection Tests, $\dot{m}_j$ = 0.026 lb/sec

Test No.	Centerline Temperature at Exit of Combustor, °F	Average T_o in Settling Chamber, °F	T_w, °F	T'_w, °F
10	--	1110	490	135
18	--	1275	535	160
22	--	1320	505	135
26	--	1400	610	180
35	--	1490	535	160
37	--	1500	710	215
41	--	1545	700	225
47	--	1570	555	160
50	--	1585	665	170
55	--	1630	590	180
57	--	1640	630	195
58	1880	1640	655	205
59	--	1645	600	180
60	1835	1655	645	250
63	1950	1695	730	320
66	1890	1725	655	220
69	1960	1740	790	320
71	1995	1750	805	410
77	1985	1790	720	310
81	2045	1820	750	365
85	2050	1830	700	335
86	2015	1840	710	340
93	2095	1925	845	480
95	2135	1960	785	400

Table 5. Typical Temperature Measurements for Kerosene Injection Tests, $\dot{m}_j$ = 0.026 lb/sec

Test No.	Centerline Temperature at Exit of Combustor, °F	Average T_o in Settling Chamber, °F	T_w, °F	T'_w, °F
9	--	1075	480	250
15	--	1250	525	290
25	--	1390	455	280
27	--	1400	590	300
34	--	1485	570	315
39	--	1535	710	345
45	--	1560	685	345
49	--	1585	645	330
63	1845	1695	675	390
67	1900	1735	780	400
70	1870	1745	790	430
74	1940	1770	680	400
79	1970	1805	745	425
82	1995	1820	820	450
87	1980	1845	700	425
88	2010	1850	775	440
89	2010	1860	840	450
90	2040	1865	795	455
91	2030	1915	840	460
92	2125	1925	900	480
94	2090	1935	785	470
96	2120	1965	840	480

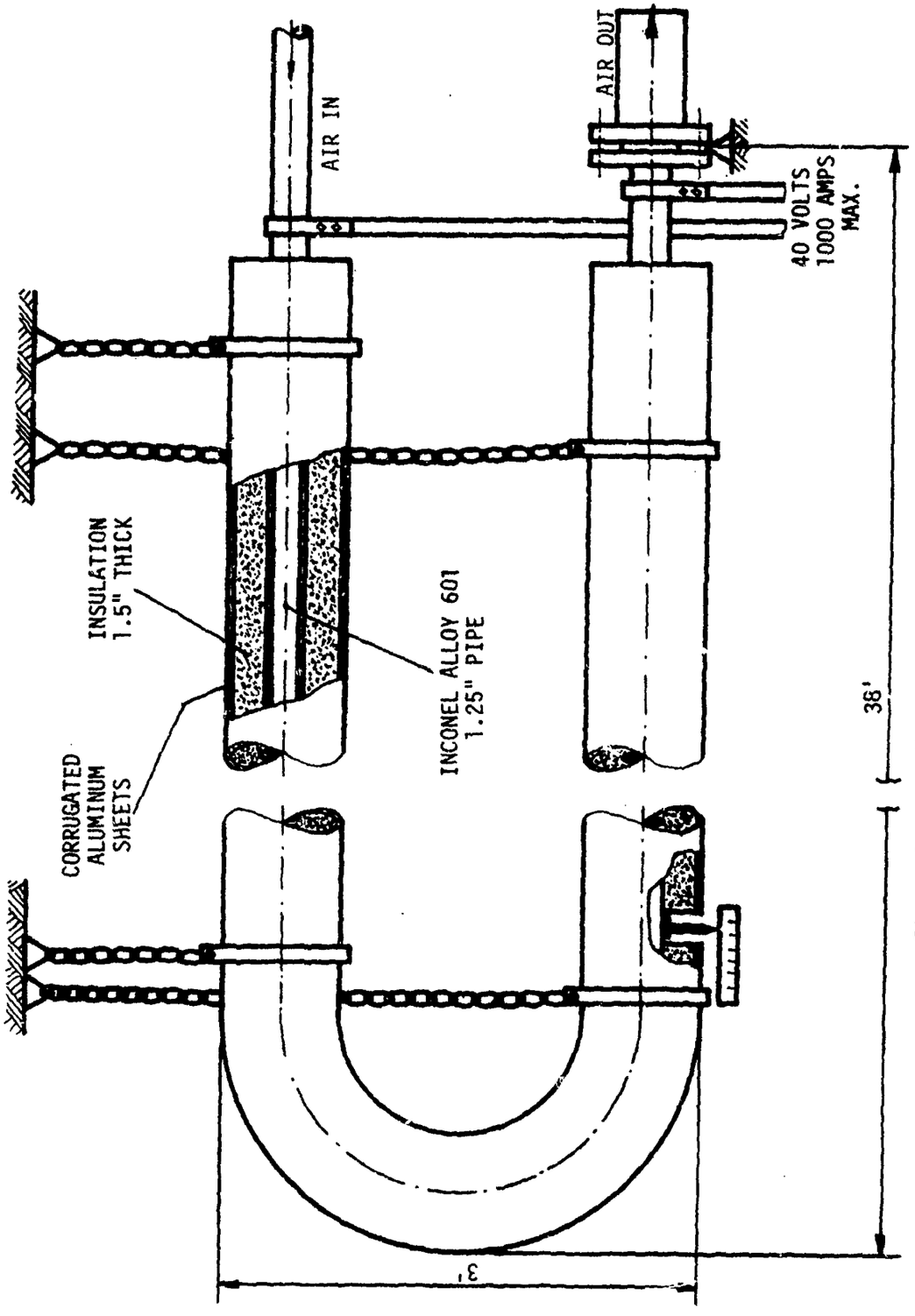

Figure 1: Details of the Heated Air Facility.

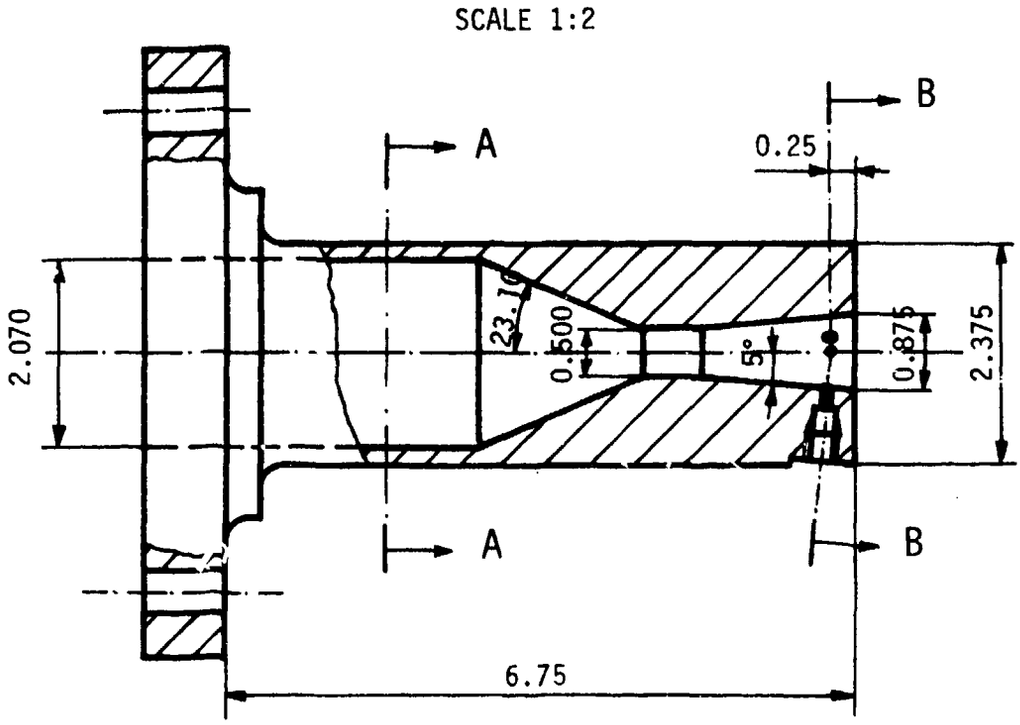

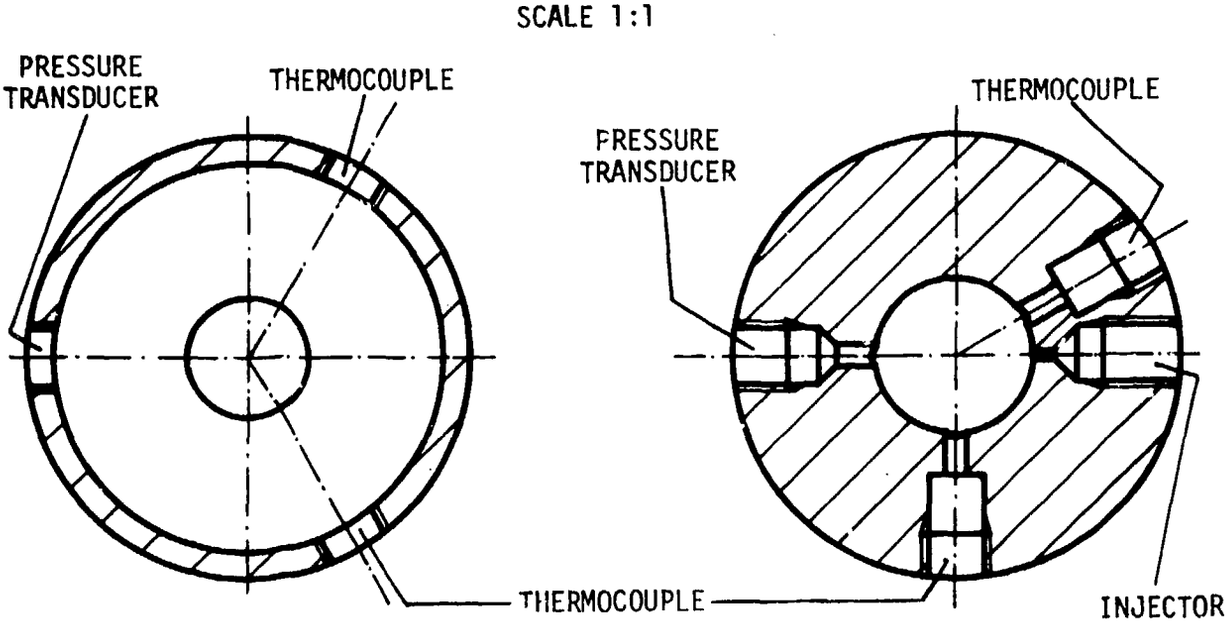

Figure 2: Test Nozzle

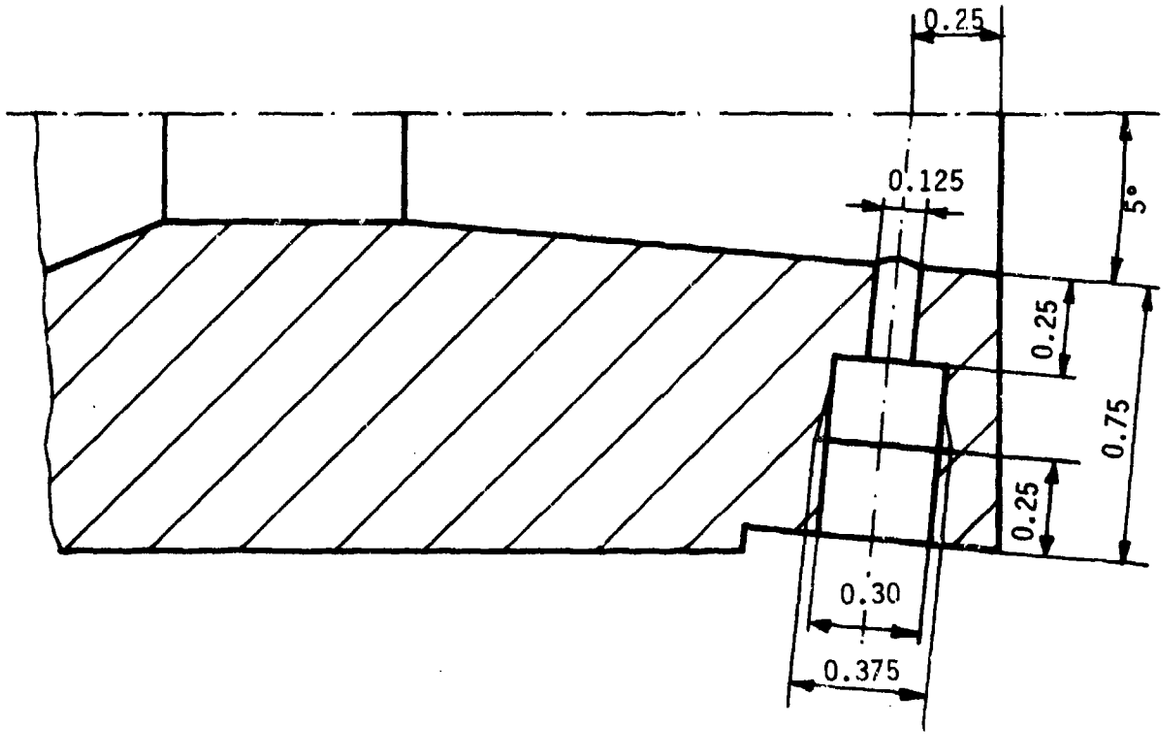

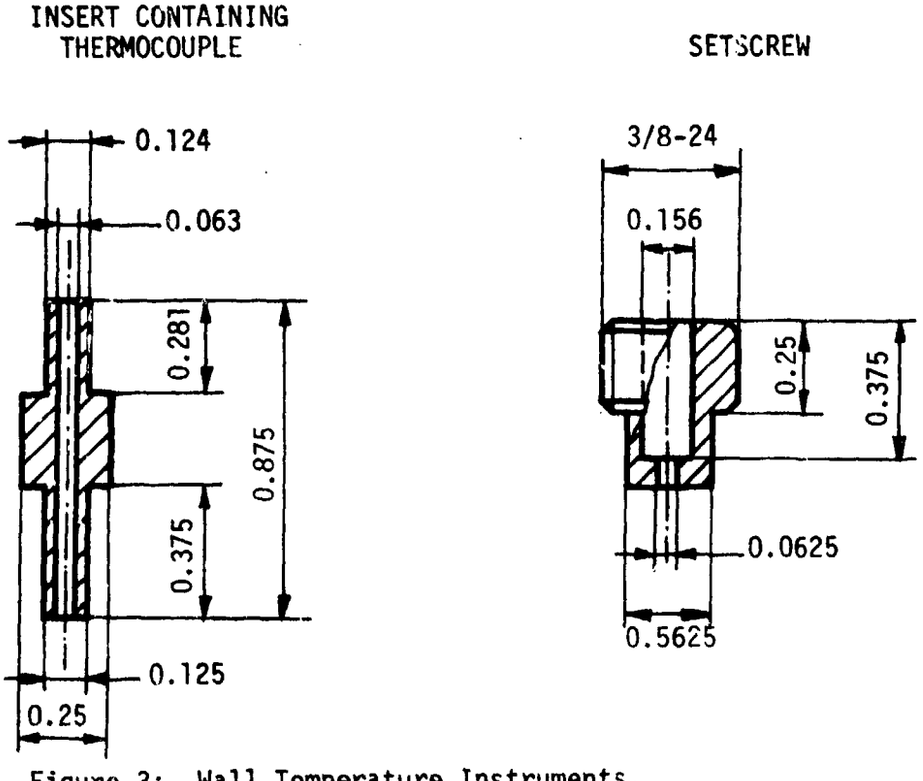

Figure 3: Wall Temperature Instruments.

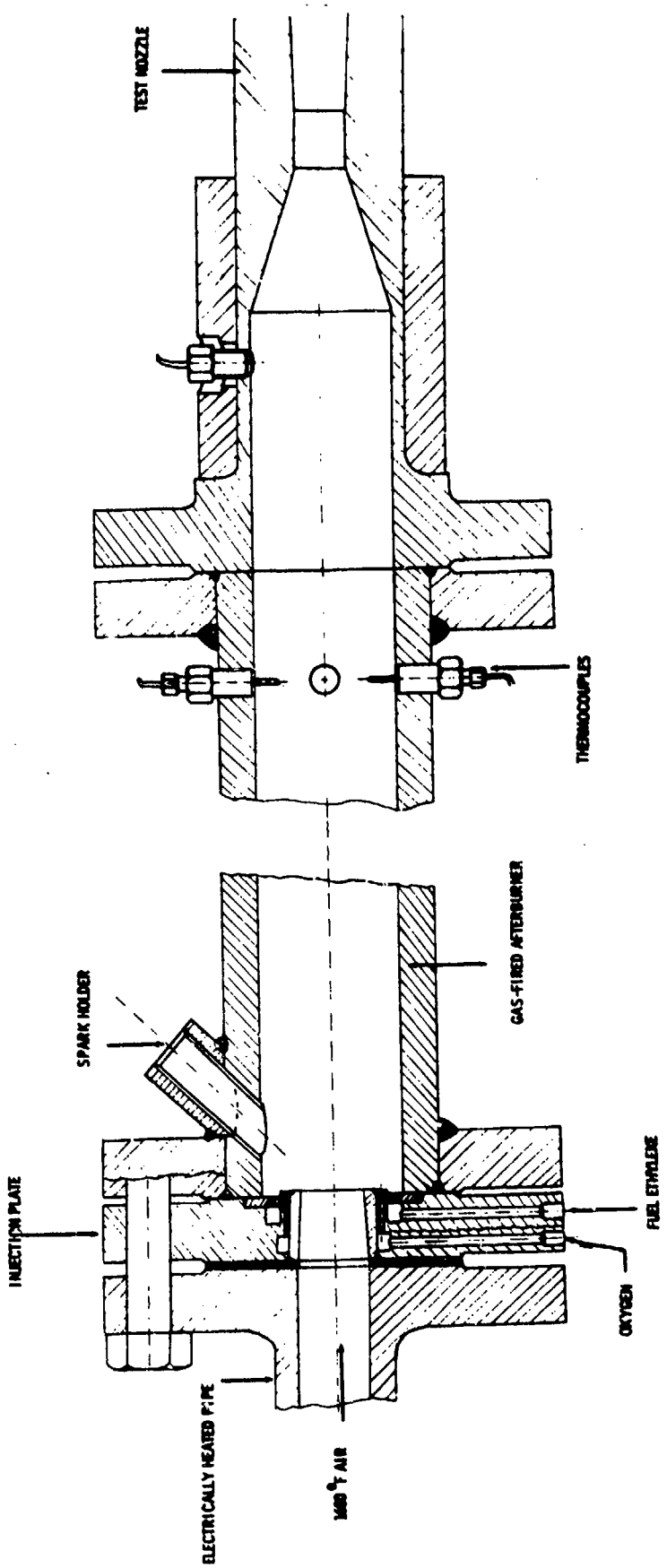

Figure 4: Cross-Section of Gas-Fired Afterburner.

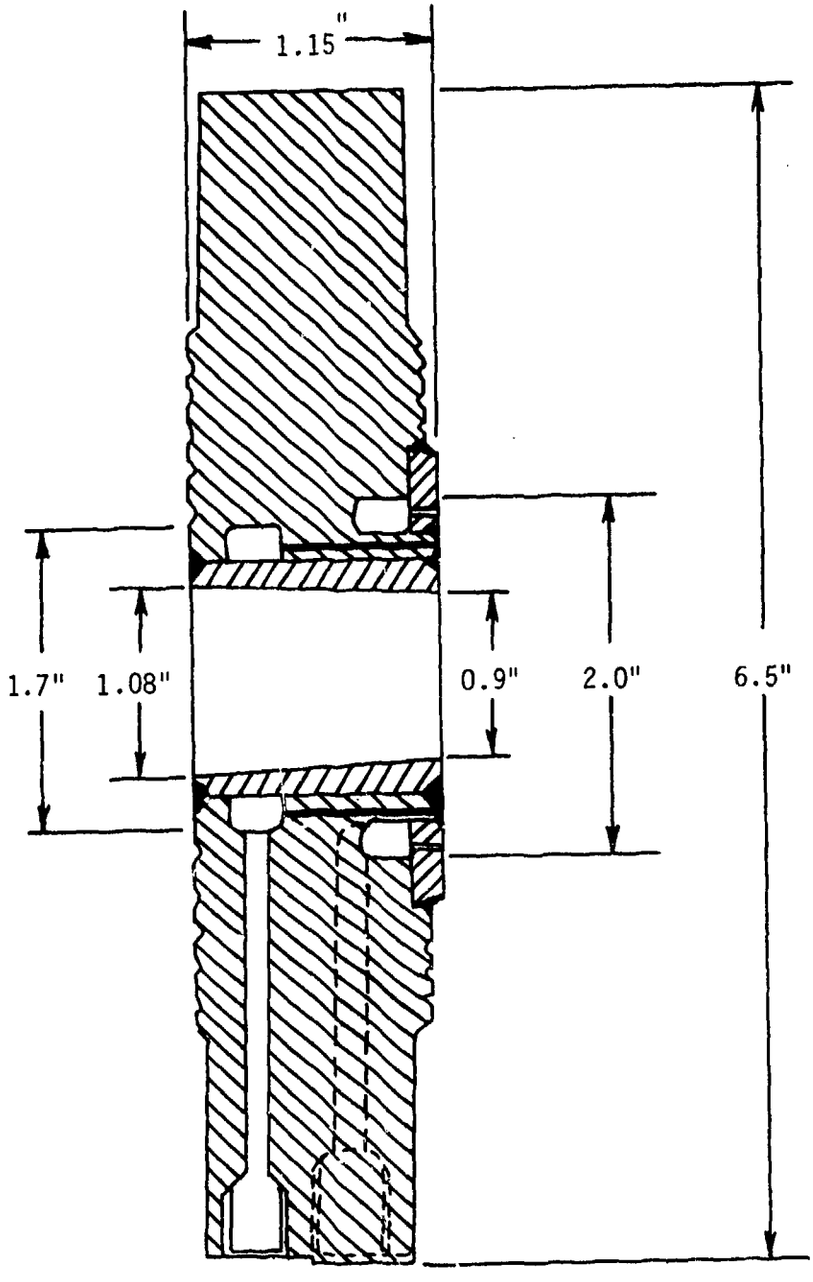

Figure 5: Cross-Section of Injection Plate for Gas-Fired Afterburner.

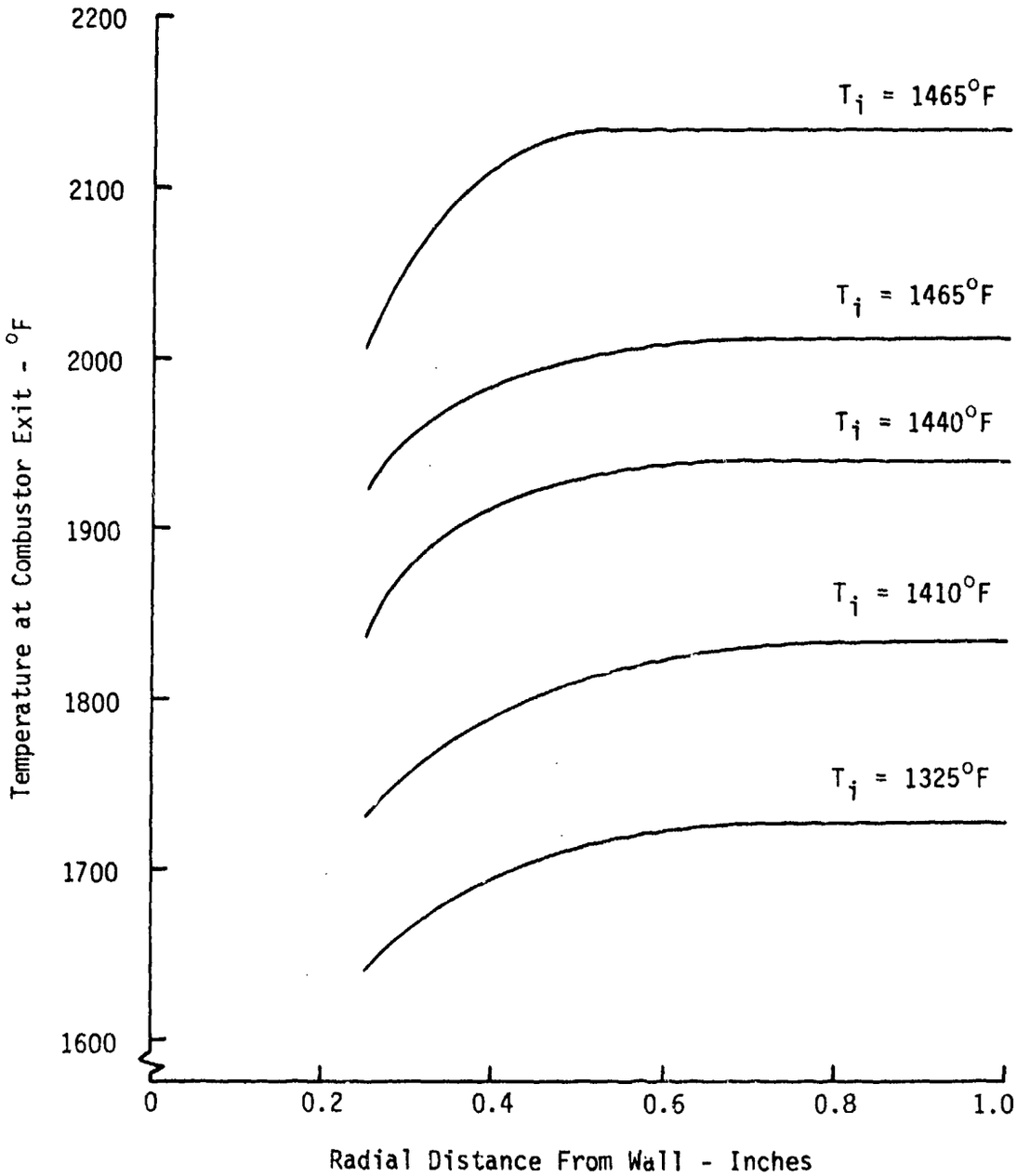

Figure 6: Radial Temperature Variation at Combustor Exit.

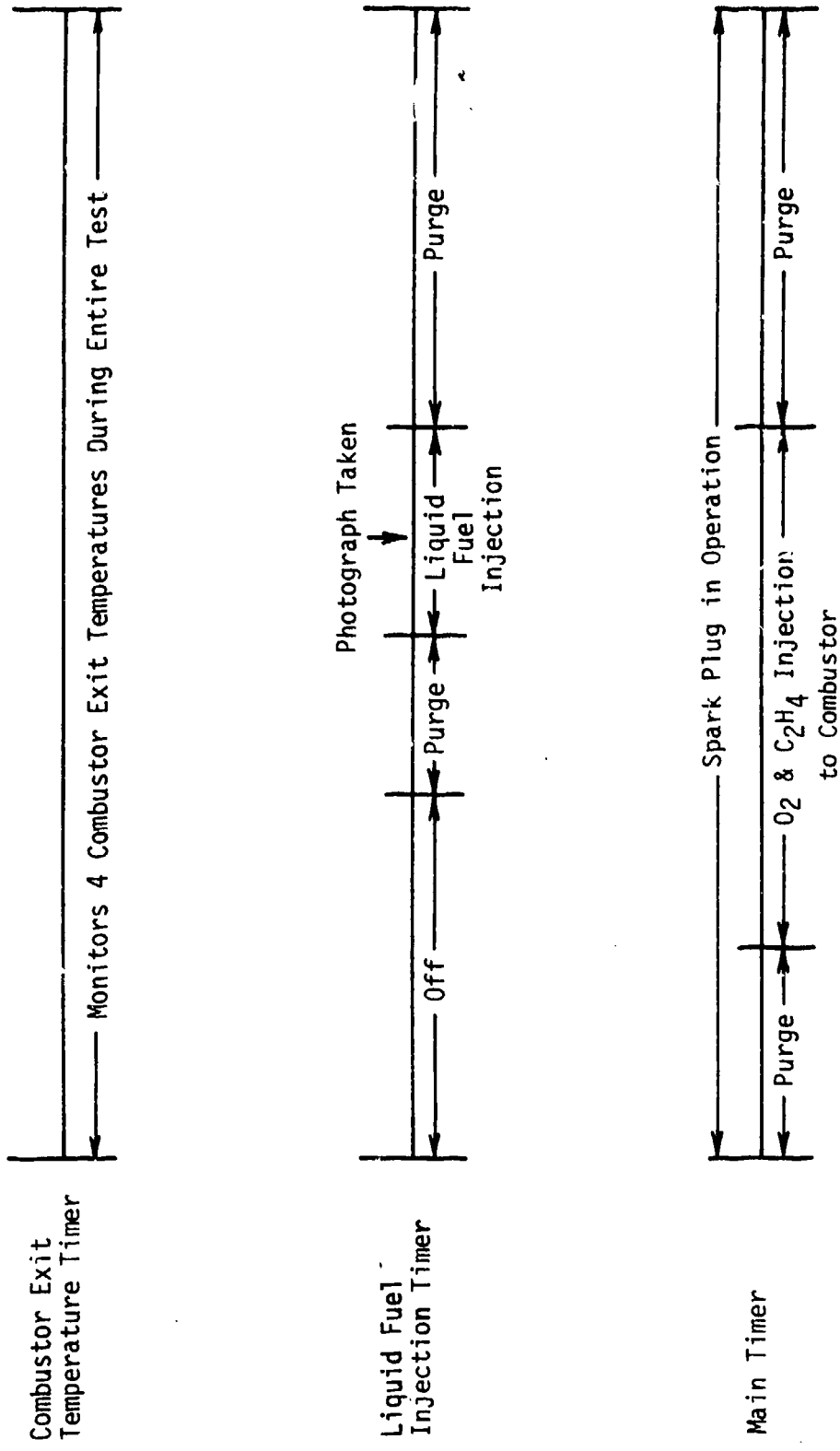

Figure 7: Schematic of Timer Sequences.

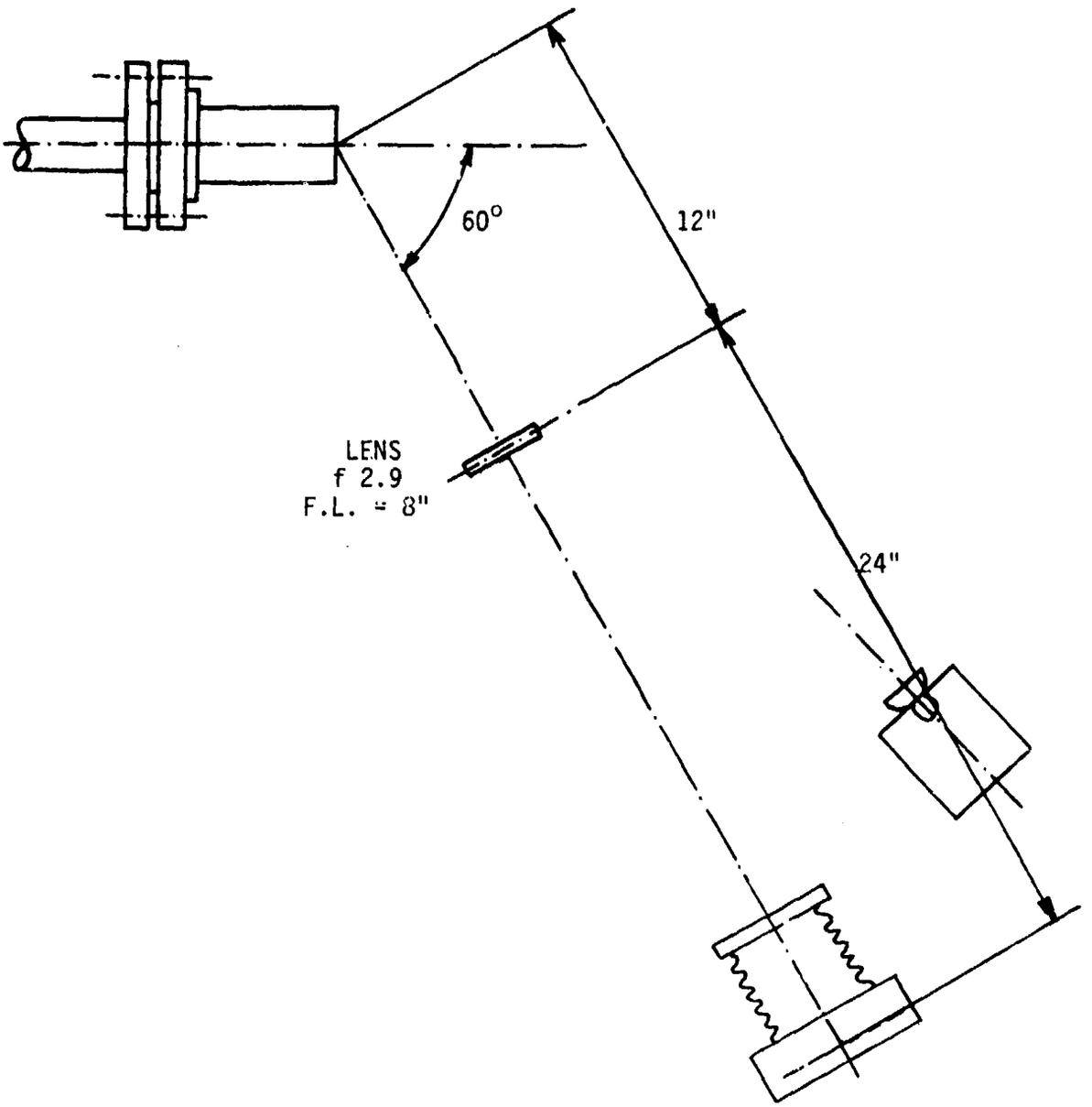

Figure 8: Optical Layout for Direct Photographs.

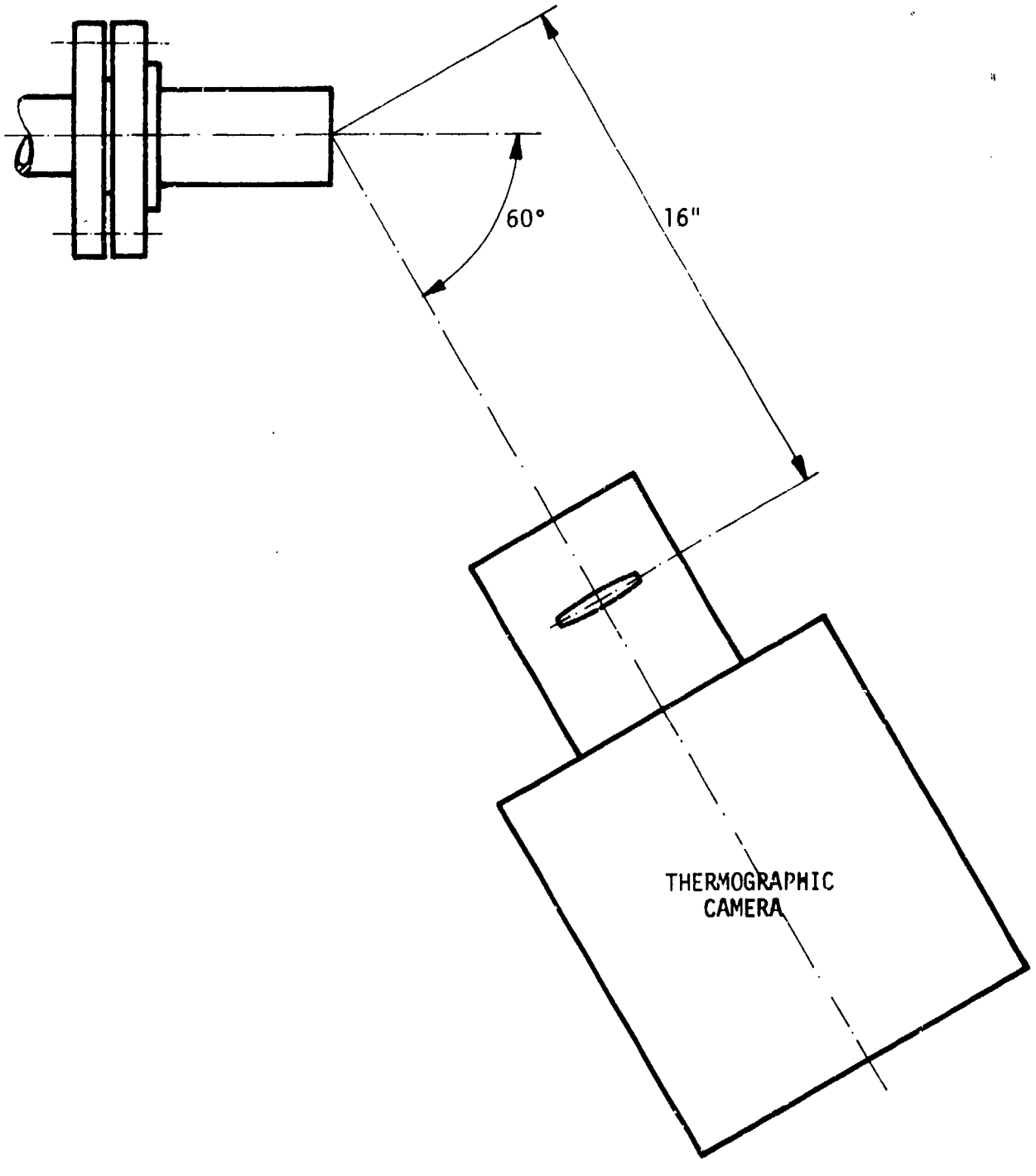

Figure 9: Optical Layout for Thermographic Photographs.

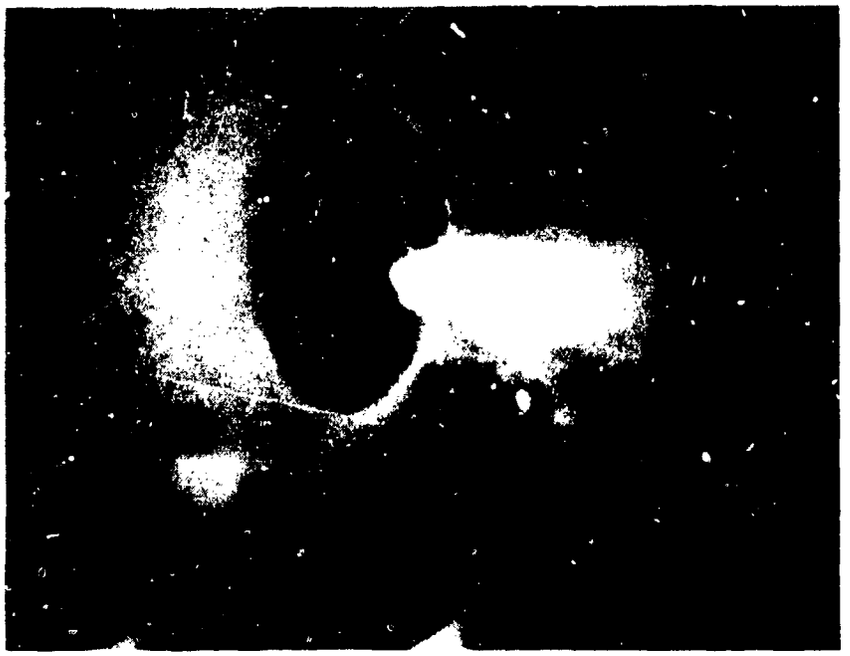

(a) T_o = 780°F, T_w = 320°F, T_w' = 145°F

(b) T_o = 1800°F, T_w = 700°F, T_w' = 215°F

Figure 10: Direct Photos of H_2O Injection, $\dot{m}_j$ = 0.026 lb/sec.

(a) T_o = 1400°F, T_w = 510°F, T_w' = 157°F

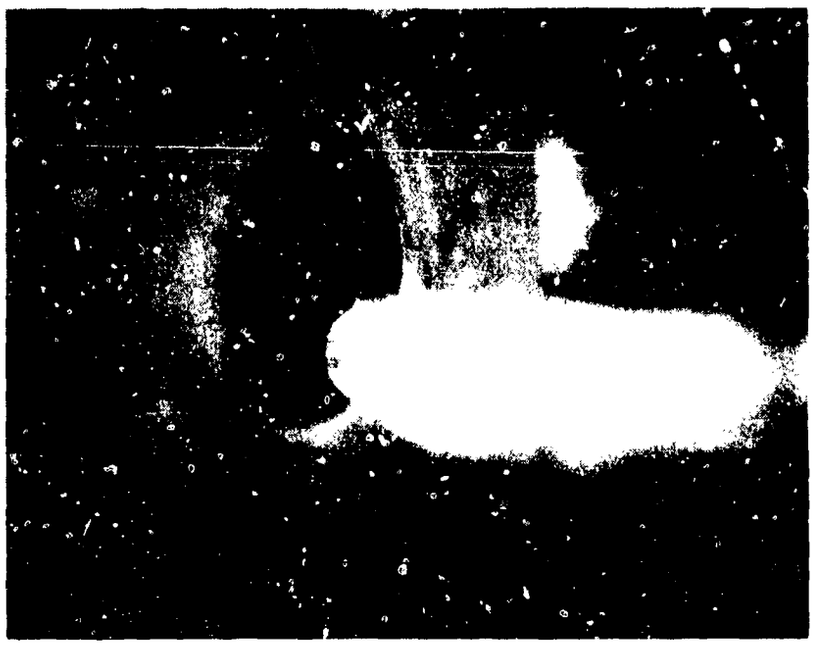

(b) T_o = 1800°F, T_w = 700°F, T_w' = 250°F

Figure 11: Direct Photos of CS_2 Injection, $\dot{m}_j$ = 0.026 lb/sec.

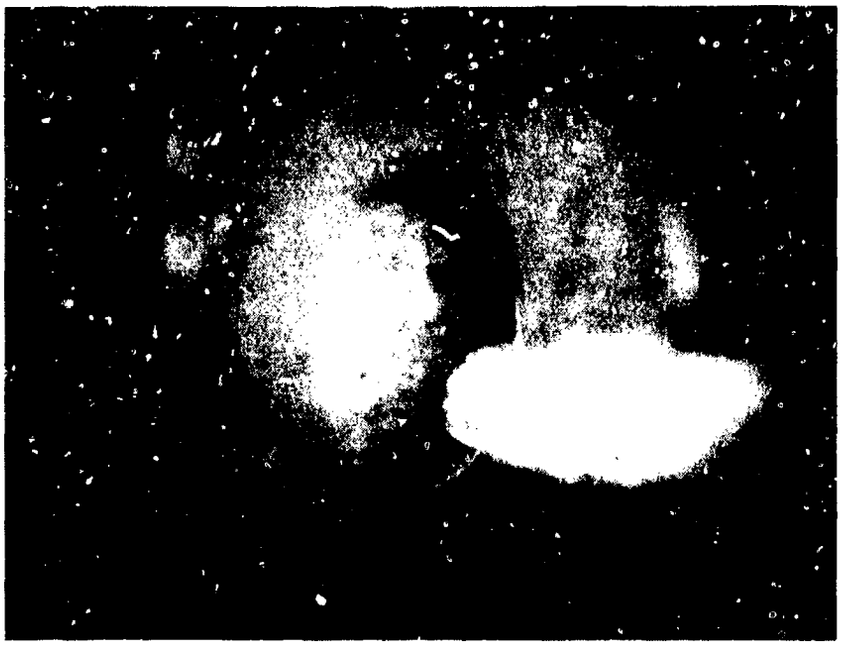

(a) T_o = 1750°F, T_w = 780°F, T_w' = 400°F

(b) T_o = 1950°F, T_w = 900°F, T_w' = 482°F

Figure 12: Direct Photos of Kerosene Injection, m_j = 0.026 lb/sec.

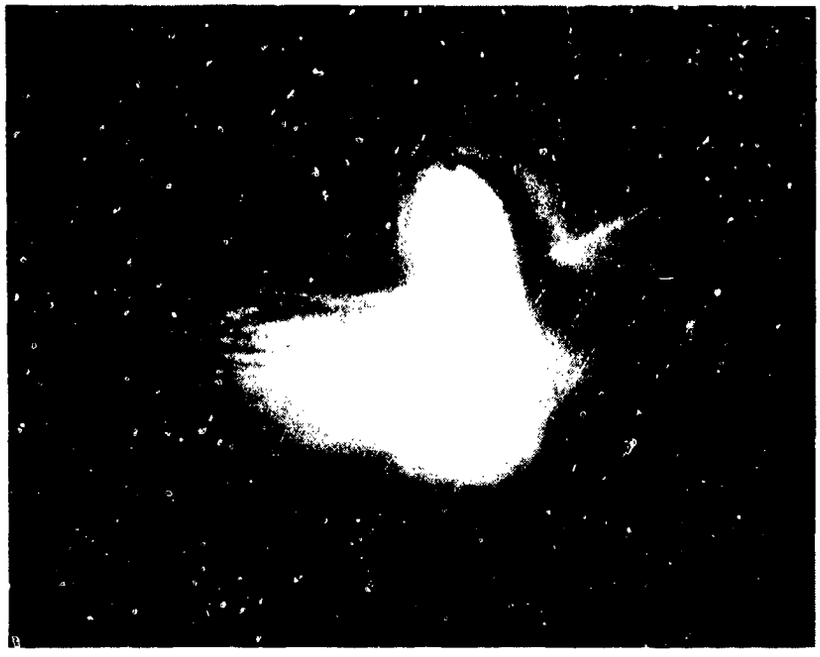

(a) T_o = 1500°F

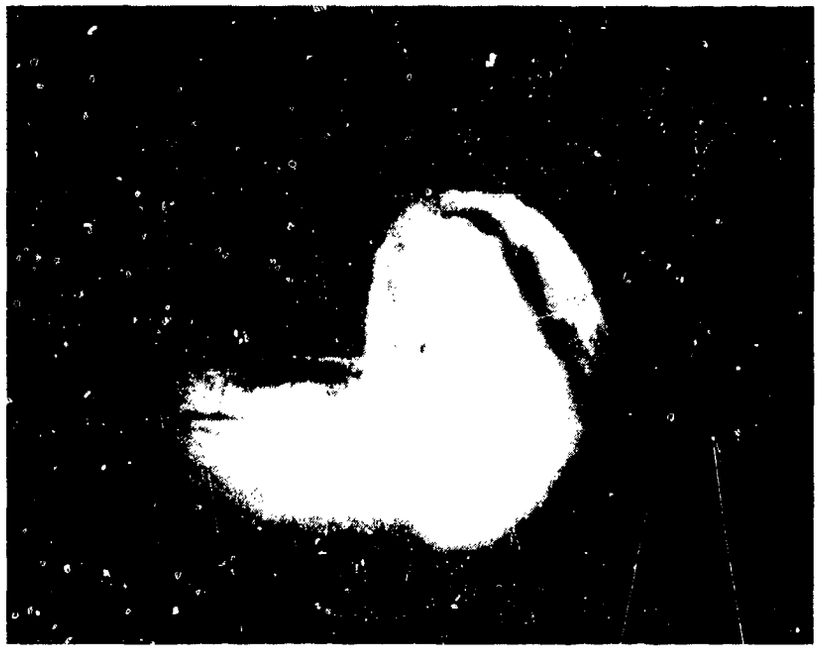

(b) T_o = 1600°F

Figure 13: Direct Photos of Kerosene Injection (Larger Magnification)

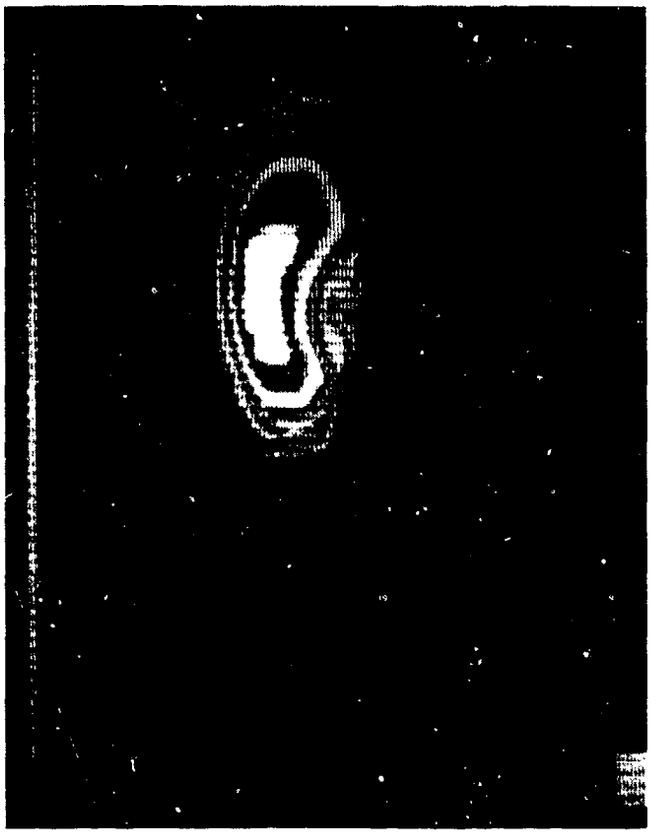

$T_o = 1500^{\circ}F$, $T_w = 655^{\circ}F$, $T_w' = 200^{\circ}F$

Figure 14: Photo of Thermographic Image, H_2O Injection.

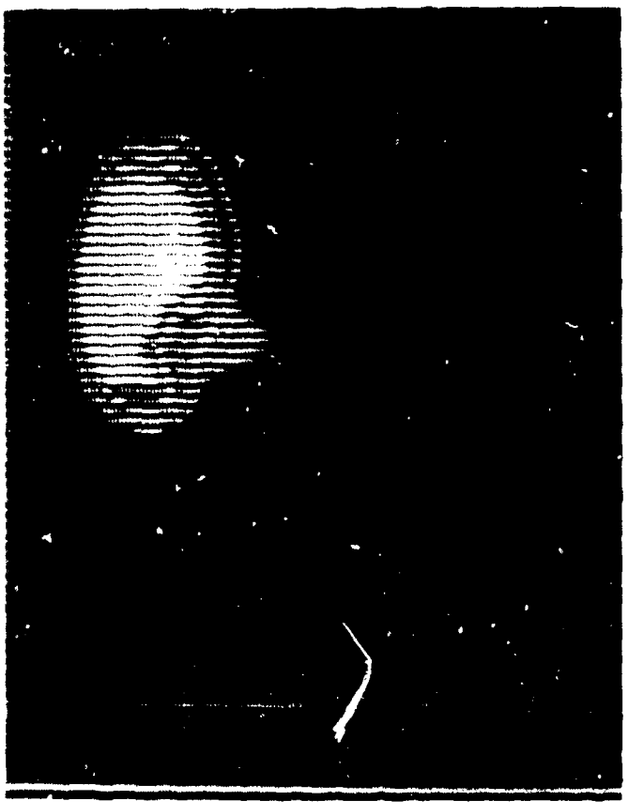

$T_o = 1950^oF$, $T_w = 780^oF$, $T_w' = 400^oF$

Figure 15: Photo of Thermographic Image, CS_2 Injection.

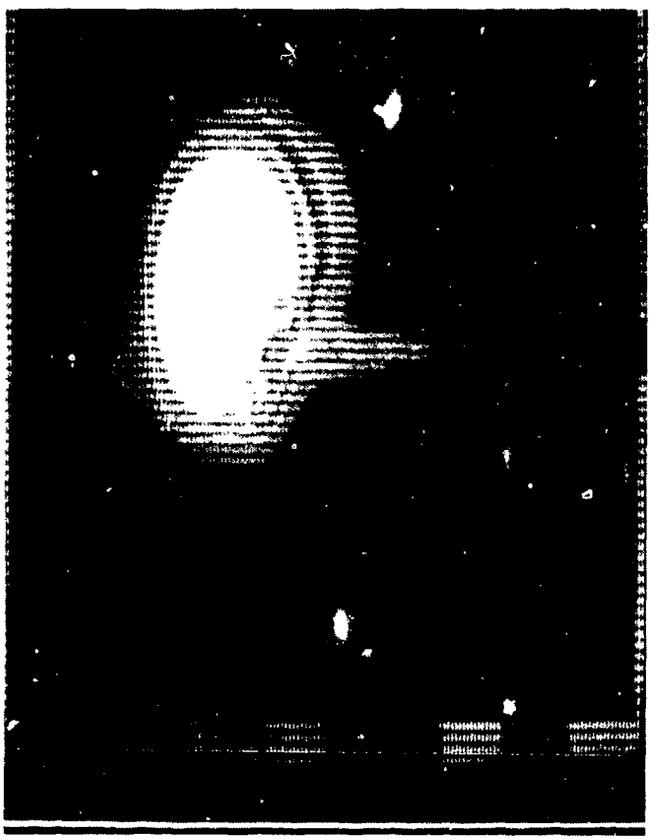

$T_o = 1950^oF$, $T_W = 840^oF$, $T_W' = 480^oF$

Figure 16: Photo of Thermographic Image, Kerosene Injection.

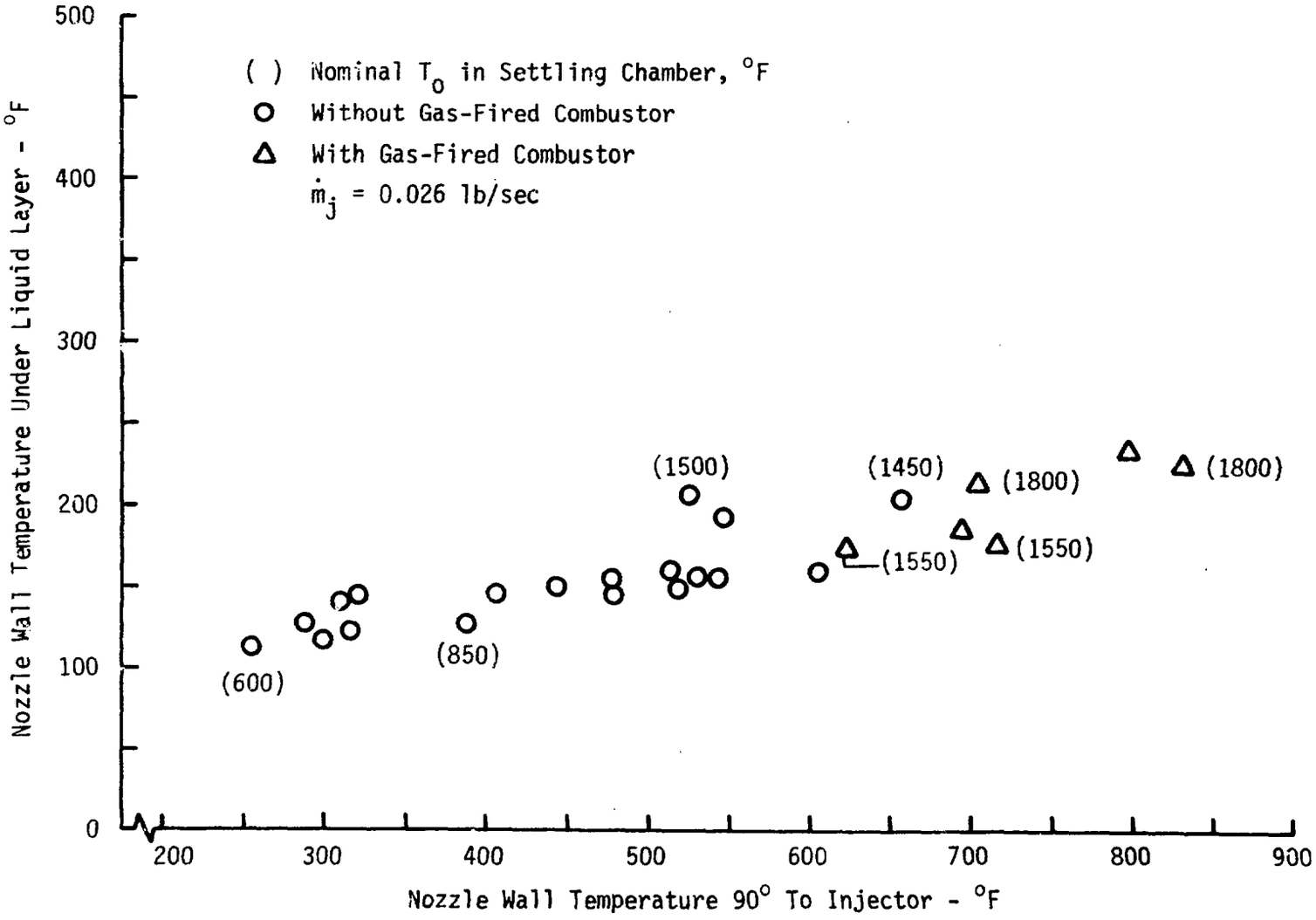

Figure 17: Wall Temperature Comparison, Water Injection.

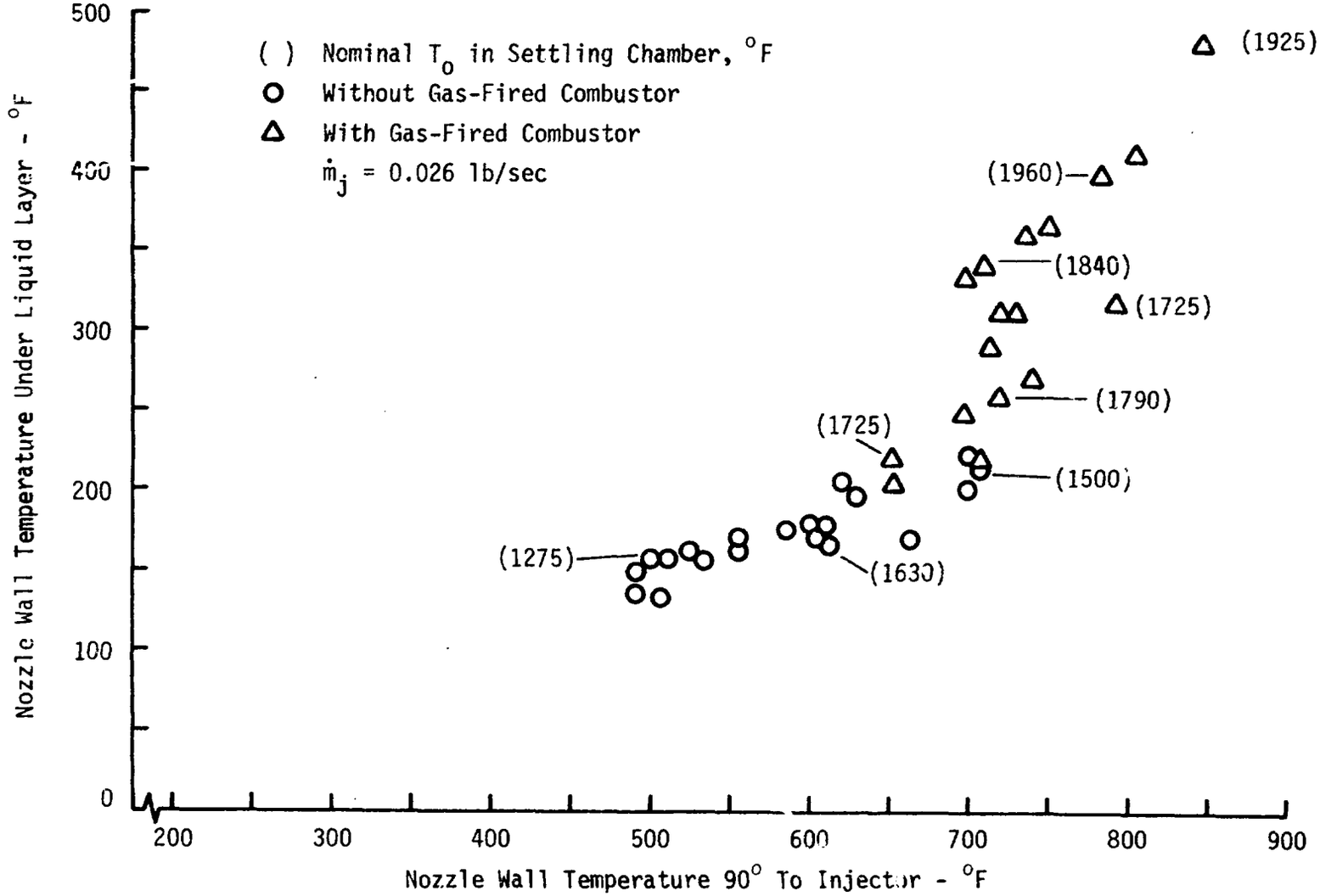

Figure 18: Wall Temperature Comparison, Carbon Disulfide Injection.

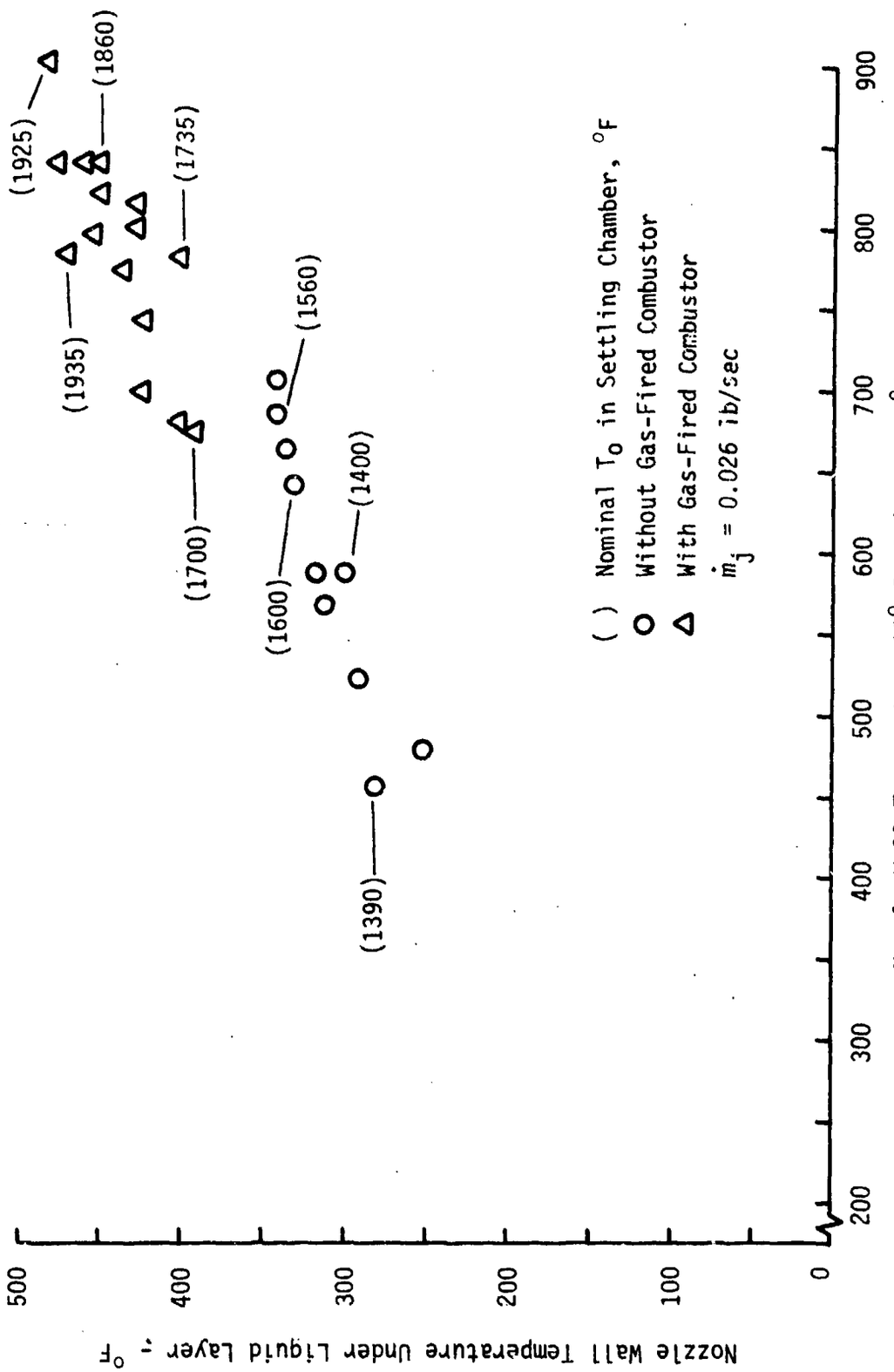

Figure 19: Wall Temperature Comparison, Kerosene Injection.

PART B: INJECTION INTO SUBSONIC AIRSTREAMS

I. BACKGROUND

1.1 Liquid Injection Into High Subsonic Air Streams and Applications

The problem of predicting the behavior of liquid jets injected normal to an airstream has attracted attention of many researchers due to its variety of applications. These include side force attitude control, thrust vector control, transpiration cooling of re-entry vehicles in order to provide local cooling in the region of communication antennae to alleviate the "black-out" period, and perhaps most important of all, injection and burning of liquid fuels in ramjet combustors and "dump" combustors. Even though the re-entry vehicle enters the earth's atmosphere at hypersonic speeds there is a region of subsonic speeds immediately behind the normal shock which is common for blunt re-entry bodies, and the coolant liquid may be injected in this region of the flow. In conventional ramjets, air is captured and decelerated to a subsonic velocity by an inlet diffuser, before fuel is added to the airstream. Such applications and others demand the study of liquid jets injected normal to a subsonic airstream.

The idea of supersonic combustion ramjets triggered the study of the behavior of liquid jets injected normal to the supersonic airstream, and much data is now available for this case; but, there is very little data available for a transverse liquid jet in a high subsonic or transonic airstream. Although supersonic combustion ramjets are potentially very attractive, conventional ramjets are still in use.

Like any other powerplant, the overall efficiency and the size of the ramjet depends upon the combustion efficiency and the size of the combustion chamber. The efficiency of the combustion process in the combustion chamber is controlled by efficient mixing of liquid fuel with air, which in turn depends upon the injector characteristics such as size, shape and orientation with respect to the free stream. The penetration of fuel jets in the airstream is one of the parameters which decides the combustor size. This too is influenced by the injector characteristics mentioned above. This shows that the role of injector geometry merits a detailed investigation.

Since phenomena like penetration, the existence of a liquid surface layer, jet structure and droplet size distribution seem to be important from a combustor design point of view; the study of effect of injector characteristics on the above parameters was the goal of the present investigation. In particular, penetration of the jet was given the major emphasis. The purpose behind this undertaking was to obtain experimental penetration and droplet size distribution data for engineering use and to investigate, if possible, theoretical correlations which incorporate the governing physical quantities.

1.2 Literature Review

As pointed out by Joshi and Schetz,[24] the literature on liquid injection into a high speed gas stream can be grouped into five categories.

(a) work related to droplet formation, droplet size and distribution, etc.

(b) work related to thrust vector control applications,

(c) work related to both supersonic combustion and thrust vector control,

(d) work directly related to supersonic combustion: Measurements and analytical predictions of liquid jets penetration, lateral spread, droplet size, etc.

(e) work related to combustion of liquid injected into supersonic air streams.

Here results related to the works of categories (a) and (d) will be presented. Results from the rest will be presented only if they are relevant to the present investigation.

Rothrock[1] was one of the pioneers to study liquid spray injected normal to a subsonic air stream. He concluded that injection counter to the air stream has more effect on spray dispersion than normal injection. Castleman[2] proposed a jet breakup model based on ligament shedding and concluded that atomization is a surface phenomena. Nukiyama and Tanasawa[3] in 1940 measured the droplet sizes and distribution experimentally. Briton[4] was one of the first to study experimentally the atomization of liquids by supersonic airjets. He verified the applicability of the empirical droplet size relations obtained by Nukiyama and Tanasawa. However, he wrongly concluded that the same mechanism applies to subsonic atomization, too. Ingebo and Foster[5] employed high speed camera and sampling techniques to study the drop-size distribution of liquid jets injected into a high velocity (subsonic) cross stream. They modified the results of Nukiyama and Tanasawa. Weiss and Worsham[6] performed excellent experimental work by injecting liquid wax into concurrent high velocity airstream. They concluded that relative velocity

between the liquid and the air stream is the most important factor controlling atomization and that physical properties of the injectant had less critical effect. Clark[7] measured the variation of jet diameter along its axis by using electrical resistance measurements. In his investigation, he interpreted the waves on the jet surface as due to considerable turbulence at the entry region of the injector. Adelberg[8] considered both capillary and the acceleration waves generated by a gas stream on the surface of a liquid jet. He estimated analytically the mean droplet size and obtained reasonably good agreement with experimental data by choosing appropriate constants in his analysis. Morell[9], Morell and Povinelli[10] studied liquid jet breakup by a transverse shock wave. Ranger and Nicholls[11] found that the spherical drop is deformed into an ellipsoid and the breakup is due to the shearing action exerted by high speed flow on the liquid surface.

Dowdy and Newton[12] were first to present penetration data for liquids. Forde, et. al.[13] obtained experimental data on penetration for water injected normal to a Mach 3 air stream for small diameter injectors at different angles of inclination. Adelberg[14] developed an analysis for liquid jet penetration into a gas stream of large dynamic pressure. Under these conditions, the waves generated on the windward surface of the jet grow and ligaments are shed from these waves. He derived equations for variation of jet diameter along its axis and also for the centre-line trajectory. These involve surface tension of the injectant and show dependence of jet penetration on surface tension. Kolpin, et. al.[15] developed empirical relationships connecting the ratio of penetration to injector diameter with the free stream Mach number,

ratio of injectant pressure to free stream static pressure and injectant vapor pressure. Catton, et. al.[16] studied experimentally liquid jet penetration into a hypersonic air stream. They developed equations to predict the penetration of a liquid jet at arbitrary angle of injection and dynamic pressure ratio. Horn and Reichenbach[17] developed a correlation for lateral spread of the jet including the effect of the free stream Mach number. Yates and Rice[18] correlated experimental data to connect the jet penetration with the jet to the free stream dynamic pressure ratio and the ratio of distance downstream of the injector to the injector diameter.

Sherman and Schetz[19] were the first to study the structure of liquid jets and sheets using photomicrographs and established that the breakup mechanism is characterized by a gross jet fracture at a wave trough. Moreover, they reported this process to be repetitive occurring at a certain frequency. Reichenbach and Horn[20] investigated the effect of injectant properties on liquid jet penetration into supersonic airstream. The work of Sherman[21] was extended by Kush and Schetz[22,23]. They performed extensive experiments to study the effect of various parameters such as free stream Mach number, free stream total pressure, injector diameter, injector shape and injectant properties on jet penetration and instantaneous jet structure. They also reported quantitative data on wavelengths, amplitudes and wavelengths, amplitudes and wave speed on the jet surface. Further, they noted that injector geometry has a significant effect on penetration and the presence of liquid surface layer around the jet due to interaction of three dimensional shock surface with the boundary layer. Joshi and Schetz[24] carried this work further to study the effect

of injector geometry on penetration, spread and structure of the liquid jet. They formulated semiempirical relation between penetration and dynamic pressure ratio. They also found the functional dependence of penetration on injector geometry characterized by the ratio of frontal dimension to the streamwise dimension. They reported that for given free stream conditions and for the given mass flow rate of the injectant the rectangular injector gave largest penetration as well as largest spread.

Newton and Spaid[25] reported that penetration affects the mixing of the injectant with the free stream. Schetz, et. al.[26] discussed the problem of tangential injection of gases, liquid injection through porous wall and transverse injection of gases through circular and rectangular orifices. They concluded that for gaseous injection, the penetration is not a very strong function of injector geometry. Edelman, et. al.[27] while experimenting on combustion of liquid hexane in a Mach 2 air stream measured penetration of the liquid jet and compared with the semi-analytical prediction of Ref. 14 and 15. The agreement between the two was good.

1.3 Outline of Present Work

The aim of the present work was to study the effect of:

1) Shape of the injector,
2) Size of the injector, and
3) Orientation of the injector with respect to the air stream

on the observable characteristics of the jet:

1) penetration,
2) structure of the jet column,

3) droplet size distribution, and

4) possible existence of liquid surface layer.

The motivation for the present investigation comes from the work of Kush and Schetz[22,23], Joshi and Schetz[24] who observed that a liquid jet injected normal to the supersonic airstream through a rectangular slot aligned with the free stream gives significantly higher penetration than through a circular hole of the same area.

Although most of the present study involved experimental work, a small theoretical investigation was carried out, also. In the experimental investigation gross (macroscopic) properties of the liquid jet (e. g. penetration) were studied through relatively long exposure wide view photographs of the jet (e. g. streak photographs). The 'microscopic' properties like structure of the jet and the droplet size distribution were studied using short exposure photomicrographs.

Any theoretical work could also be classified as 'macroscopic' and 'microscopic'. In 'microscopic' analysis, one may take into account details like breakup mechanism, whereas, in 'macroscopic' approach, one would consider the entire jet and the broken liquid particles to be enclosed in a control volume and apply simple physical laws to obtain an integral picture of jet. In the theoretical part of the present investigation, the major emphasis was on 'macroscopic' analysis, since it preserves the physics of the problem. This procedure is described in Chapter II. Given below is the brief outline of the experimental approach.

The effect of injector geometry was studied using circular and rectangular injectors. Effect of orientation was studied by placing the rectangular slot aligned with or transverse to the free stream. Each

injector and its orientation was studied in two different free stream Mach numbers for at least six different mass flow rates of the injectant. The injectant that was used in all the tests was water, because of its availability and easy handling. The penetration data was obtained using long exposure photographs, whereas, data about the structure of the jet and the droplet sizes was obtained using short exposure photomicrographs. The details of the experimental procedure are presented in Chapter III, and in Chapter IV results of the investigation are presented.

II. ANALYSIS FOR CORRELATION PARAMETERS

In the present work, a 'macroscopic' view of the theoretical analysis was emphasized. Gross aspects of the jet behavior such as penetration are given the main consideration. The details of the jet structure and unsteadiness are not considered. The jet and the clumps of the liquid broken from the jet are imagined to be enclosed in a control volume which presents an obstacle to the free stream. This approach neglects the effects of vaporization and hence, may not work well with high vapor pressure injectants. This simple analysis is expected to yield the functional dependence of penetration on injectant variables and the injector geometry.

The effects of mass flow rate, free stream Mach number and injection size and shape on the mean droplet size were investigated. Weiss and Worsham[6] had concluded that the relative velocity between the liquid and air stream is the most important factor controlling atomization and geometry had less critical effect. In their experiments, the liquid was injected into a concurrent airstream. This differs from the present work since here the injectant is introduced normal to the airstream. Due to this, there is no parameter like relative velocity between the liquid injected and the airstream. As the jet bends backwards in the direction of the airstream, it has velocity component in that direction and hence, will have a velocity relative to the airstream. This relative velocity will finally become zero as the jet attains free stream velocity. This can be varied by two methods. Firstly, by changing the mass flow rate, keeping the free stream Mach number constant and secondly, by keeping the mass flow rate constant while changing the free stream Mach number. The

effect of the injector geometry can be studied by using injectors of different sizes and shapes.

Penetration:

Fig. 1 shows the control volume used in the analysis of penetration. Since this is only a macroscopic view of the jet, the details of wave disturbances on the liquid surface are not considered. The face S of the Control volume is normal to the free stream direction and sufficiently downstream so that the liquid particles have attained free stream velocity.

The liquid jet being three dimensional, the drag force N acts perpendicular to the jet trajectory. The component of this normal to the free stream acts downward and dissipates the normal momentum of the jet. The net streamwise momentum of the jet is given by

$\mu_{s1} = 0$; at the injector orifice and

$\mu_{s2} = \dot{m}V_\infty$; at the face S of the control volume.

Hence, the rate of change of streamwise momentum of the jet for given free stream conditions

$$\frac{d}{dt}(mV_\infty) = \dot{m}V_\infty.$$

This should be equal to the streamwise component of the drag force N, which can be written as

$$H = \tfrac{1}{2}\rho_\infty V^2 S_f C_D = \dot{m}V_\infty$$

Here C_D is the drag coefficient of the obstacle presented by the control volume which will be called an equivalent body hereafter. S_f is the frontal projected area of the jet. Now, let it be assumed that the frontal area S_f is proportional to the product hd_f, where h is the penetration defined as the maximum physical distance the liquid jet penetrates into the free stream and d_f is the frontal linear dimension of the injector.

Therefore,

$$S_f = C_1 h d_f \quad , \qquad C_1 = \text{constant of proportionality and}$$

$$\dot{m} = \left(\frac{C_1}{2} \rho_\infty V_\infty C_D\right) h d_f \tag{2.1}$$

Now ρ_∞ and V_∞ are constant for any given free stream condition. C_D is a function of the free stream Mach number and the shape of the equivalent body. The equivalent body shape is a function of the injectant properties, injection pressure, free stream conditions and the injector geometry. Hence, for given injectant and the free stream conditions, the equivalent body shape and its size will be the functions of only injector geometry and injection pressure. It is expected that injector geometry will govern the shape of the equivalent body. The size of the injector and the change in the injection pressure will affect only size of the equivalent body. By definition, C_D depends on the equivalent body shape and not on the size of it. Putting all this together implies that for the given Mach number of the free stream C_D is the same for all injectors of the same shape and orientation with respect to the free stream. This shows that for given free stream conditions ρ_∞ and V_∞, and for given shape of the injector

$$\frac{C_1}{2} \rho_\infty V_\infty C_D = \text{constant} = C_2$$

Hence, equation (2.1) becomes

$$C_2 h d_f = \dot{m} \tag{2.2}$$

i.e.

$$h d_f \propto \dot{m}$$

This result is intuitively obvious, since for a given injector and its orientation with respect to free stream higher $\dot{m}$ means higher normal momentum of the jet as it comes out of the injector and hence, larger

penetration. Afterwards, the experiments will verify the validity of the equation (2.2) thereby, justifying the underlying assumptions.

Next, the penetration will be related to the customary variable of jet/free stream dynamic pressure ratio, $\bar{q}$, and to the injector geometry.

By definition,

$$\bar{q} = \frac{\frac{1}{2}\rho_j V_j^2}{\frac{1}{2}\rho_\infty V_\infty^2}$$

and since $\dot{m} = \rho_j A_j V_j C_d$ the above equation results into the following:

$$\bar{q} = \frac{\dot{m}^2}{\rho_\infty V_\infty^2 \rho_j A_j^2 C_d^2} \tag{2.3}$$

Substituting for $\dot{m}$ from equation (2.1)

$$\bar{q} = \frac{4\, C_1^2 \rho_\infty C_D^2 h^2 d_f^2}{\pi^2 \rho_j d_{eq}^4 C_d^2}$$

$$= \frac{4\, C_1^2}{\pi^2} \left(\frac{\rho_\infty}{\rho_j}\right)\left(\frac{C_D^2}{C_d^2}\right)\left(\frac{h}{d_f}\right)^2 \left(\frac{d_f}{d_{eq}}\right)^4$$

or

$$\frac{h}{d_f} = \text{const.} \quad \frac{\rho_j}{\rho_\infty} \quad (\bar{q})^{\frac{1}{2}} \left(\frac{C_d}{C_D}\right)\left(\frac{d_{eq}}{d_f}\right)^2 \tag{2.5}$$

$\frac{h}{d_f}$ = non-dimensional penetration.

Since C_D is unknown, it can be combined with other known quantities to form undetermined constant C, such that

$$\frac{h}{d_f} = C\, (\bar{q})^{\frac{1}{2}}\, C_d \left(\frac{d_{eq}}{d_f}\right)^2 \tag{2.6}$$

Since C includes C_D, it is a function of injector shape.

Starting again with the definition of $\bar{q}$ and using measurable quantites

$$\bar{q} = \frac{\frac{1}{2}\rho_j V_j^2}{\frac{1}{2}\rho_\infty V_\infty^2} = \frac{2(P_{oj} - p_1)}{\gamma\, p_\infty M_\infty^2}$$

$$= \frac{2}{\gamma\, M_\infty^2}\left(\frac{P_{oj}}{p_\infty} - \frac{p_1}{p_\infty}\right) \qquad (2.7)$$

Here p_1 is the static pressure at the base of the jet. At the base, the jet itself is approximately normal to the free stream, and hence, p_1 can be said to be approximately equal to the free stream static pressure since the free stream is subsonic. Hence,

$$\frac{p_1}{p_\infty} \simeq 1$$

Here it should be noted that $\frac{P_{oj}}{p_\infty} > \frac{p_1}{p_\infty}$. Now combining equations (2.6) and (2.7) gives

$$\frac{hM_\infty}{d_f} = \text{const.}\sqrt{\left(\frac{\rho_j}{\rho_\infty}\right)}\left(\frac{P_{oj}}{p_\infty} - \frac{P_1}{p_\infty}\right)^{\frac{1}{2}}\left(\frac{C_d}{C_D}\right)\left(\frac{d_{eq}}{d_f}\right)^2 \qquad (2.8)$$

where constant has absorbed the effect of γ.

The following observations can be made from this equation:

For given free stream conditions and the injector geometry C_D can be assumed to be constant. Then ——

(i) Penetration is proportional to the square root of the injection pressure at least to the first approximation.

(ii) Penetration is proportional to the square root of the injectant density when injectant pressure is constant.

For the given injector geometry and the injection pressure, the effect of the free stream conditions is as follows:

(i) Penetration decreases with an increase in the free stream Mach number.

(ii) Although C_D is constant over a wide range of subsonic Mach numbers, it increases sharply as the transonic Mach numbers are reached.

This further decreases the penetration.

Observations (i) and (ii) together mean that an increase in the free stream Mach number has a two-fold effect in decreasing penetration.

(iii) Penetration decreases with increase in the free stream static pressure and the free stream density when the free stream stagnation pressure is held constant. Alternately, if free stream stagnation pressure is held constant and the stagnation temperature is increased, the penetration will also increase.

III. EXPERIMENTAL INVESTIGATION

3.1 Test Facility

Tests were carried out in the V.P.I. & S.U. 9" x 9" supersonic/transonic blowdown wind tunnel. The test section nozzle block of this tunnel was modified to obtain variable Mach number, subsonic flow. The Mach number of the flow in the test section could be adjusted to any value between 0.45 and 0.75 by adjusting the throat area of this modified nozzle. The stagnation temperature was at ambient atmospheric value in all the tests. Free stream Mach numbers of 0.45 and 0.75 were used during the test schedule. The stagnation pressure of the free stream was held at about 24.4 psia for M = 0.75 and at about 30.0 psia for M = 0.45. Fig. 2 shows the test section with the test model mounted for testing.

3.2 Flat Plate Model

The injection experiments were carried out over a 4" x 5" flat plate with a wedge type leading edge. The front edge of the model was rounded. The plate was mounted on a sting and was located approximately at the center of the test section. Calibration of the test section in the direction transverse to the flow direction showed uniform velocity distribution over the entire cross-section of the test section ensuring that the whole jet will be subjected to the same free stream velocity. The injectors were in the form of the interchangeable brass inserts which fitted beneath the flat plate and the orifice was flush with the flat surface. This was necessary since injectors of different

shapes and sizes were to be tested. Each injector had smooth conical entry passage followed by 1/16" straight run. A 1" inside diameter plenum chamber was fitted to the plate underneath the injector using an O-ring to provide seal. This plenum chamber size was large compared to the orifice size, and pressure in the plenum chamber could be assumed to be approximately equal to the injectant stagnation pressure. Injectant was supplied to the plenum chamber using 1/4" copper feed line and the pressure in the plenum chamber was measured by using another small tubing used to connect pressure transducer to the plenum chamber. The orifice was located 2" downstream of the leading edge of the flat plate.

Three static pressure taps of 1/32" diameter were made on the plate surface and two 1/16" diameter stainless steel tubes were attached to the plate model to measure total pressure in front of the model. All the three static pressure taps gave the same readings, both in wet (with injection) and dry (without injection) runs, indicating, thereby, that the proper static pressure was being recorded. The same was true with the total pressure readings.

Injectors of two different geometries -- circular and rectangular with rounded corners were used. Rounding of the corners gives more uniform flow of the injectant over the whole area of the slot.

Fig. 3a shows the flat plate model as seen from the top, whereas Fig. 3b shows the bottom view of the model. Table I gives the list of the injectors and the test conditions investigated.

3.3 Experimental Set-up and Instrumentation

The experimental arrangement is shown schematically in Fig. 4. The injectant was stored in a reservoir, which was pressurized by means of compressed air. This pressure could be regulated and would be kept constant throughout a set of test runs. The injectant, under pressure, would flow through a needle valve, then through a solenoid valve and finally, through a rotometer type flowmeter before entering the plenum chamber. The needle valve could be adjusted to obtain the desired mass flow rate. The solenoid valve could be opened and closed remotely to start and stop the injection.

The flowmeter was Brooks Flowmeter Series 6408-69887/1. This was calibrated for water, the injectant which was used throughout these tests. The solenoid valve (size 1/4") was manufactured by Skinner Electric Valve Division.

The pressure measurements and transducers used were as given below:

Free stream stagnation pressure measured in front of the flat plate model---

0-50 psid Statham Transducer (Model PM 280 TC±50-350)

Free stream static pressure measured on the flat plate model---

0-50 psid Statham Transducer (Model PM 60 TC±50-350)

Total pressure of water measured in the plenum chamber---

0-500 psia CEC transducer (Type 4-326).

The outputs of all the transducers were recorded on Honeywell strip chart recorders.

The flat plate was mounted vertically for top view observations and horizontally for all other experimental work.

3.4 Photographic Techniques

(a) Streak photographs:

Streak photographs are relatively long exposure photographs (exposure time = 2.5 milliseconds) which give time averaged pictures of the highly unsteady jet. Such pictures were used for the measurements of the penetration. The pictures were taken at a magnification of 3.25:1. Magnification was provided by an 8" focal length, f2 lens. A [illegible] mercury arc lamp was used as a continuous source of light. Light from this source was reflected from a parabolic mirror to obtain a parallel-ray light beam incident on the jet. The camera was a simple bellow-box arrangement using a Polaroid sheet film holder at the focal plane. The photographic film Polaroid Type 57, 3000 ASA, was used for all the photographs. The shutter speed was set at 1/400 of a second.

Fig. 5 shows the schematic diagram of the set-up used for obtaining the above photographs, and Fig. 6 shows a sample photograph of this type.

The above mentioned photographs give time averaged views of the jet and are useful for measuring gross characteristics of the jet like penetration. To obtain any kind of microscopic details of the jet, stop action photographs are required. Such photographs give instantaneous views of the jet. The exposure time to be used is determined by the

type of details desired. In the present investigation, two types of short exposure photographs were obtained.

(b) Stop action photographs:

1) Spark shadowgraphs:

These are short exposure photographs with the exposure time of the order of a microsecond (0.8 microsecond). A General Radio Strobotac strobe flash unit was used as a source of light. This would flash on the jet for a period of 0.8 microsecond. On the other side of the jet, the same camera arrangement as used for obtaining streak photographs was set, but now the shutter was left open all the time. Extreme care was taken to keep the room dark throughout such runs. The photographs obtained using such a procedure show details of the jet and are useful in studying wave pattern on the jet surface and the break-up mechanism of the jet.

Fig. 7 shows the schematic diagram of the set-up used for obtaining spark shadowgraphs, and Fig. 8 shows a sample photograph of this kind.

2) Nanosecond Photographs:

These are spark shadowgraphs with extremely short exposure time (exposure time of 2.5 nanosecond) and magnification of 3.25:1. The optical arrangement for obtaining these is similar to that used for spark shadowgraphs, except the light source. The light in this case is a nanolamp (approx. 15×10^{-9} sec.). The field of view in these photographs was extremely narrow. These photographs show microscopic details of the jet such as droplets and hence, are used to obtain data about droplet size.

The schematic diagram of the optical setup is shown in Fig. 9, and Fig. 10 shows a typical back lighted photomicrograph.

(c) Top Views:

To study liquid layer, the flat plate model was mounted vertically, and front-lighted streak pictures looking down at the jet were taken. An ordinary projector lamp was used as a light source. The camera arrangement was the same as for back lighted streak photographs.

3.5 Experimental Procedure:

Some of the earlier investigators (Ref. 15, 19, 21) have reported that penetration is relatively insensitive to the injectant properties. Hence, water at room temperature, due to its availability and easy handling, was used for all the tests.

Injectors of two shapes - circular and rectangular - were tested in two free stream Mach numbers. Each rectangular injector was tested with two orientations - aligned with free stream and transverse to the free stream. Each configuration was tested for different values of mass flow rate.

During each run, free stream stagnation pressure, static pressure in the test section, volume flow rate of injectant, and total pressure of the injectant in the plenum chamber were recorded. The description of a typical run will be as follows.

1) The tunnel room was made completely dark and film was loaded into the camera.
2) The remote control timer was turned on.

3) The remote control timer in turn would start the strip chart recorders. Then, it would start the tunnel, and two seconds later the liquid jet was started.

4) Two seconds after this, the photograph was taken and a rotameter reading was taken by the operator.

5) The timer shuts off the jet, the wind tunnel, and the strip chart recorder, in that order.

6) Barometric pressure was recorded for each set of runs.

Duration of a typical run was between 7 and 10 seconds. The operator always had manual control over the running of the tunnel for safety reasons.

IV. RESULTS AND DISCUSSION

4.1 Jet Penetration

As mentioned in section 3.4 (a), the long exposure streak photographs were used for measuring penetration. Penetration is a function of, "x", downstream of the injector and assumes an asymptotic value as the jet loses its normal momentum. In the present work, all the measurements were taken at $x/d_{eq} = 6.25$ downstream of the centre of the injector. This distance was sufficient for the jet to attain its asymptotic value of penetration. Actual penetration was calculated from the penetration measured from the photographs by taking magnification into account, which was approximately 3.25 for all the photographs. The jet to free stream dynamic pressure ratio was calculated from the recorded data of pressures. Measured penetration was plotted against measured mass flow rate of injectant for different values of d_f/d_s. Examples are presented in Figs. 11, 12, and 13. Next, the plots were made of non-dimensional penetration, h/d_f vs. non-dimensional $q^{-1/2}\ C_d\ (\frac{d_{eq}}{d_f})^2$. (e.g. figs. 14, 15 and 16) These give a family of curves with parameter (d_f/d_s).

As developed in Sec. 2.2,the equation of non-dimensional penetration for given injectant and the free stream conditions is

$$\frac{h}{d_f} = C\ (\bar{q})^{1/2}\ \ C_d\ (\frac{d_{eq}}{d_f})^2 \qquad (2.6)$$

where C is a function C_D and, hence, of injector shape. If the injector shapes are characterized by d_f/d_s, then

$$C = C\ (\frac{d_f}{d_s}) \qquad (4.1)$$

According to eqn. (2.6), C is a slope of the curve h/d_f vs $(\bar{q})^{1/2} C_d (d_{eq}/d_f)^2$. Hence, C can be found out from the plots of h/d_f vs $(\bar{q})^{1/2} C_d \left(\frac{d_{eq}}{d_f}\right)^2$ made previously. These are listed in Table II. Now, if it is assumed that

$$C = c_3 \left(\frac{d_f}{d_s}\right)^{c_4} \tag{4.2}$$

where C_3 and C_4 are constants.

Then,

$$\log C = \log C_3 + C_4 \log \left(\frac{d_f}{d_s}\right) \tag{4.3}$$

To evaluate C_3 and C_4 plot of log C vs log $\left(\frac{d_f}{d_s}\right)$ was made (Fig. 17), which was a straight line.

The equation of this straight line is

$$\log C = 1.13 + 0.416 \log \left(\frac{d_f}{d_s}\right) \tag{4.4}$$

or

$$C = 13.5 \left(\frac{d_f}{d_s}\right)^{0.416}$$

When this form of C is substituted in the equation (2.6) it becomes

$$\frac{h}{d_f} = 13.5 (\bar{q})^{1/2} C_d \left(\frac{d_{eq}}{d_f}\right)^2 \left(\frac{d_f}{d_s}\right)^{0.416} \tag{4.5}$$

The penetration data for all the injectors tested clusters around a single straight line defined by the above equation as seen in the Fig. 18.

Effect of injector shape of given area.

In combustion applications, a definite amount of fuel is added

to the air stream to achieve the desired fuel/air ratio. The main concern is of getting better mixing of fuel and air. This is determined by penetration and droplet size. For given mass flow rate, the penetration itself is governed by injector shape and hence, it is necessary to know what injector shape will give better penetration. To do this, substitute $\bar{q}$ from equation (2.3) in equation (4.5)

$$h = \text{const.} \frac{\dot{m}}{\rho_\infty^{1/2} \rho_j^{1/2} V_\infty} (d_f/d_s)^{0.416} \frac{1}{d_f}$$

For given free stream conditions and the given injectant

$$h = \text{const.}\ \dot{m}\ (d_f/d_s)^{0.416} \frac{1}{d_f} \tag{4.6}$$

Now for prescribed mass flow rate

$$h = k\ (d_f/d_s)^{0.416} \frac{1}{d_f} \tag{4.7}$$

where $k = \text{const.}$

If a circular injector is considered -

$$d_f = d_s = d_{eq}$$

$$h_{circ.} = k/d_{eq} \tag{4.8a}$$

Next, consider injector of rectangular geometry with $d_f/d_s = 1/5$ and having the same area as the above circular injector.

(This will be aligned orientation of the injector).

$$h_{aligned} = \frac{k\ (0.2)^{0.416}}{d_{eq}}$$

$$0.512 \frac{k}{d_f} \tag{4.8b}$$

If the same rectangular injector is placed in transverse orientation, then $d_f/d_s = 5$, and

$$h_{transverse} = (5)^{0.416} \frac{k}{d_g}$$

$$= 1.953 \frac{k}{d_g} \qquad (4.8c)$$

If an injector with $d_{eq} = 0.09375"$ is considered, then the sides of the equivalent rectangular injectors are 0.038" and 0.19" and are in the ratio 1:5.

For such a case,

$h_{circ.} = 10.67\ k$

$h_{aligned} = 12.56\ k$

$h_{transverse} = 10.28\ k$

This shows that

$$h_{aligned} > h_{circ.} \geq h_{transverse}$$

It should be noted that difference between $h_{circ.}$ and $h_{transverse}$ is not very much for this case.

If rectangular injectors of side ratio 1:3 are used, equations (4.8) a, b, c become

$$h_{circ.} = k/d_{eq} \qquad (4.9a)$$

$$h_{aligned} = 0.633 \frac{k}{d_f} \qquad (4.9b)$$

$$h_{transverse} \quad 579 \frac{k}{d_f} \qquad (4.9c)$$

For injectors of d_{eq} = 0.09375", these become

$h_{circ.}$ = 10.67 k

$h_{aligned}$ = 12.71 k

$h_{transverse}$ = 10.6 k

The validity of these can be observed from Fig. 19 and 20. In general, it is concluded that $h_{aligned} > h_{circ.} \gtrsim h_{transverse}$.

Effect of injector size of given shape:

For given injector shape d_f/d_s; C_D can be assumed to be constant when M_∞ is constant. For these conditions, equation (2.6) becomes

$$\frac{h}{d_f} = \text{const.} \; (\bar{q})^{1/2} \; C_d \; \left(\frac{d_{eq}}{d_f}\right)^2$$

Substituting equation (2.3) in this gives

$$h = \text{const.} \; \frac{\dot{m}}{d_f} \tag{4.10}$$

i.e. for a given mass flow rate, penetration is inversely proportional to the frontal dimension.

Comparison with results of other investigators:

Yates and Rice[18] obtain the following empirical expression for water injected normal to Mach 3 air stream, valid for circular injectors.

$$\frac{h}{d_{eq}} = 1.15 \; (\bar{q})^{1/2} \; \ln \left(1 + 6 \; \frac{x}{d_{eq}}\right) \tag{4.11}$$

Here, x is the distance downstream of the injector at which pentration

is measured. In the present study, all measurements were taken at $x/d_{eq} = 6.25$, for which equation (4.11) reduces to

$$\frac{x}{d_{eq}} = 4.2\ (\bar{q})^{1/2} \tag{4.12}$$

Equation (4.5) for circular injector becomes

$$\frac{x}{d_{eq}} = 13.5\ (\bar{q})^{1/2}\ C_d \tag{4.13}$$

Although the constants in (4.12) and (4.13) do not match exactly, their form is the same. The difference in the constants may be explained by the difference in the free stream Mach number.

The important difference between the present results and those of previous investigators is observed when the results of Joshi and Schetz[24] are considered. They concluded that

$$h_{aligned} > h_{transverse} \gtrsim h_{circ}$$

Effect of Mach number

As mentioned in the Chapter II penetration decreases with an increase in the free stream Mach number. This can be seen from Fig. 21, in which plot of penetration vs. mass flow rate is made for a given injector for two different Mach numbers.

4.2 Jet Breakup

A qualitative study of the effect of injector geometry on jet breakup and instantaneous structure was carried out. In the present investigation, back lighted photomicrographs with two different exposure times were used to obtain information about jet breakup and structure.

Observations from spark shadowgraphs:

(i) The axial distance to the gross fracture increases with increases in $\bar{q}$,

(ii) With an increase in $\bar{q}$, the amplitude and the wave length of surface waves reduces.

(Fig. 22 is representative of these observations.)

(iii) The effect of injector geometry for given $\bar{q}$ were as follows (Fig. 23):

(a) the axial distance to the fracture is largest for aligned rectangular slot and least for the transverse slot and (b) clump size is largest for the rectangular slot in the aligned orientation and smallest for the transverse orientation.

4.3 Drop Size Measurements

The measurements of droplet size were made using a microscope with magnification of 62.5 with the nanosecond photographs. All the measurements were made at a plane normal to the free stream at a downstream distance of $x/d_{eq} = 6.25$. The sample back lighted photomicrograph in Fig. 10 shows a darker core along the centre line of the jet. This is due to the presence of either liquid clumps or masses of liquid droplets in distinguishable from one another. Due to this, droplet size measurements were impossible to make in this region of the jet. Hence, measurements were made only in the region where individual droplets were clearly visible, i.e., at the edge of the

core and away from the darker portion. Droplets were not very clear for low mass flow rates of the injectant, and large equivalent diameters. Figs. 24 and 25 show a representative histograms for droplet size.

The following observations were made about the mean drop sizes:

(i) The mean droplet size was of the order of 10^{-2} inch.

(ii) For a given injector and free stream conditions, mass flow rate did not effect droplet size greatly. For example, for d_{eq} of 0.03125" and M_∞ = 0.45, the mean droplet size was 0.0138 inch with standard deviation of 0.00064 inch.

(iii) Decreasing d_{eq} increased mean droplet size. For example, for d_{eq} of 0.0625" and M_∞ = 0.45, the mean droplet size increased to 0.0155"; an increase of 12.3% (Compare to (i) above).

(iv) Increasing M_∞ decreased mean droplet size. For d_{eq} of 0.03125" and M_∞ = 0.75 mean droplet size was 0.012" about 15% decrease. (Compare to (i) above).

(v) Injector geometry had a major effect on mean droplet size. The rectangular injector oriented aligned with the free stream decreased mean droplet size whereas, when it was oriented transverse, the mean droplet size increased. For example, with the rectangular slot of d_{eq} = 0.0625" in M_∞ = 0.45 when aligned gave $\bar{d}$ = 0.0128" and when transverse gave $\bar{d}$ = 0.0182".

Two observations can be made when the above results are compared with those of Weiss and Worsham.[6] Firstly, the droplet size as determined in

the present investigation is of the order of 10^{-2} in., much larger as compared to that measured by Weiss and Worsham which was of the order of a few microns. This difference in the measured diameters can be explained in the following manner. In the present investigation, the sampling plane was at $x/d_{eq} = 6.25$ where as it was at $x/d_{eq} = 123$ to 218 in the experiments of Weiss and Worsham. It can be argued that the droplets were not fully developed at the time of measurements in the present investigation, and the results might well have been comparable if higher values of x/d_{eq} had been used in the present study. Secondly, the number of droplets investigated in the present study is much too small compared to that studied by Weiss and Worsham. This is due to a deficiency of the measuring technique used. In the photographic measuring technique, measurements are made only for a very short duration of time and at a single plane. This gives information about only a few droplets. In the method used by Weiss and Worsham sampling time is large and hence larger number of sample droplets can be obrained. Of course, the "hot-wax" technique has obvious limitations and cannot be generally employed.

4.3 Liquid Surface Layer:

The top view photographs and visual observations showed that there was no liquid surface layer present near the injection port. The liquid surface layer has been supposed to be a product of shock-boundary layer interaction.[23,24] Since in the subsonic flow there is no shock, no such interaction exists and absence of liquid surface layer is consistent with this reasoning.

V. CONCLUSIONS

The theoretical analysis of the problem indicated that for given free stream conditions and for a given injectant

$$\frac{h}{d_f} = C \ (\bar{q})^{\frac{1}{2}} \ C_d \left(\frac{d_{eq}}{d_f}\right)^2 \tag{5.1}$$

where C was a function of the injector geometry. Hence, for a given injector, geometry C could be assumed to be a constant. To obtain the functional dependence of C on the injector geometry which was characterized by $d_f:d_s$, plots of non-dimensional penetration h/d_f vs. $(\bar{q})^{1/2} C_d (d_{eq}/d_f)^2$ were made for different values of $(d_f:d_s)$. These were straight lines through the origin as predicted theoretically by eqn. (5.1)

When values of log C calculated from these plots were plotted against log $(d_f:d_s)$, the following functional dependence was observed

$$C = 13.5 \ (d_f/d_s)^{0.416}$$

When substituted in equation (5.1) this gives

$$\frac{h}{d_f} = 13.5 \ (\bar{q})^{\frac{1}{2}} \ C_d \left(\frac{d_{eq}}{d_f}\right)^2 \left(\frac{d_f}{d_s}\right)^{0.416} \tag{5.2}$$

This equation explicitly shows the effect of injector geometry.

The following conclusions about the effect of injector geometry can be drawn:

For given free stream conditions and injectant mass flow rate, the penetration depends upon the injector geometry in the following fashion:

(i) For a given injector area, the rectangular slot aligned with the free stream gives maximum penetration, whereas the same

slot placed transverse to the free stream gives minimum penetration. This result holds for $d_f:d_s$ up to 5:1.

(ii) A circular injector gives penetration which is less than that given by an aligned equivalent rectangular slot but slightly more than that given by a transverse rectangular slot.

(iii) For a given injector shape (d_f/d_s ratio), the penetration is inversely proportional to the frontal dimension when the area of the injector is varied.

(iv) Increasing Mach number decreases penetration.

Studies of spark shadowgraphs of the jet structure and break-up indicated that:

(i) An increase in $\bar{q}$ increases the axial distance to the gross fracture of the jet.

(ii) An increase in $\bar{q}$ decreases the amplitude and wave length of the surface waves.

(iii) The axial distance to the gross fracture is the largest for the aligned rectangular slot and the least for transverse rectangular slot.

On the basis of the measurements made, the following observations about the mean drop size were made:

(i) The mean droplet size was of the order of 10^{-2} inch.

(ii) Decreasing d_{eq}, increases mean droplet size.

(iii) Increasing free stream Mach number decreases mean droplet size.

There was no trace of a liquid surface layer near the injection port under any condition tested and it was concluded that the liquid surface layer does not exist for liquid injection into subsonic flow.

REFERENCES

1. Rothrock, C., "Effect of High Velocities on the Distribution and Penetration of a Fuel Spray," NACA TN 376, 1931.
2. Castleman, R., "The Mechanism of Atomization Accompanying Solid Injection," NACA Report 440, 1932.
3. Nukiyama, S. and Tanasawa, Y., "Experiments on the Atomization of Liquids in an Air Stream," Rept. 6, Transactions of the Society of Mechanical Engineers (Japan), Vol. 6, No. 23, 1940, p. 11 (Translated by Defense Research Board (Canada), March 18, 1950).
4. Bitron, M., "Atomization of Liquids by Supersonic Air Jets," Ind. and Eng. Chem., Vol. 47, No. 1, Jan. 1955, p. 23.
5. Ingebo, R. and Foster, H., "Drop Size Distribution for Cross-Current Break-up of Liquid Jets in Air Stream," NACA TN 4087, Oct. 1957.
6. Weiss, C. and Worsham, C., "Atomization in High Velocity Air Streams," ARS Journal, Vol. 29, No. 4, April 1959, p. 252.
7. Clark, B., "Break-up of a Liquid Jet in a Transverse Flow of Gas," NASA TN D-2424, Aug. 1964.
8. Adelberg, M., "Mean Drop Size Resulting from the Injection of a Liquid Jet into a High Speed Gas Stream," AIAA Journal, Vol. 6, No. 6, June 1968, pp. 1143-1147.
9. Morrell, G., "Rate of Liquid Jet Breakup by a Transverse Shock Wave," NASA TN D-1728, May 1963.

10. Morrell, G. and Povinelli, F., Breakup of Various Liquid Jets by Shock Waves and Applications to Resonant Combustion," NASA TN D-2423, Aug. 1964.

11. Ranger, A. and Nicholls, J., "Aerodynamic Shattering of Liquid Drops," AIAA Journal, Vol. 7, No. 2, May 1969, pp. 285-290.

12. Dowdy, M. and Newton, J., "Investigation of Liquid and Gaseous Secondary Injection Phenomena on a Flat Plate with M = 2.01 to M = 4.54," TR 32-542, Dec. 1963, Jet Propultion Lab.

13. Forde, J., Molder, S., and Szpiro, E., "Secondary Liquid Injection into a Supersonic Airstream," Journal of Spacecraft and Rockets, Vol. 3, No. 8, Aug. 1966, pp. 1173-1176.

14. Adelberg, M., "Breakup Rate and Penetration of a Liquid Jet in a Gas Stream," AIAA Journal, Vol. 5, No. 8, Aug. 1967, pp. 1408-1415.

15. Kolpin, M., Horn, K., and Reichenbach, R., "Study of Penetration of a Liquid Injectant into a Supersonic Flow," AIAA Journal, Vol. 6, No. 5, May 1968, pp. 853-858.

16. Catton, I., Hill, D., and McRae, R., "Study of Liquid Jet Penetration in a Hypersonic Stream," AIAA Journal, Vol. 6, No. 11, Nov. 1968, pp. 2084-2089.

17. Horn, K., and Reichenbach, R., "Further Experiments on Spreading of Liquids Injected into a Supersonic Flow," AIAA Journal, Vol. 7, No. 2, Feb. 1969, pp. 358-359.

18. Yates, C. and Rice, J., "Liquid Jet Penetration," Research and Development Programs Quarterly Report, U-RQR/69-2, Applied Physics Lab., Johns Hopkins Univ., 1969.

19. Sherman, A. and Schetz, J., "Breakup of Liquid Sheets and Jets in a Supersonic Gas Stream," AIAA Journal, Vol. 9, No. 4, Apr. 1971, pp. 666-673.

20. Reichenbach, R. and Horn, K., "Investigation of Injectnat Properties on Jet Penetration in a Supersonic Stream," AIAA Journal, Vol. 9, No. 3, Mar. 1971, pp. 469-472.

21. Sherman, A., "Investigations into the Breakup of Liquid Sheets and Jets in a Supersonic Gas Stream," Ph.D. Thesis, Univ. of Maryland, 1969.

22. Kush, E., "Decomposition of a Liquid Jet Injected Normal to a Supersonic Air Stream," Ph.D. Thesis, Virginia Polytechnic Institute and State Univ., 1972.

23. Kush, E. and Schetz, J., "Liquid Jet Injection into a Supersonic Flow," AIAA Paper No. 72-1180, AIAA/SAE 8th Joint Propulsion Specialist Conference, New Orleans, La., Nov. - Dec. 1972.

24. Joshi, P. and Schetz, J., "Effect of Injector Shape on Penetration and Spread of Liquid Jets," AIAA Paper No. 74-1156, AIAA Journal, Vol. 13, No. 9, Sept. 1975, pp. 1137-1138.

25. Newton, J. and Spaid, F., "Interaction of Secondary Injectants and Rocket Exhaust for Thrust Vector Control," ARS Journal, Vol. 32, No. 8, Aug. 1962, pp. 1203-1211.

26. Schetz, J. and Gilreath, H., and Lubard, S., "Fuel Injection and Mixing in a Supersonic Stream," 12th Symposium (International) on Combustion. The Combustion Institute, Pittsburg, Pa., 1965,

27. Edelman, R., Schmotolocha, S., and Slutsky, S., "Combustion of Liquid Hydrocarbons in a High Speed Air Stream," AIAA Journal, Vol. 9, No. 7, July 1971, pp. 1357-1364.

TABLE I

Test Conditions

Cross flow Mach numbers = 0.75 and 0.45

Cross flow total temperature = ambient

Injectant - Water

Temperature of injectant - Room temperature

Injectors Used*

Inj.	Rectangular**				Circular
	Width d	b	Length L	L/d	Dia.
1	---	---	---	---	1/8
2	0.0665	0.133	0.199	3	---
3	0.0506	0.203	0.253	5	---
4	---	---	---	---	3/32
5	0.0498	0.0995	0.149	3	---
6	0.0380	0.152	0.190	5	---
7	---	---	---	---	1/16
8	0.0332	0.0664	0.0996	3	---
9	---	---	---	---	1/32

* All dimensions in inches

** Refer to Fig. B-1 in Appendix B.

TABLE II

No.	d_f:d_s	d_f/d_s	Slope C	log d_f/d_s	log C
1	1:5	0.20	6.5	- 0.6990	0.813
2	1:3	0.33	8.6	- 0.4771	0.934
3	Circle	1.00	13.5	0.0000	1.130
4	3:1	3.00	23.7	0.4771	1.375
5	5:1	5.00	26.67	0.6990	1.426

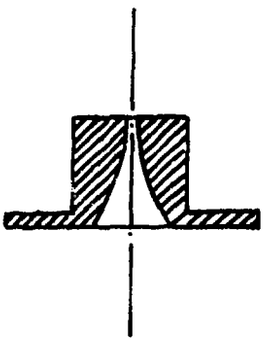

INJECTOR
CROSS - SECTION

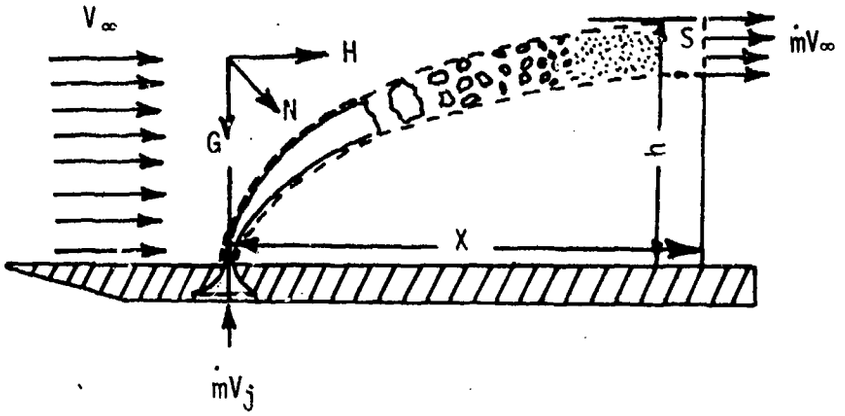

Fig. 1 Control Volume for Jet Penetration

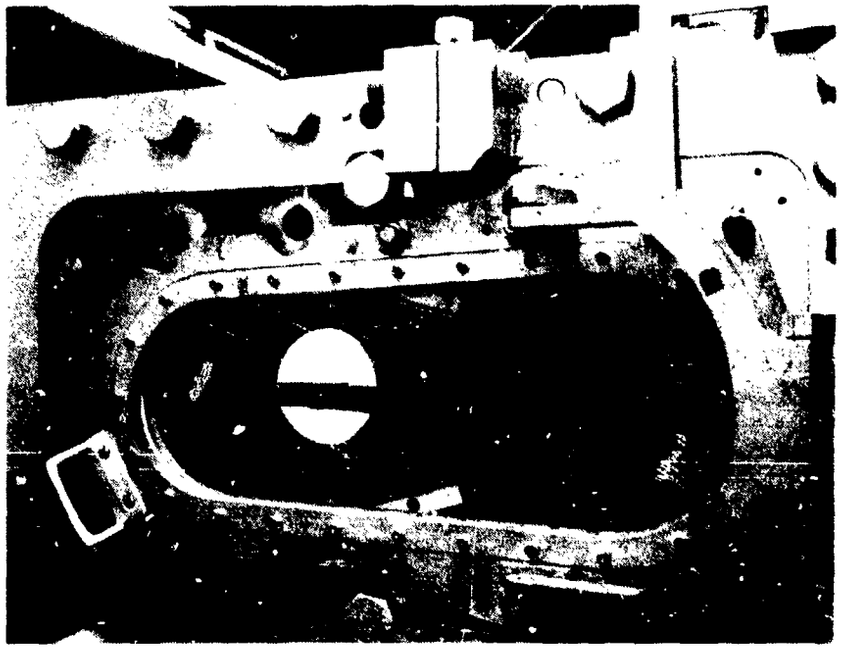

Fig. 2 Test Section With Model Mounted for Testing

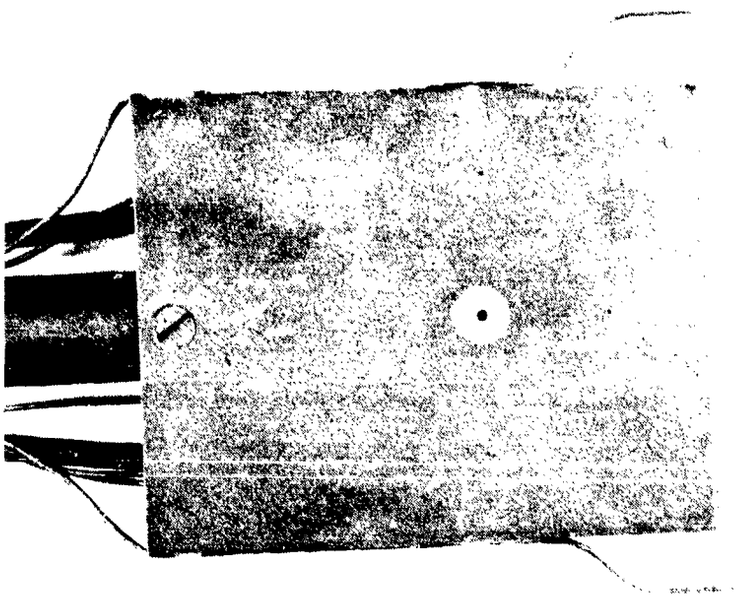

Fig. 3a FLAT PLATE MODEL (TOP VIEW)

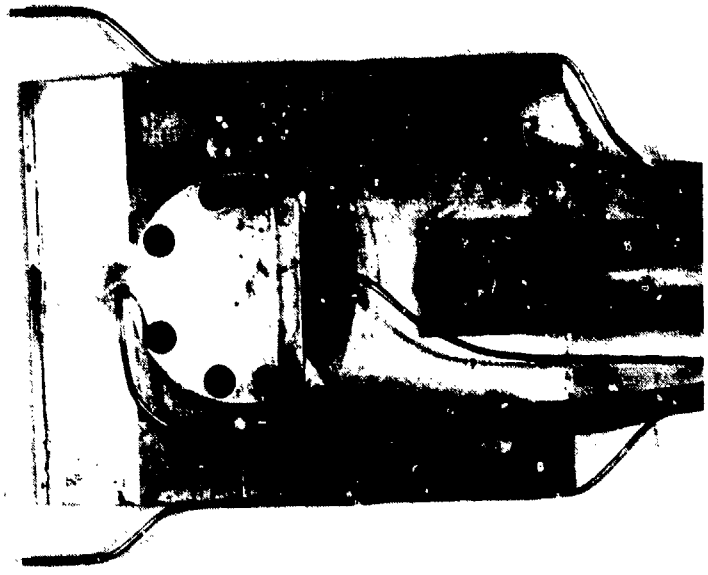

Fig. 3b FLAT PLATE MODEL (BOTTOM VIEW)

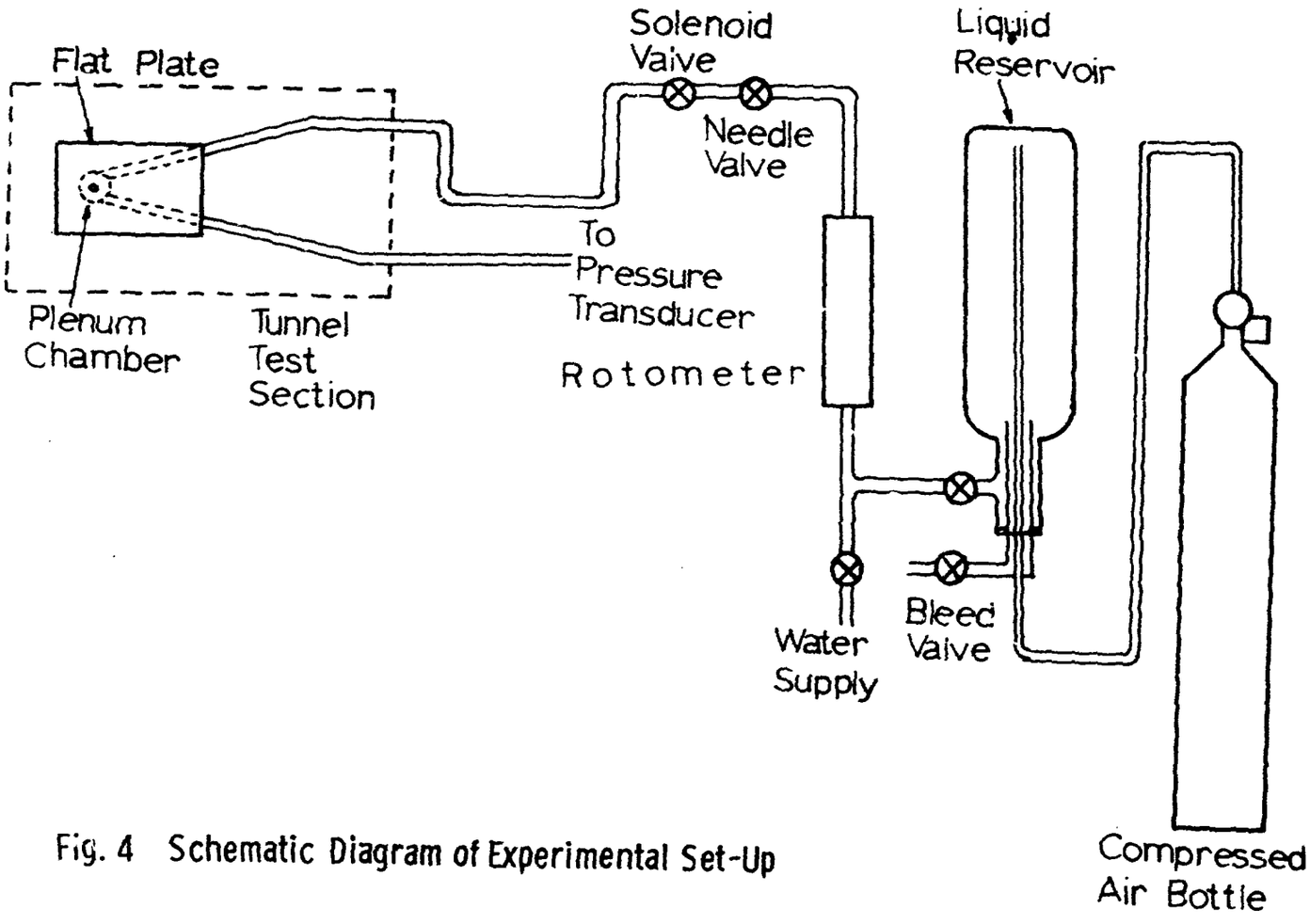

Fig. 4 Schematic Diagram of Experimental Set-Up

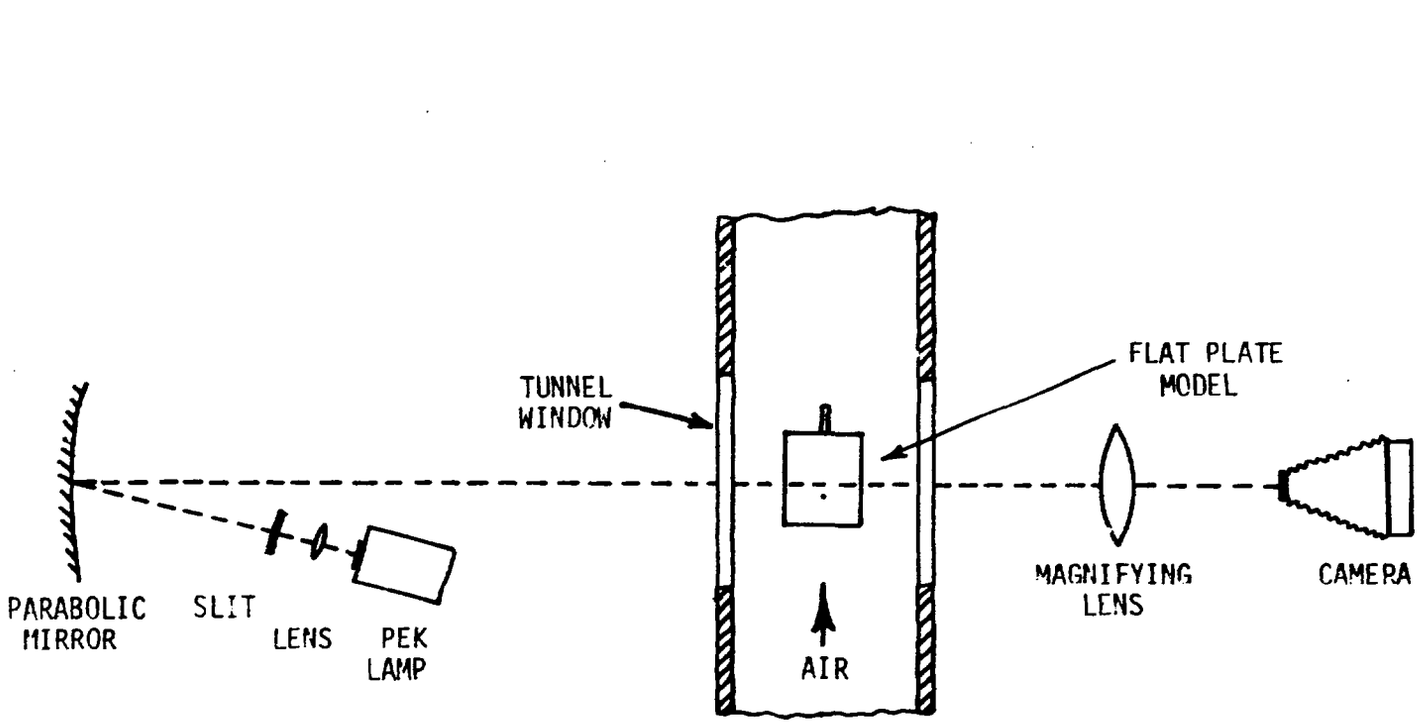

Fig. 5 Schematic Optical Set-Up for Streak Pictures

Fig. 6 TYPICAL STREAK PHOTOGRAPH

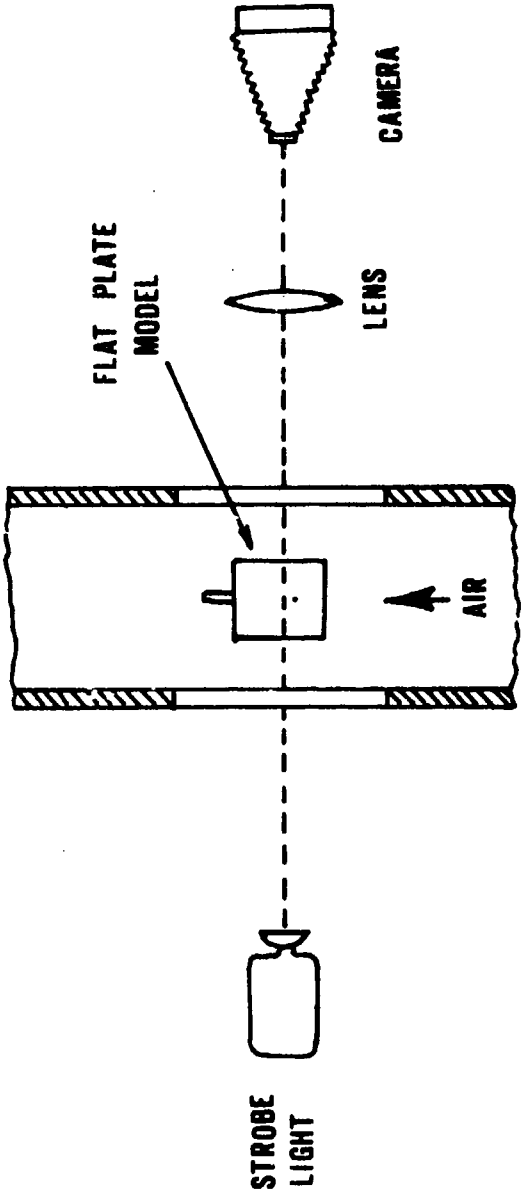

Fig. 7 Schematic Optical Set-Up for Spark Shadowgraphs

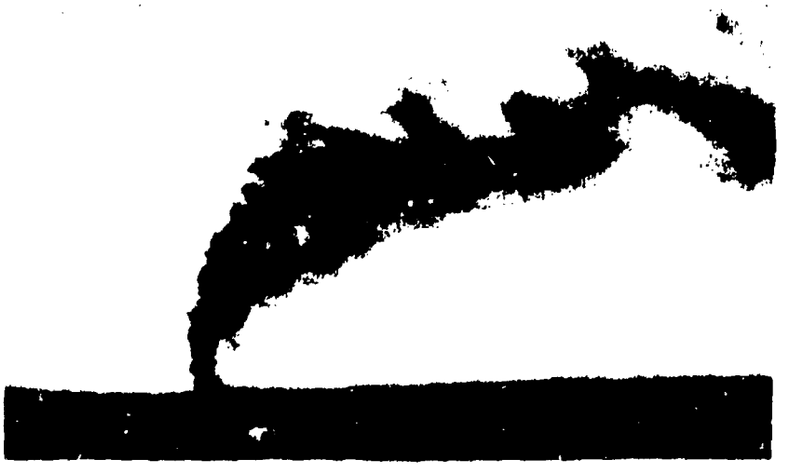

Fig. 8 SAMPLE OF SPARK SHADOWGRAPH

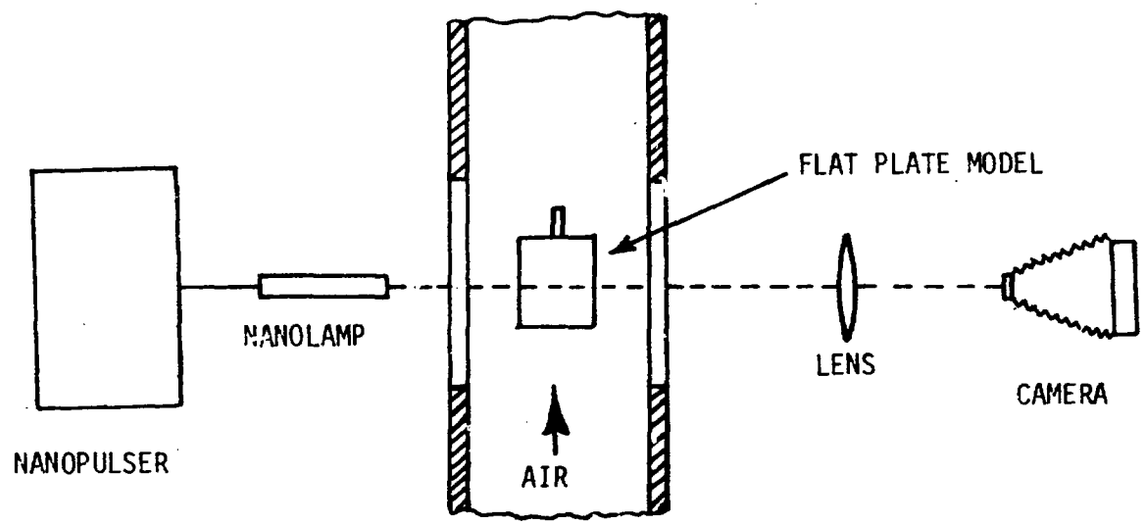

Fig. 9 Schematic Optical Set-Up for Back Lighted Photomicrograph

Fig. 10 REPRESENTATIVE BACK LIGHTED PHOTOMICROGRAPH

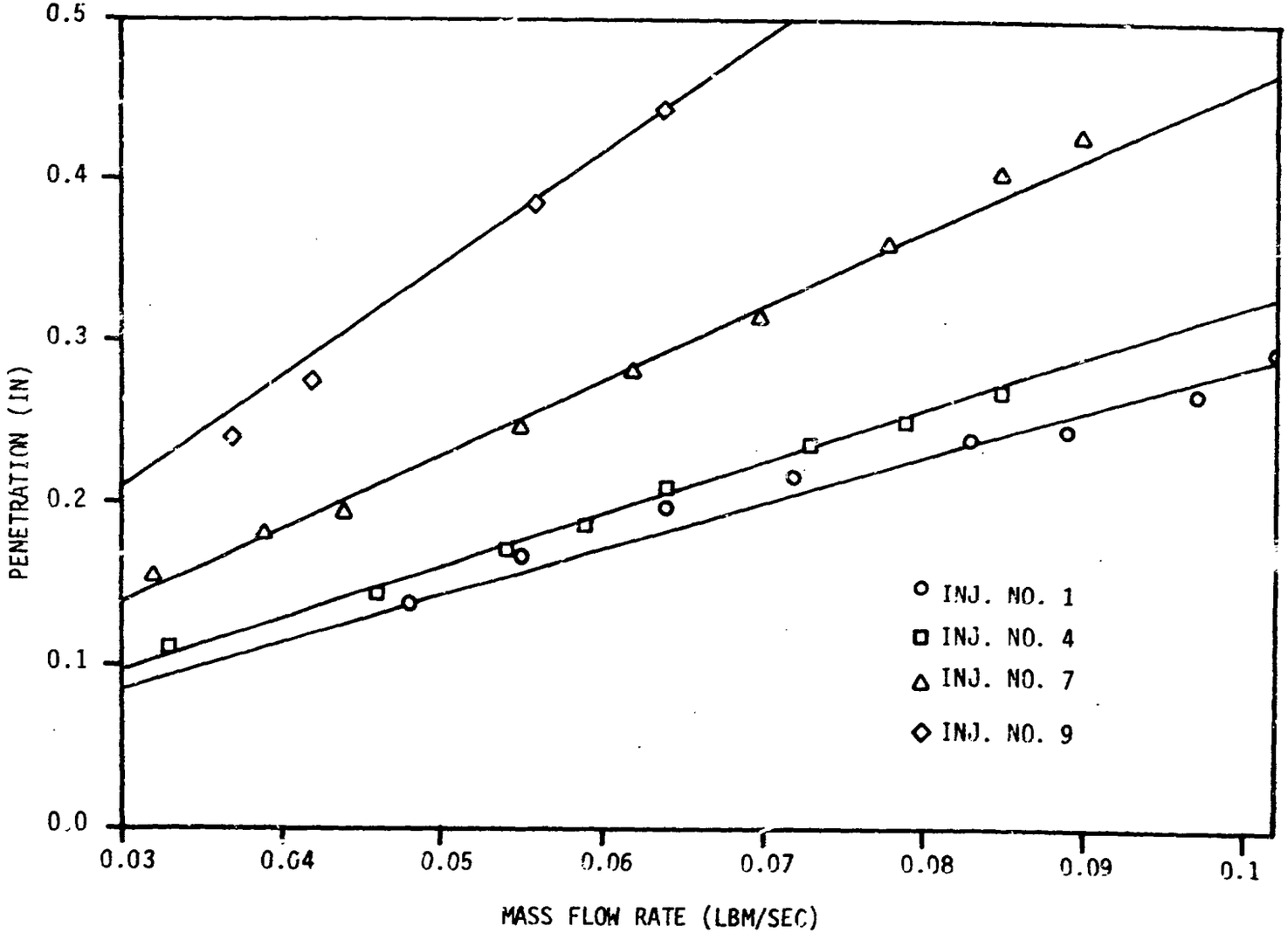

Fig. 11 Penetration Vs. Mass Flow Rate - Rectangular Injectors (d_f:d_s::1:1)

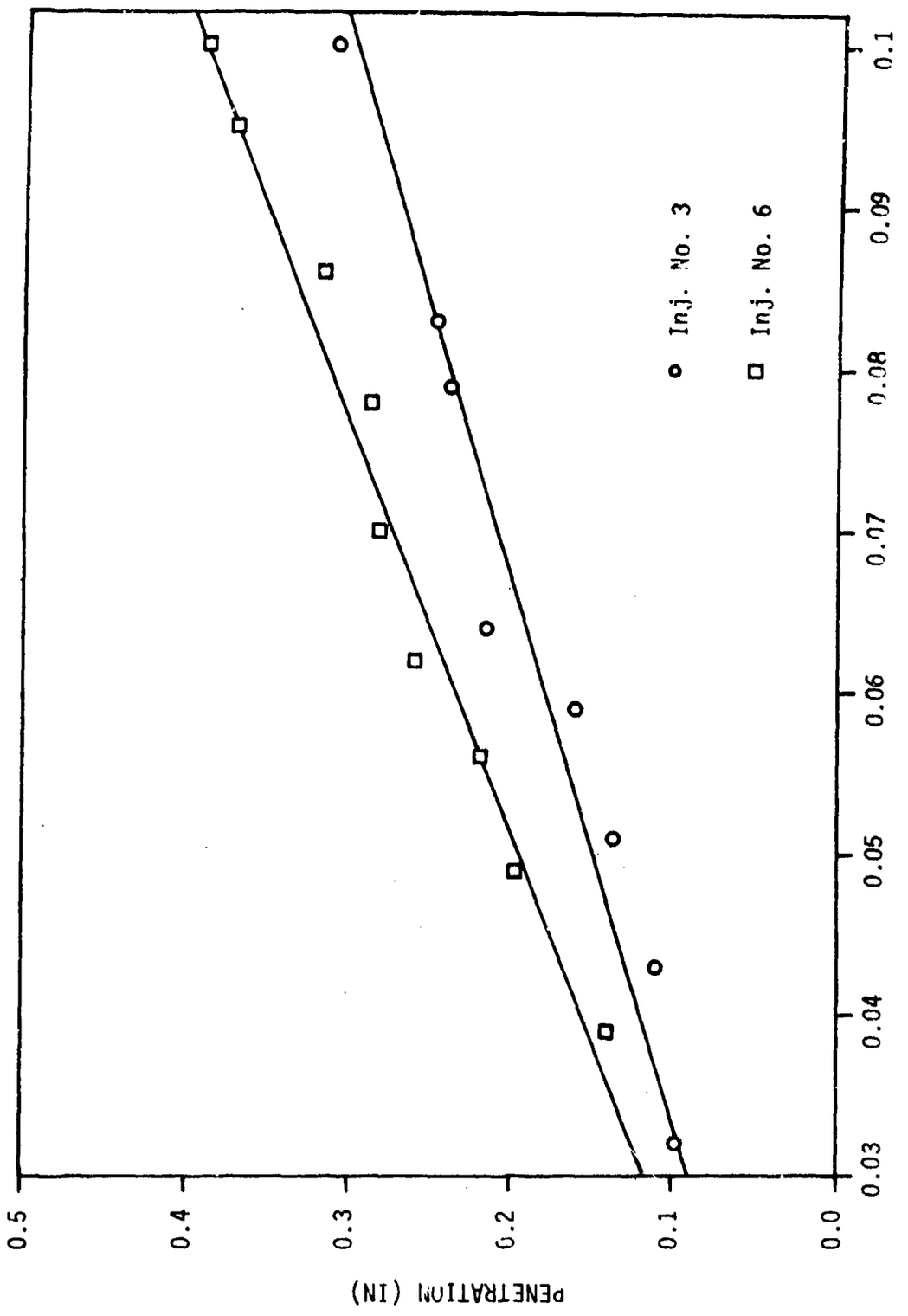

Fig. 12 Penetration Vs. Mass Flow Rate - Rectangular Injectors (d_f:d_s::1:5)

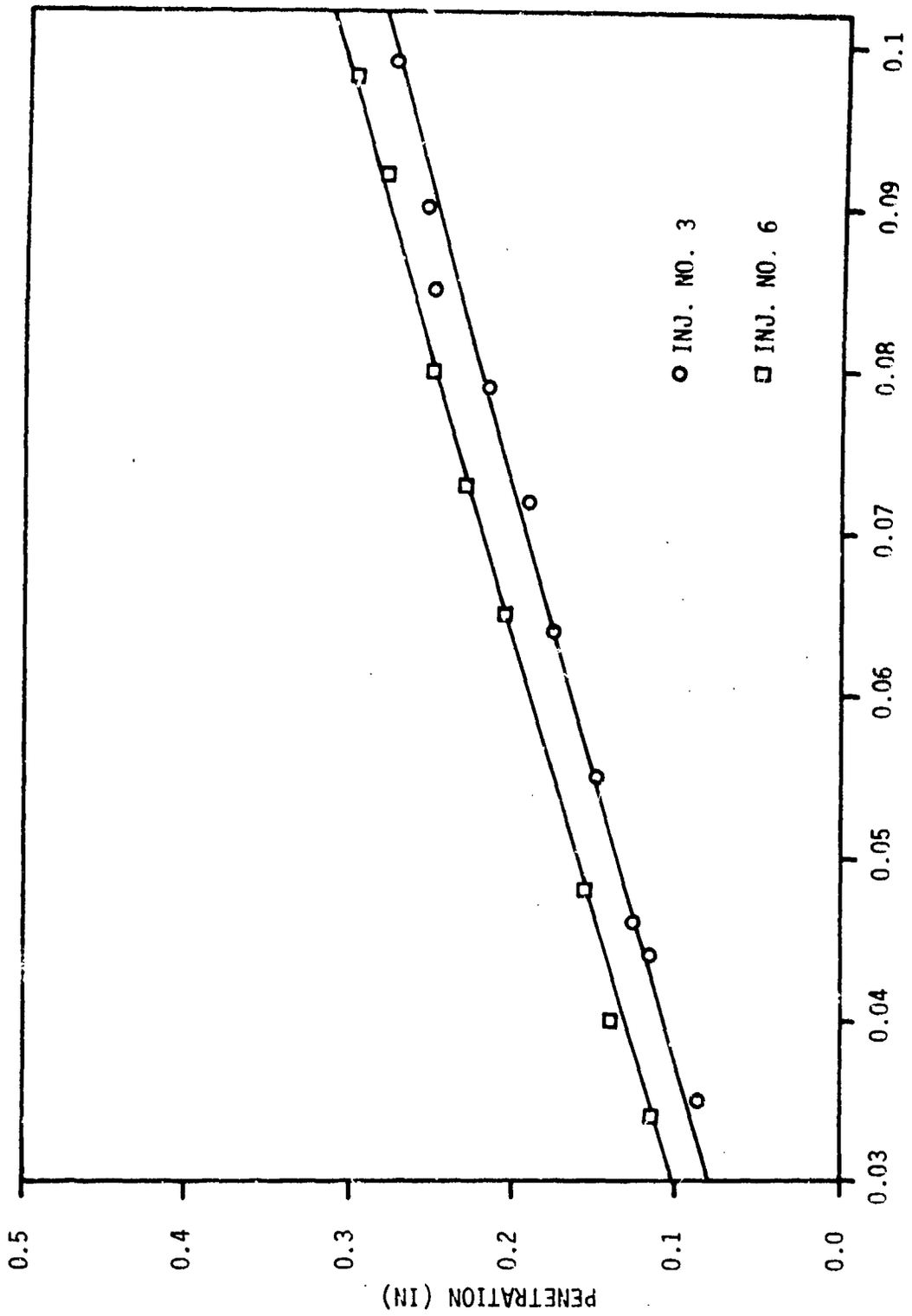

Fig. 13 Penetration Vs. Mass Flow Rate - Rectangular Injectors (d_f:d_s::5:1)

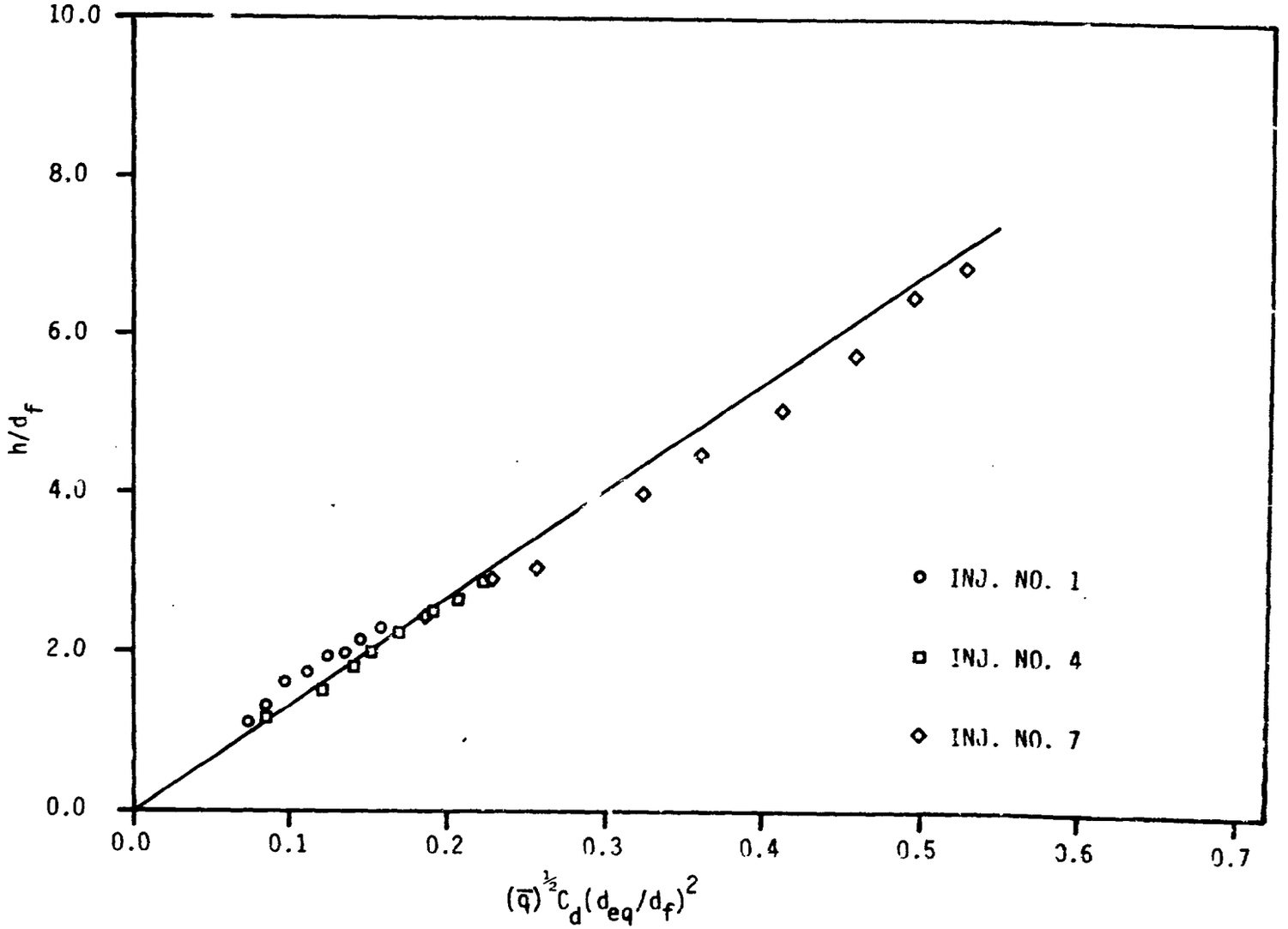

Fig. 14 Penetration Correlation For Circular Injectors

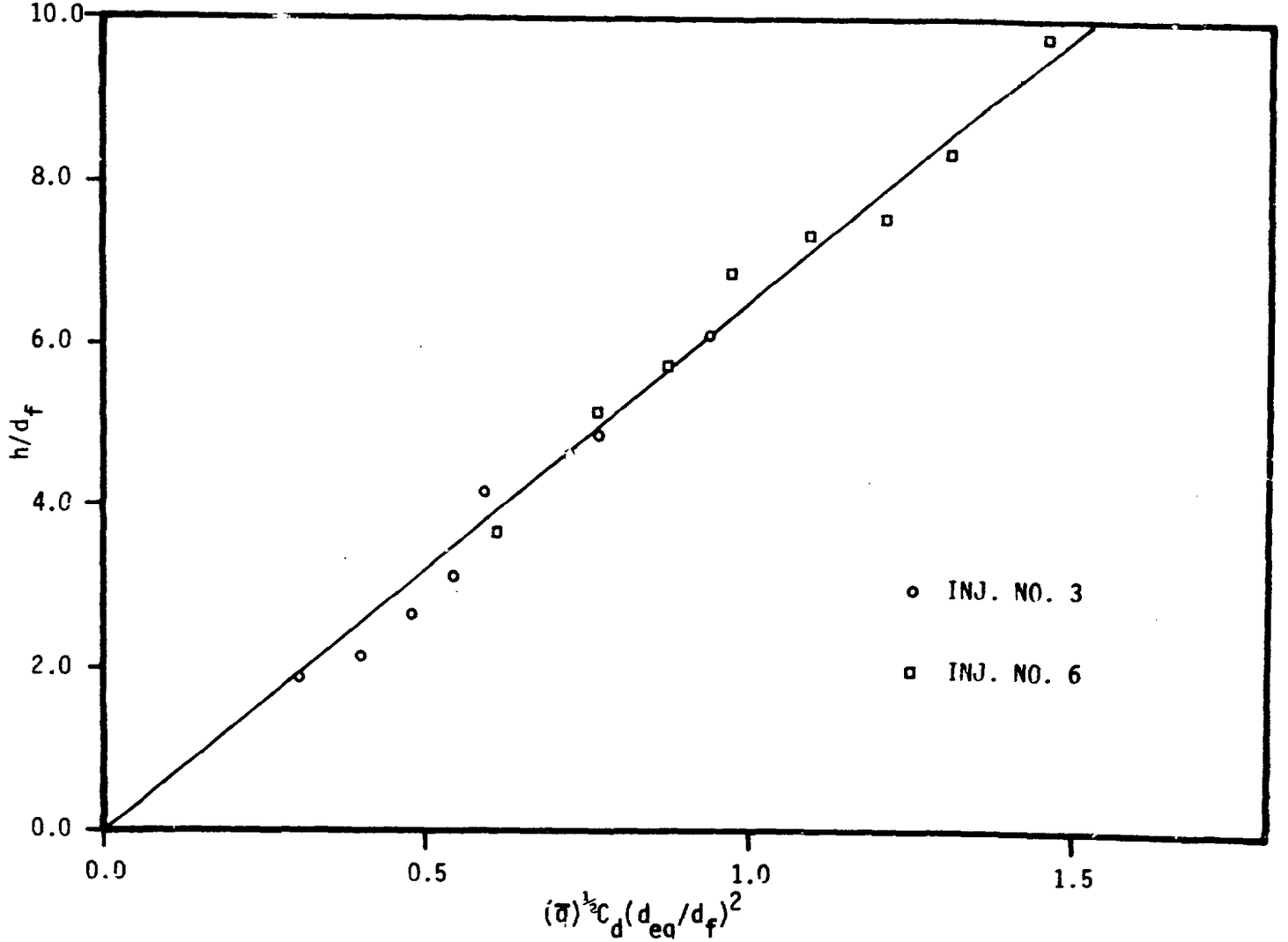

Fig. 15 Penetration Correlation for Rectangular Injectors (d_f:d_s::1:5)

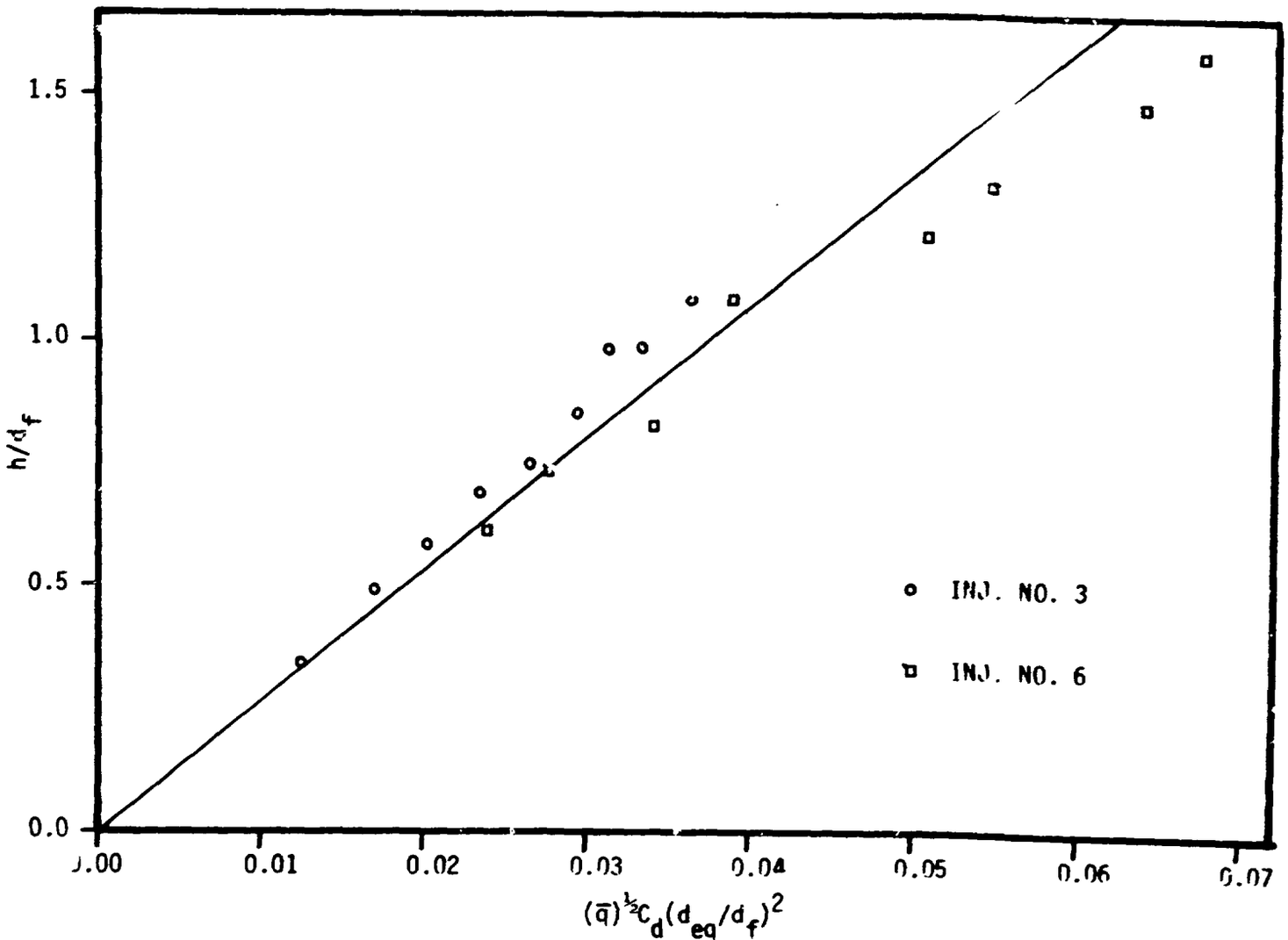

Fig. 16 Penetration Correlation for Rectangular Injectors (d_f:d_s::5:1)

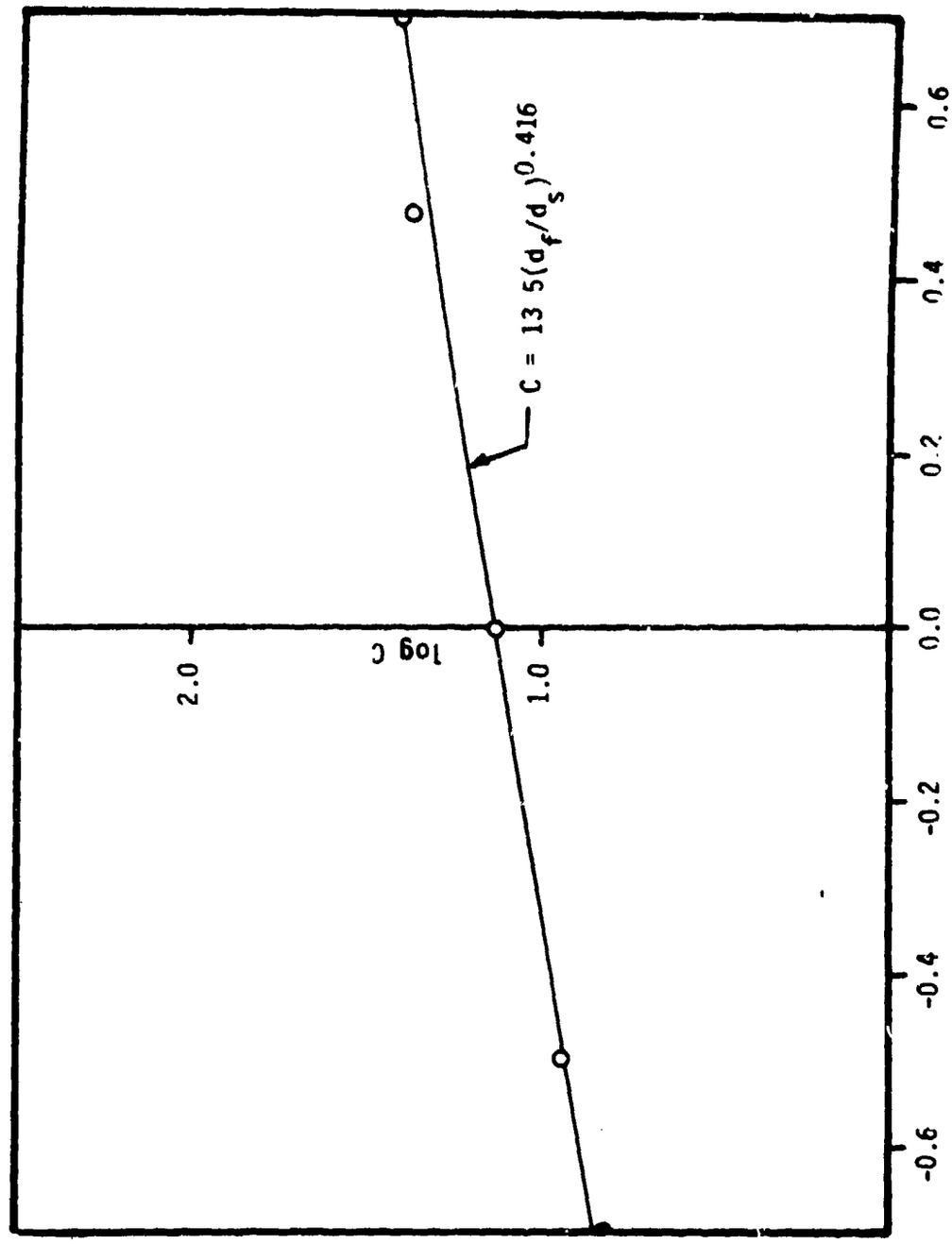

Fig. 17 Log C Vs. Log (d_f/d_s)

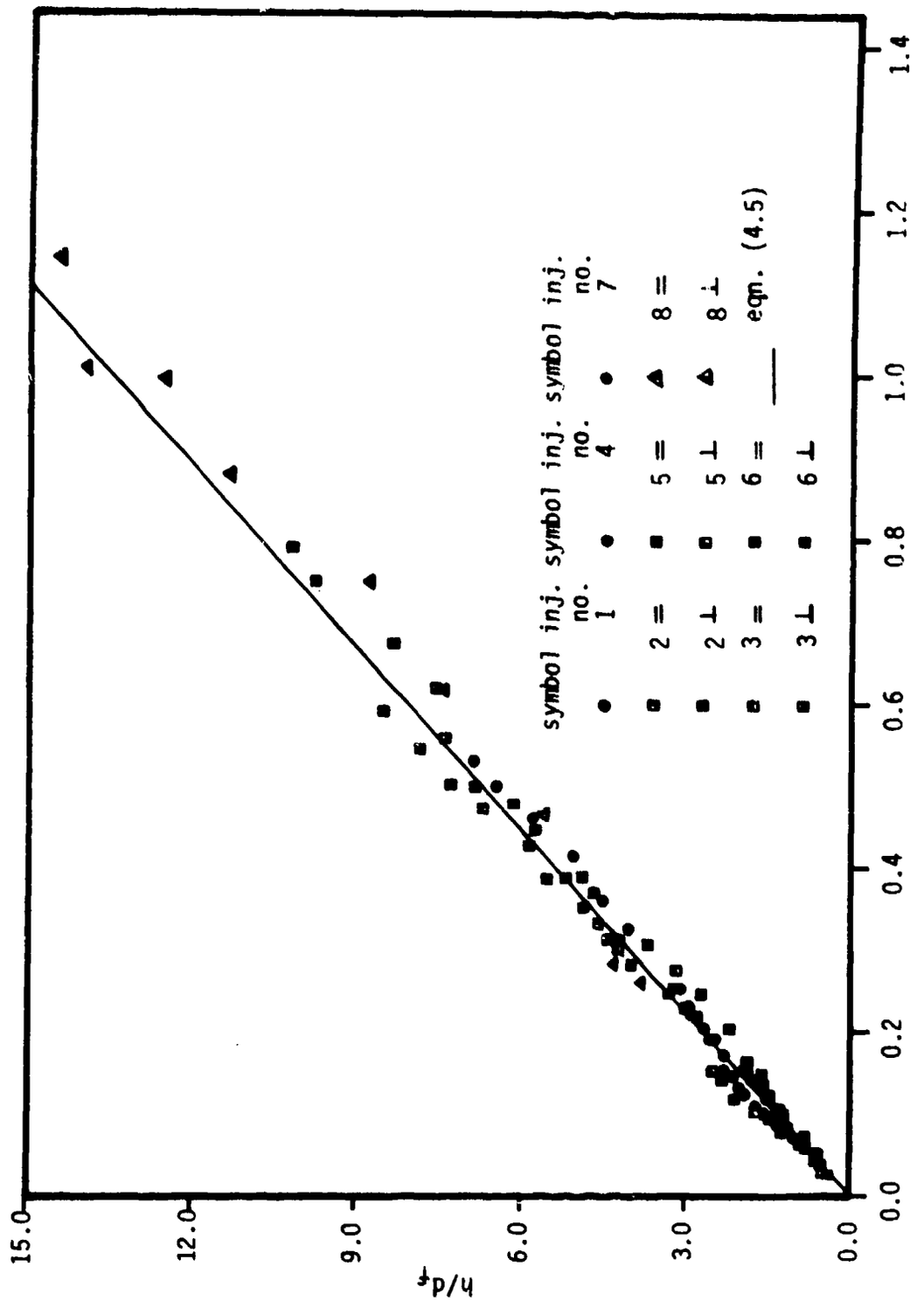

Fig. 18 Penetration Correlation for All Injectors Tested

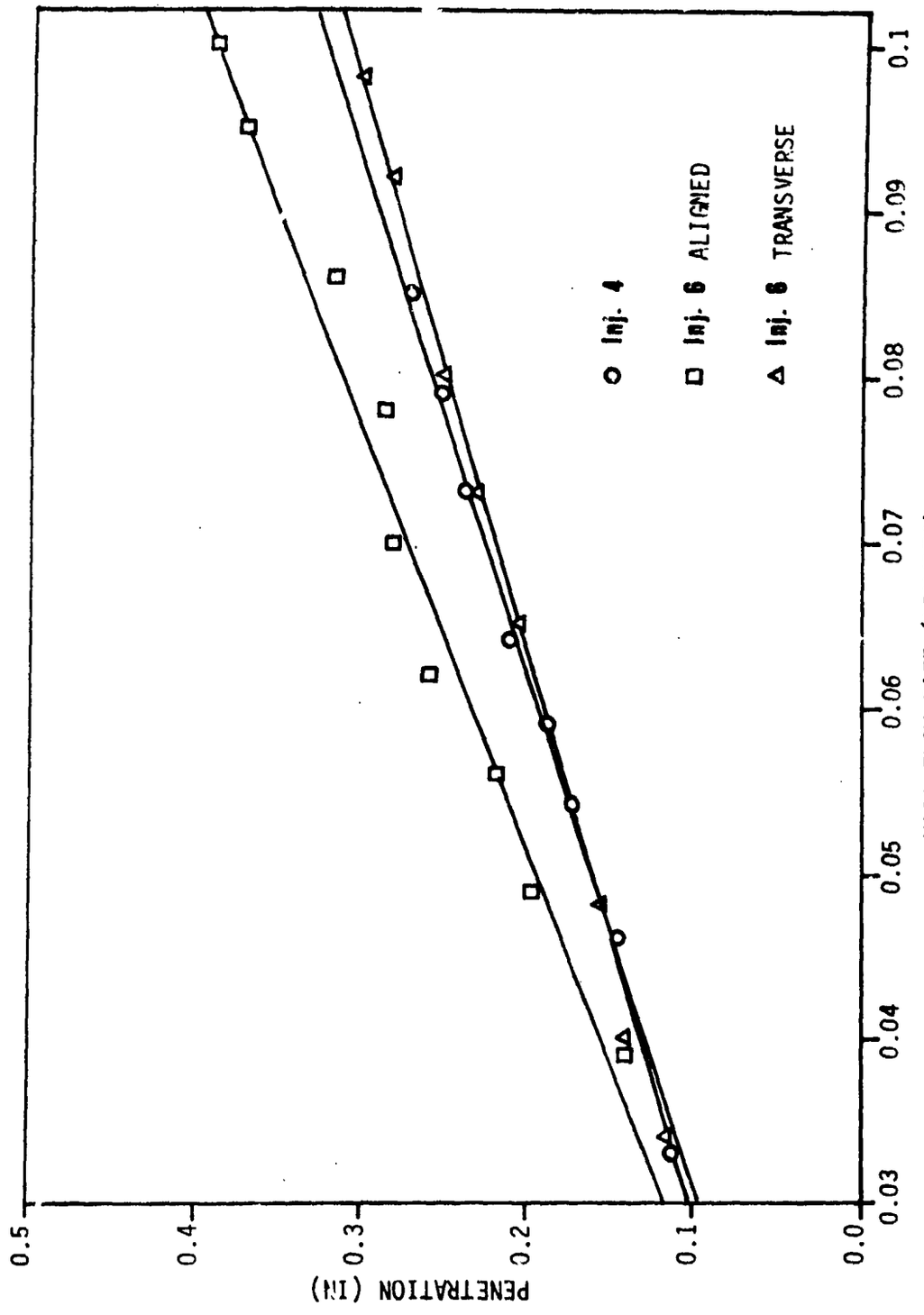

Fig. 19 Comparison of Circular and Rectangular Injectors Having Same Area

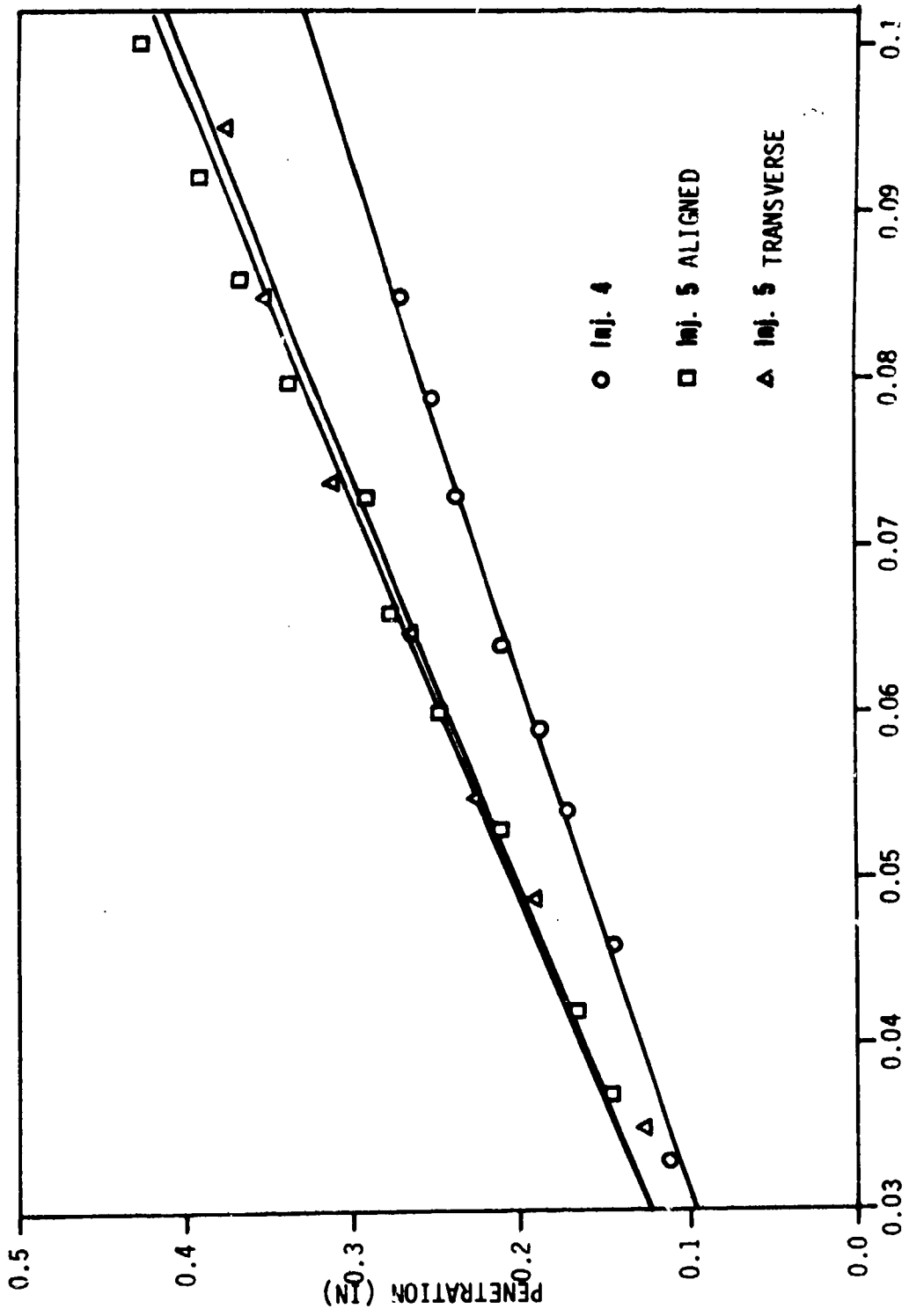

Fig. 20 Comparison of Circular and Rectangular Injectors Having Same Area

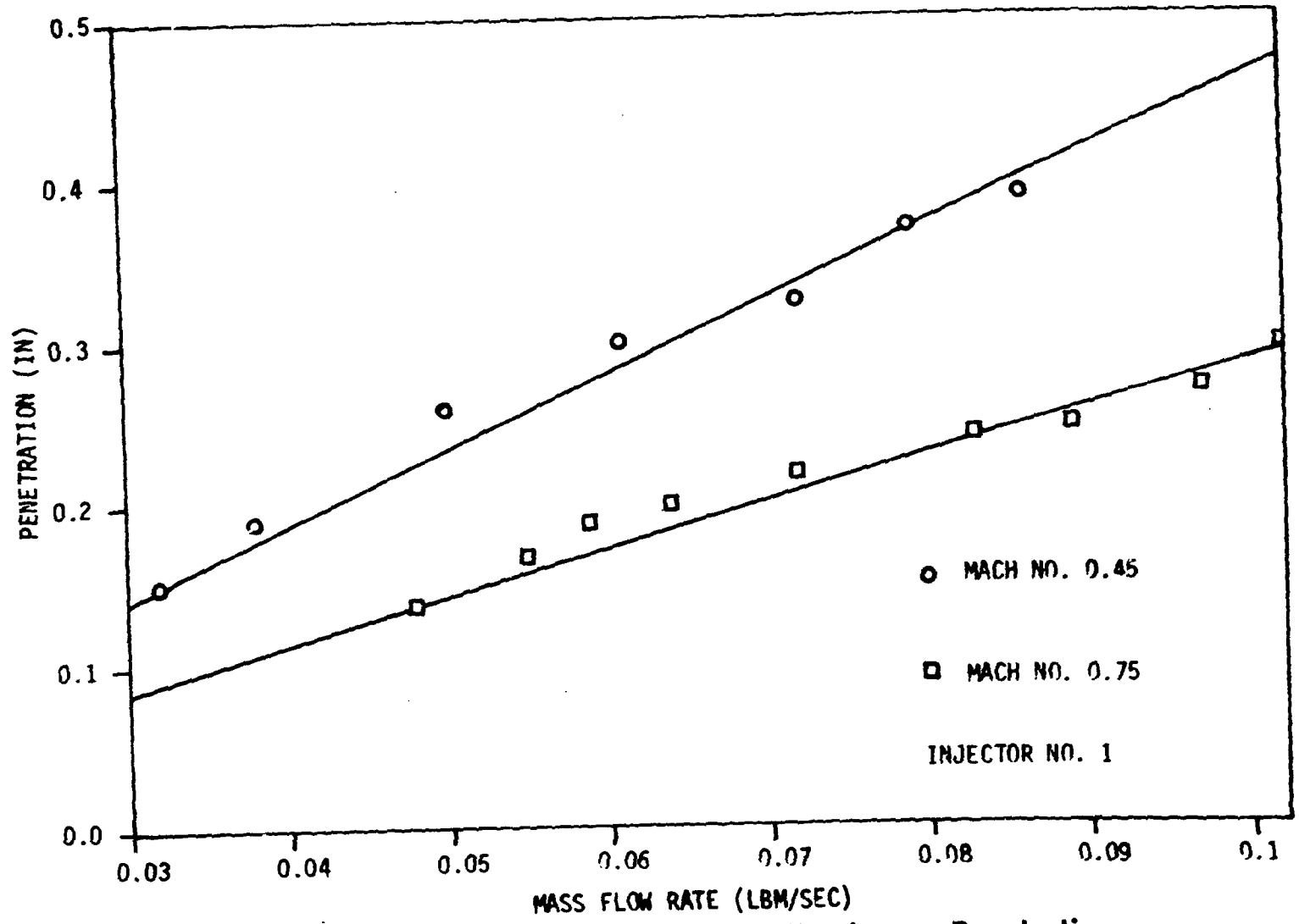

Fig. 21 Effect of Free Stream Mach Number on Penetration

(a) Inj. No. 5 Transverse $\overline{q}$ = 2.061

(b) Inj. No. 5 Transverse $\overline{q}$ = 0.76

Fig. 22 EFFECT OF CHANGE IN $\overline{q}$ ON JET STRUCTURE

(a) Inj. No. 5 Transverse $\bar{q}$ = 2.061

(b) Inj. No. 5 Aligned $\bar{q}$ = 2.05

Fig. 23 EFFECT OF IJECTOR GEOMETRY ON JET STRUCTURE

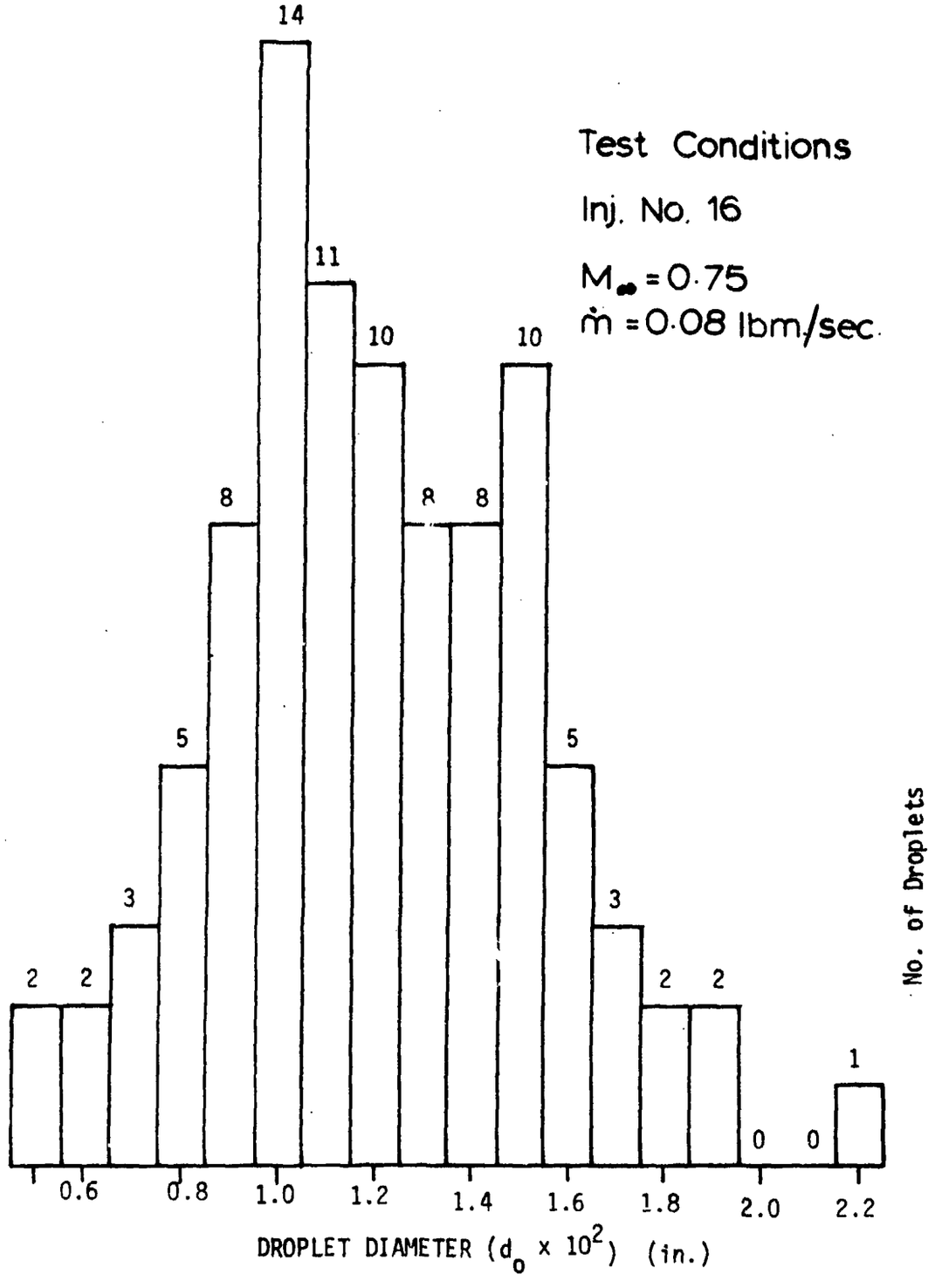

Fig. 24 Droplet Size Distribution - Histogram

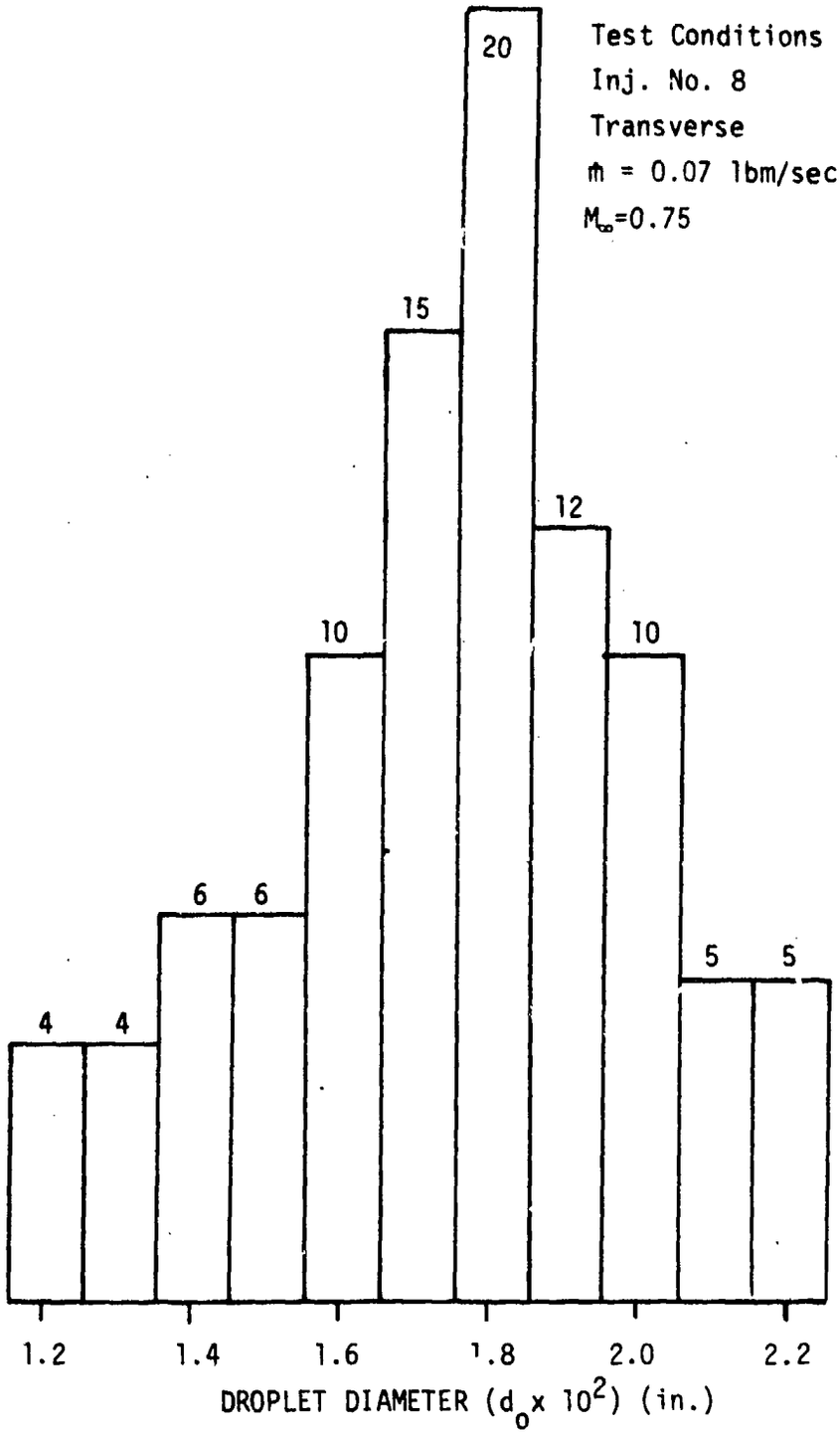

Fig. 25 Droplet Size Distribution - Histogram

APPENDIX A

TABULARIZED PENETRATION DATA

TABLE A-1

Injector No. 1

Area = 0.01227 in.^{2}

Frontal Dimension = 0.125 in.

Shape - Circle

Sr. No.	P_{oj}	$\dot{m}$	V_j	$\bar{q}$	h	h/d_f	$(\bar{q})^{\frac{1}{2}} C_d \frac{d_{eq}}{d_f}^2$
	psia	lbm./sec.	ft./sec.		in.		
1	18.63	0.048	17.32	0.019	0.068	0.544	0.072
2	18.76	0.055	17.87	0.021	0.083	0.664	0.084
3	19.23	0.064	19.73	0.025	0.1	0.8	0.096
4	19.31	0.072	20.03	0.026	0.108	0.864	0.110
5	19.69	0.083	21.39	0.029	0.12	0.96	0.124
6	20.06	0.089	22.64	0.033	0.123	0.984	0.134
7	20.31	0.097	23.44	0.035	0.135	1.08	0.144
8	20.81	0.102	24.98	0.04	0.148	1.184	0.154

TABLE A-2

Injector No. 2

Area = 0.01227 $in.^2$

Frontal Dimension = 0.0665 in.

Shape - Rectangular

Orientation - Aligned

Sr. No.	P_{oj}	$\dot{m}$	V_j	$\bar{q}$	h	h/d_f	$(\bar{q})^{\frac{1}{2}} C_d$	d_{eq}/d_f ^{2}
	psia	lbm./sec.	ft./sec.		in.			
1	18.26	0.043	14.73	0.014	0.053	0.797	0.226	
2	18.61	0.049	16.4	0.017	0.062	0.932	0.258	
3	18.64	0.056	16.54	0.018	0.087	1.308	0.303	
4	19.21	0.065	18.52	0.022	0.093	1.398	0.346	
5	19.36	0.069	19.5	0.024	0.100	1.504	0.361	
6	19.74	0.076	20.9	0.028	0.108	1.624	0.402	
7	20.44	0.085	23.26	0.034	0.132	1.985	0.443	
8	21.49	0.094	26.4	0.044	0.147	2.211	0.497	
9	22.24	0.099	28.43	0.051	0.152	2.286	0.519	

TABLE A-3

Injector No. 2

Area = 0.01227 $in.^2$

Frontal Dimension = 0.199 in.

Shape - Rectangular

Orientation - Transverse

Sr. No.	P_{oj}	$\dot{m}$	V_j	$\bar{q}$	h	h/d_f	$(\bar{q})^{\frac{1}{2}} C_d \, d_{eq}/d_f^2$
	psia	lbm./sec.	ft./sec.		in.		
1	18.8	0.031	17.75	0.02	0.04	0.201	0.0184
2	19.06	0.04	18.81	0.023	0.052	0.261	0.0239
3	19.43	0.049	20.21	0.026	0.062	0.312	0.0293
4	19.78	0.059	21.46	0.029	0.08	0.402	0.0349
5	20.3	0.068	23.19	0.034	0.09	0.452	0.0400
6	20.68	0.077	24.38	0.038	0.109	0.548	0.0454
7	21.98	0.086	28.06	0.050	0.123	0.618	0.0512
8	22.88	0.094	30.35	0.059	0.138	0.693	0.0556
9	23.76	0.100	32.43	0.067	0.145	0.729	0.0592

TABLE A-4

Injector No. 3

Area = 0.01227 in.^{2}

Frontal Dimension = 0.0506 in.

Shape - Rectangular

Orientation - Aligned

Sr. No.	P_{oj}	$\dot{m}$	V_j	$\bar{q}$	h	h/d_f	$(\bar{q})^{\frac{1}{2}} C_d \left(\frac{d_{eq}}{d_f}\right)^2$
	psia	lbm./sec.	ft./sec.		in.		
1	17.78	0.032	12.9	0.011	0.048	0.949	0.301
2	18.41	0.043	16.13	0.017	0.055	1.087	0.398
3	18.78	0.051	17.75	0.02	0.068	1.344	0.475
4	18.91	0.059	18.29	0.021	0.08	1.58	0.539
5	19.29	0.064	19.77	0.025	0.107	2.115	0.589
6	20.16	0.079	22.81	0.033	0.118	2.332	0.721
7	20.31	0.083	23.29	0.035	0.123	2.43	0.765
8	22.29	0.1	28.92	0.054	0.155	3.063	0.936

TABLE A-5

Injector No. 3

Area = 0.01227 $in.^2$

Frontal Dimension = 0.253

Shape - Rectangular

Orientation - Transverse

Sr. No.	P_{oj}	$\dot{m}$	V_j	$\bar{q}$	h	h/d_f	$(\bar{q})^{\frac{1}{2}} C_d \, d_{eq}/d_f^2$
	psia	lbm./sec.	ft./sec.		in.		
1	19.12	0.035	18.65	0.022	0.043	0.170	0.0127
2	19.28	0.046	19.27	0.024	0.063	0.249	0.0170
3	20.08	0.055	22.14	0.031	0.074	0.292	0.202
4	20.86	0.064	24.62	0.038	0.088	0.348	0.0233
5	21.16	0.072	25.51	0.042	0.095	0.375	0.0265
6	21.66	0.079	26.93	0.046	0.108	0.427	0.0293
7	22.33	0.085	28.72	0.052	0.125	0.494	0.0312
8	23.08	0.090	30.59	0.059	0.125	0.494	0.0332
9	24.08	0.099	32.93	0.069	0.138	0.545	0.0365

TABLE A-6

Injector No. 4

Area = 0.0069 $in.^2$

Frontal Dimension = 0.09375 in.

Shape - Circle

Sr. No.	P_{oj}	$\dot{m}$	V_j	$\bar{q}$	h	h/d_f	$(\bar{q})^{\frac{1}{2}} C_d \, d_{eq}/d_f^2$
	psia	lbm./sec.	ft./sec.		in.		
1	20.03	0.033	19.00	0.022	0.055	0.587	0.86
2	20.68	0.046	21.39	0.028	0.071	0.757	0.12
3	21.78	0.054	24.92	0.038	0.085	0.907	0.14
4	22.03	0.059	25.66	0.039	0.093	0.992	0.152
5	22.43	0.064	26.79	0.044	0.105	1.12	0.168
6	23.18	0.073	28.79	0.05	0.118	1.259	0.19
7	23.78	0.079	30.30	0.056	0.125	1.333	0.206
8	24.18	0.085	31.27	0.059	0.135	1.44	0.221

TABLE A-7

Injector No. 5

Area - 0.0069 $in.^2$

Frontal Dimension = 0.0498 in.

Shape - Rectangular

Orientation - Aligned

Sr. No.	P_{oj}	$\dot{m}$	V_j	$\bar{q}$	h	h/d_f	$(\bar{q})^{\frac{1}{2}} C_d \frac{d_{eq}}{d_f}^2$
	psia	lbm./sec.	ft./sec.		in.		
1	20.61	0.037	21.87	0.029	0.072	1.446	0.344
2	21.56	0.042	24.89	0.038	0.082	1.647	0.394
3	23.16	0.053	29.28	0.053	0.105	2.108	0.498
4	24.61	0.06	32.75	0.066	0.122	2.45	0.555
5	26.16	0.066	36.1	0.08	0.138	2.771	0.611
6	27.66	0.073	39.06	0.094	0.145	2.912	0.674
7	30.16	0.08	43.56	0.117	0.167	3.353	0.752
8	31.71	0.086	46.13	0.131	0.182	3.655	0.795
9	34.76	0.092	50.8	0.159	0.195	3.916	0.862
10	37.96	0.1	55.29	0.188	0.212	4.257	0 937

TABLE A-8

Injector No. 5

Area = 0.0069 $in.^2$

Frontal Dimension = 0.149 in.

Shape - Rectangular

Orientation - Transverse

Sr. No.	P_{oj}	$\dot{m}$	V_j	$\bar{q}$	h	h/d_f	$(\bar{q})^{\frac{1}{2}} C_d \, d_{eq}/d_f^2$
	psia	lbm./sec.	ft./sec.		in.		
1	21.35	0.035	24.38	0.037	0.062	0.416	0.0366
2	22.1	0.042	26.57	0.043	0.08	0.537	0.0435
3	23.35	0.049	29.86	0.055	0.095	0.638	0.0511
4	24.5	0.055	32.59	0.065	0.102	0.685	0.0575
5	26.75	0.065	37.37	0.086	0.131	0.879	0.0673
6	29.1	0.074	41.79	0.108	0.155	1.04	0.0768
7	33.1	0.085	48.38	0.144	0.175	1.174	0.0886
8	37.25	0.095	54.38	0.182	0.188	1.262	0.0980

TABLE A-9

Injector No. 6

Area = 0.0069 $in.^2$

Frontal Dimension = 0.038 in.

Shape - Rectangular

Orientation - Aligned

Sr. No.	P_{oj}	$\dot{m}$	V_j	$\bar{q}$	h	h/d_f	$(\bar{q})^{\frac{1}{2}} C_d \frac{d_{eq}}{d_f}^2$
	Psia	lbm./sec.	ft./sec.		in.		
1	21.75	0.039	23.09	0.031	0.07	1.842	0.611
2	22.75	0.049	26.11	0.04	0.098	2.579	0.767
3	23.75	0.056	28.82	0.049	0.109	2.868	0.876
4	24.75	0.062	31.29	0.057	0.13	3.421	0.974
5	26.41	0.07	35.01	0.072	0.14	3.684	1.094
6	28.25	0.078	38.72	0.088	0.143	3.763	1.210
7	30.25	0.086	42.39	0.101	0.158	4.158	1.315
8	33.01	0.095	46.49	0.125	0.185	4.868	1.463
9	34.65	0.100	49.05	0.139	0.194	5.105	1.543

TABLE A-10

Injector No. 6

Area = 0.0069 $in.^2$

Frontal Dimension - 0.190

Shape - Rectangular

Orientation - Transverse

Sr. No.	P_{oj}	$\dot{m}$	V_j	$\bar{q}$	h	h/d_f	$(\bar{q})^{\frac{1}{2}} C_d \, d_{eq}/d_f^2$
	psia	lbm./sec.	ft./sec.		in.		
1	18.54	0.034	24.41	0.044	0.058	0.305	0.0240
2	19.54	0.04	26.76	0.052	0.07	0.368	0.0278
3	20.04	0.048	29.38	0.065	0.078	0.411	0.0341
4	22.04	0.055	33.85	0.085	0.103	0.542	0.0390
5	25.09	0.073	39.99	0.119	0.115	0.605	0.0512
6	27.44	0.08	43.13	0.133	0.125	0.658	0.0550
7	30.44	0.092	48.62	0.174	0.140	0.737	0.0640
8	32.99	0.098	51.96	0.195	0.150	0.789	0.0677

TABLE A-11

Injector no. 7

Area = 0.00307 $in.^2$

Frontal Dimension = 0.0625 in.

Shape - Circle

Sr. No.	P_{oj}	$\dot{m}$	V_j	$\bar{q}$	h	h/d_f	$(\bar{q})^{\frac{1}{2}} C_d \left(\frac{d_{eq}}{d_f}\right)^2$
	psia	lbm./sec.	ft./sec.		in.		
1	23.57	0.032	30.52	0.058	0.0765	1.224	0.188
2	24.82	0.039	33.65	0.07	0.09	1.44	0.23
3	26.82	0.044	37.41	0.086	0.095	1.52	0.258
4	30.32	0.055	43.65	0.116	0.125	2.00	0.324
5	36.87	0.062	53.39	0.172	0.14	2.24	0.361
6	37.87	0.07	55.02	0.185	0.158	2.52	0.413
7	43.87	0.078	62.6	0.239	0.18	2.88	0.460
8	48.12	0.085	67.56	0.28	0.203	3.24	0.497
9	49.72	0.09	69.3	0.295	0.214	3.424	0.53

TABLE A-12

Injector No. 8

Area = 0.00307 in.^{2}

Frontal Dimension = 0.0332 in.

Shape - Rectangular

Orientation - Aligned

Sr. No.	P_{oj}	$\dot{m}$	V_j	$\bar{q}$	h	h/d_f	$(\bar{q})^{\frac{1}{2}} C_d \frac{d_{eq}}{d_f}^2$
	psia	lbm./sec.	ft./sec.		in.		
1	25.68	0.035	35.16	0.076	0.093	2.801	0.733
2	31.73	0.047	45.74	0.126	0.123	3.705	0.969
3	34.48	0.056	54.95	0.188	0.145	4.367	1.183
4	48.23	0.067	67.62	0.28	0.188	5.663	1.388
5	56.23	0.075	76.19	0.361	0.208	6.265	1.576
6	65.61	0.083	84.51	0.435	0.232	6.988	1.730
7	73.36	0.087	90.99	0.501	0.24	7.229	1.806

TABLE A-13

Injector No. 8

Area - 0.00307 $in.^2$

Frontal Dimension - 0.0996 in.

Shape - Rectangular

Orientation - Transverse

Sr. No.	P_{oj}	$\dot{m}$	V_j	$\bar{q}$	h	h/d_f	$(\bar{q})^{\frac{1}{2}} C_d \, d_{eq}/d_f^2$
	psia	lbm./sec.	ft./sec.		in.		
1	31.73	0.04	43.41	0.106	0.095	0.954	0.0885
2	36.48	0.049	50.61	0.142	0.115	1.155	0.1083
3	39.73	0.054	55.31	0.171	0.13	1.305	0.1189
4	49.23	0.064	66.87	0.249	0.152	1.526	0.1415
5	58.85	0.073	76.82	0.329	0.192	1.928	0.1626
6	67.23	0.081	84.45	0.396	0.215	2.159	0.1784

TABLE A-14

Injector No. 9

Area = 0.00077 in.^{2}

Frontal Dimension - 0.03125 in.

Shape - Circle

Sr. No.	P_{oj}	$\dot{m}$	V_j	$\bar{q}$	h	h/d_f	$(\bar{q})^{\frac{1}{2}} C_d \frac{d_{eq}}{d_f}^2$
	psia	lbm./sec.	ft./sec.		in.		
1	45.3	0.037	62.17	---	0.12	3.84	---
2	65.68	0.042	82.68	---	0.138	4.416	---
3	100.68	0.056	109.87	---	0.192	6.144	---
4	151.30	0.064	140.0	---	0.222	7.104	---
5	247.55	0.074	184.05	---	0.265	8.48	---
6	263.65	0.08	190.73	---	0.28	8.96	---
7	301.15	0.086	204.81	---	0.295	9.44	---
8	326.71	0.09	210.49	---	0.32	10.24	---

APPENDIX B

COMPARISON OF CIRCULAR AND RECTANGULAR INJECTORS

Comparison of Circular and rectangular injectors:

The expression for penetration in terms of mass flow rate, as given by Eqn. (4.6), is

$$H_{rect} = k\dot{m} \left(\frac{d_f}{d_s}\right)^{0.416} \frac{1}{d_f} \tag{B.1}$$

where k is a constant. In general, this equation applies to rectangular injectors with round edges. For a special case of a circular hole of the same area, $d_f = d_s = d_{eq}$

Hence

$$h_{circ} = k \frac{\dot{m}}{d_{eq}} \tag{B.2}$$

Dividing Eqn. (B.1) by Eqn. (B.2)

$$\frac{h_{rect}}{h_{circ}} = \frac{d_{eq}}{d_f} \left(\frac{d_f}{d_s}\right)^{0.416} \tag{B.3}$$

This equation holds for prescribed free stream conditions and injectant mass flow rate.

For a given injector area, with reference to Fig. B-1,

$$\frac{\pi d_{eq}^2}{4} = \frac{\pi d_f^2}{4} + d_f (d_s - d_f) \tag{B.4a}$$

for aligned injector and

$$\frac{\pi d_{eq}^2}{4} = \frac{\pi d_s^2}{4} + d_s (d_f - d_s) \tag{B.4b}$$

for transverse injector.

Squaring Eqn. (B.3) and substituting for d_{eq}^2 from Eqns. (B.4a) and (B.4b).

$$\left(\frac{h_{rect}}{h_{circ}}\right)^2 = \left\{1 + \frac{4}{\pi}\left(\frac{d_s}{d_f} - 1\right)\right\}\left(\frac{d_f}{d_s}\right)^{0.832}$$

for aligned injector and

$$\left(\frac{h_{rect}}{h_{circ}}\right)^2 = \left\{\frac{4}{\pi}\left(\frac{d_s}{d_f}\right) + \left(1 - \frac{4}{\pi}\right)\left(\frac{d_s}{d_f}\right)^2\right\}\left(\frac{d_f}{d_s}\right)^{0.832}$$

for transverse injector

Simplifying,

$$\frac{h_{rect}}{h_{circ}} = \left\{1.27\left(\frac{d_s}{d_f}\right)^{0.168} - 0.27\left(\frac{d_f}{d_s}\right)^{0.832}\right\}^{1/2} \qquad \text{(B.5a)}$$

for aligned injector and

$$\frac{h_{rect}}{h_{circ}} = \left\{1.27\left(\frac{d_s}{d_f}\right)^{0.168} - 0.27\left(\frac{d_s}{d_f}\right)^{1.168}\right\}^{1/2} \qquad \text{(B.5b)}$$

for transverse injector.

The range of d_f/d_s or d_s/d_f is as follows:

For aligned injectors,

$$0 < \frac{d_f}{d_s} \lesssim 1$$

and

for transverse injectors,

$$0 < \frac{d_s}{d_f} \lesssim 1$$

If the index of $\frac{d_f}{d_s}$ in Eqn. (B.1) is exactly 0.5 the following expressions are obtained.

$$\frac{h_{rect}}{h_{circ}} = 1.27 - 0.27 \left(\frac{d_f}{d_s}\right) \qquad \text{(B.6a)}$$

for aligned injectors and

$$\frac{h_{rect}}{h_{circ}} = 1.27 - 0.27 \left(\frac{d_s}{d_f}\right) \qquad \text{(B.6b)}$$

for transverse injectors.

Equations (B.5) and (B.6) are plotted in Fig. B-2. It is seen that any rectangular injector aligned with the free stream gives pene-ration higher than that given by a circular injector. In case of rectangular injector transverse to the free stream, the penetration is higher provided that the ratio d_s/d_f is higher than 4.7, otherwise, the penetration is lower than that given by the circular injector. Moreover, the difference between the penetration given by transverse slot and that given by the circular injector is not large except for small values of d_s/d_f.

The index of d_f/d_s in Eqn. (B.1), in fact, cannot be greater than 0.5. If the contrary were true, then Eqn. (B.1) predicts that a transverse slot will have greater penetration than an aligned slot. In the present experimental work, the penetration due to an aligned slot is always greater than that due to a transverse slot. Thus, the following inequality can be established:

$$h_{aligned} < h_{circle} \lesssim h_{transverse}$$

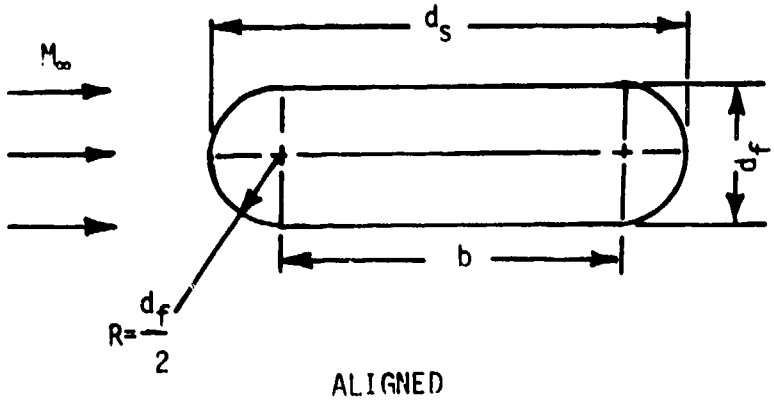

ALIGNED

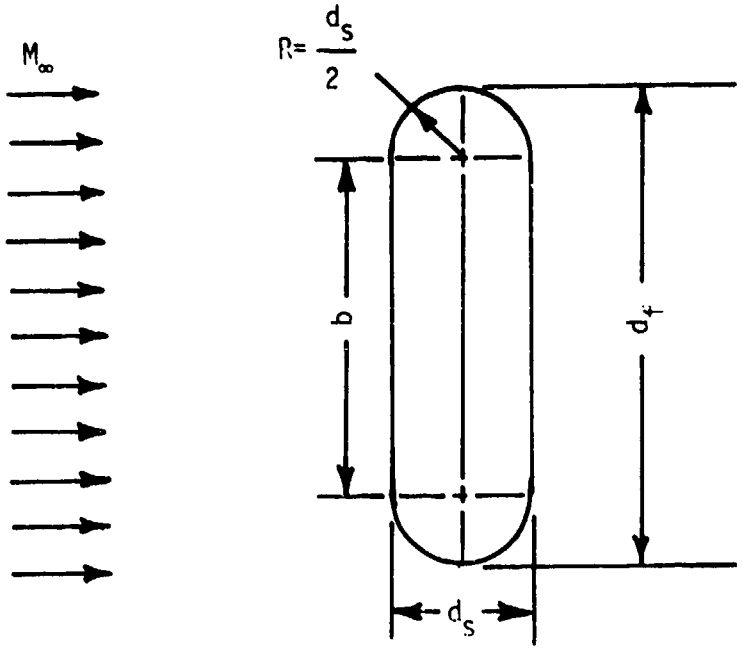

TRANSVERSE

Fig. B-1 Aligned and Transverse Orientation of A Rectangular Injector With Rounded Ends

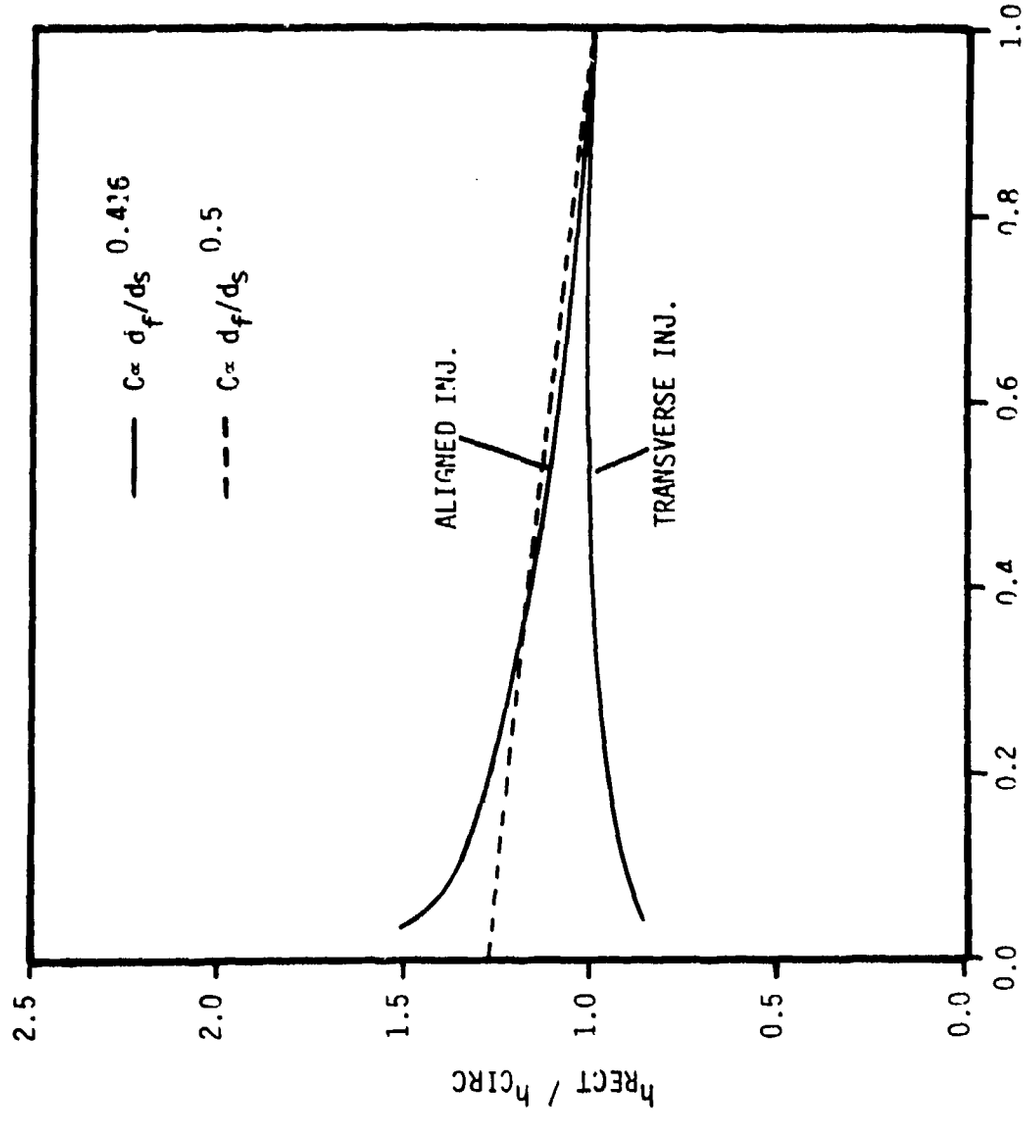

Fig. B -2 Comparison of Circular and Rectangular Injectors

APPENDIX C

TABULARIZED DROPLET SIZE DISTRIBUTION DATA

TABLE C-1

Test Conditions

Run	M_∞	Injector	Mass flow rate in lbm/sec.
1	0.45	9	0.08
2	0.45	7	0.08
3	0.45	8 transverse	0.07
4	0.45	8 aligned	0.072
5	0.75	7	0.083

TABLE C-2

Droplet size $d \times 10^2$ (in.)	Number of droplets				
	Run 1	Run 2	Run 3	Run 4	Run 5
0.45 - 0.55	2				
0.55 - 0.65	2				
0.65 - 0.75	3			2	3
0.75 - 0.85	7	7		5	6
0.85 - 0.95	8	8		11	12
0.95 - 1.05	17	8		6	8
1.05 - 1.15	14	12		15	13
1.15 - 1.25	16	4	4	10	15
1.25 - 1.35	13	7	4	19	15
1.35 - 1.45	14	11	6	10	9
1.45 - 1.55	28	8	6	7	8
1.55 - 1.65	17	4	10	5	5
1.65 - 1.75	18	12	15	5	4
1.75 - 1.85	11	8	20	3	4
1.85 - 1.95	10	0	12		
1.95 - 2.05	3	3	10		
2.05 - 2.15	0	0	5		
2.15 - 2.25	4	0	5		
2.25 - 2.35	2	0			
2.35 - 2.45		4			